NAVAL POSTGRADUATE SCHOOL

MONTEREY, CALIFORNIA

THESIS

HF OVER-THE-HORIZON RADAR SYSTEM PERFORMANCE ANALYSIS

by

Bin-Yi Liu

September 2007

Thesis Co-Advisors: Phillip E. Pace
Jeffrey B. Knorr

Approved for public release, distribution is unlimited

THIS PAGE INTENTIONALLY LEFT BLANK

REPORT DOCUMENTATION PAGE			Form Approved OMB No. 0704-0188

1. AGENCY USE ONLY *(Leave blank)*	**2. REPORT DATE** September 2007	**3. REPORT TYPE AND DATES COVERED** Master's Thesis

4. TITLE AND SUBTITLE HF Over-the-Horizon Radar System Performance Analysis	**5. FUNDING NUMBERS**
6. AUTHOR(S) Bin-Yi Liu	
7. PERFORMING ORGANIZATION NAME(S) AND ADDRESS(ES) Center for Joint Services Electronic Warfare Naval Postgraduate School, Code EC Monterey, CA 93943-5000	**8. PERFORMING ORGANIZATION REPORT NUMBER**
9. SPONSORING /MONITORING AGENCY NAME(S) AND ADDRESS(ES) Missile Defense Agency 7100 Defense Pentagon Washington, DC 20301-7100	**10. SPONSORING/MONITORING AGENCY REPORT NUMBER**

11. SUPPLEMENTARY NOTES The views expressed in this thesis are those of the author and do not reflect the official policy or position of the Department of Defense or the U.S. Government.

12a. DISTRIBUTION / AVAILABILITY STATEMENT Approved for public release; distribution is unlimited	**12b. DISTRIBUTION CODE** A

13. ABSTRACT (maximum 200 words)

The basic concept of the structure and properties of the ionosphere are discussed to explain how the performance of the over-the-horizon radar (OTHR) system is affected. An overview of the OTHR system characteristics and performance are presented along with some applications currently used around the world, including their geographic location and historical background. The waveforms used for the OTHR systems include simple pulse, pulse Doppler, phased-coded pulse, frequency modulated continuous wave (FMCW), and frequency modulated interrupt continuous wave (FMICW). Other characteristics such as target detection methods and the skywave OTHR range equation are also discussed. Simulation results indicate that the minimum required input signal-to-noise ratio (SNR) for a target with 100 m^2 cross section at 3,500 km footprint range is -52.4 dB at $f_c = 14.5$ MHz. In addition, a noncooperative intercept receiver requires a minimum input SNR of 94 dB for a square law detector and 97 dB for a linear detector for interception at a footprint range of 3,500 km at $f_c = 14.5$ MHz.

A model of the maximum detection range for the Chinese FMCW OTH backscatter (OTH-B) radar was developed in MATLAB. An intercept receiver maximum interception range is also analyzed. A ray tracing technique is also used in PROPLAB to present a more detailed analysis. The analysis includes the electron density profile, the maximum usable frequency, the critical frequency of the layers, the skip zone, and the signal quality. The simulations focused on the Chinese OTH-B radar system are to investigate the Chinese surveillance capabilities.

14. SUBJECT TERMS Over-the-Horizon, OTH, OTHR, OTH-B, ionosphere, Jindalee, JORN, HF, HFSWR, Nostradamus, Valensole, OTH-SW, CONDO-R, MADRE, WARF, AN/FPS-95, AN/FPS-112, AN/FPS-118, AN/TPS-71, waveform, simple pulse, Pulse Doppler, phased-coded pulse, FMCW, FMICW, radar equation, PROPLAB, ray tracing, signal quality	**15. NUMBER OF PAGES** 122
	16. PRICE CODE

17. SECURITY CLASSIFICATION OF REPORT	**18. SECURITY CLASSIFICATION OF THIS PAGE**	**19. SECURITY CLASSIFICATION OF ABSTRACT**	**20. LIMITATION OF ABSTRACT**
Unclassified	Unclassified	Unclassified	UU

NSN 7540-01-280-5500 Standard Form 298 (Rev. 2-89)
Prescribed by ANSI Std. 239-18

THIS PAGE INTENTIONALLY LEFT BLANK

Approved for public release; distribution is unlimited

HF OVER-THE-HORIZON RADAR SYSTEM PERFORMANCE ANALYSIS

Bin-Yi Liu
Lieutenant, Taiwan Navy
B.S., Chinese Naval Academy, 2000

Submitted in partial fulfillment of the
requirements for the degree of

MASTER OF SCIENCE IN ELECTRONIC WARFARE SYSTEMS ENGINEERING

from the

NAVAL POSTGRADUATE SCHOOL
September 2007

Author: Bin-Yi Liu

Approved by: Phillip E. Pace
Thesis Co-Advisor

Jeffrey B. Knorr
Thesis Co-Advisor

Dan C. Boger
Chairman, Department of Information Science

THIS PAGE INTENTIONALLY LEFT BLANK

ABSTRACT

The basic concept of the structure and properties of the ionosphere are discussed to explain how the performance of the over-the-horizon radar (OTHR) system is affected. An overview of the OTHR system characteristics and performance are presented along with some applications currently used around the world, including their geographic location and historical background. The waveforms used for the OTHR systems include simple pulse, pulse Doppler, phased-coded pulse, frequency modulated continuous wave (FMCW), and frequency modulated interrupt continuous wave (FMICW). Other characteristics such as target detection methods and the skywave OTHR range equation are also discussed.

A model of the maximum detection range for the Chinese FMCW OTH backscatter (OTH-B) radar was developed in MATLAB. An intercept receiver maximum interception range is also analyzed. Simulation results indicate that the minimum required input signal-to-noise ratio (SNR) for a target with 100 m^2 cross section at 3,500 km footprint range is $-52.4\,\text{dB}$ at $f_c = 14.5$ MHz. In addition, a non-cooperative intercept receiver requires a minimum input SNR of 94 dB for a square law detector and 97 dB for a linear detector for interception at a footprint range of 3,500 km at $f_c = 14.5$ MHz. A ray tracing technique is also used in PROPLAB to present a more detailed analysis. The analysis includes the electron density profile, the maximum usable frequency, the critical frequency of the layers, the skip zone, and the signal quality. The simulations focused on the Chinese OTH-B radar system are to investigate the Chinese surveillance capabilities.

THIS PAGE INTENTIONALLY LEFT BLANK

TABLE OF CONTENTS

I. INTRODUCTION....1
A. OVER-THE-HORIZON RADAR SYSTEMS....1
1. The Beginning of OTHR....1
2. Problems of the OTHR System....2
B. PRINCIPAL CONTRIBUTIONS....3
C. THESIS OUTLINE....4

II. IONOSPHERE EFFECTS ON OTHR SYSTEM....5
A. IONOSPHERE STRUCTURE....5
B. IONOSPHERIC MODEL....8

III. CURRENT OTHR SYSTEMS IN USE....15
A. AUSTRALIA....15
1. Geographically Strategic Location....15
2. Jindalee Operational Radar Network (JORN)....15
B. CANADA....18
1. Geographically Strategic Location and Defense Innovation....18
2. SWR Series High-Frequency Surface Wave Radar (HFSWR)....19
C. CHINA....20
1. An Overview of Chinese Radar Development....20
2. Over-the-Horizon Backscatter (OTH-B) Radar....20
3. Surface Wave (ground wave) Over-the-Horizon (OTH) Radar....22
4. Pulse Doppler Over-the-Horizon Backscatter (PD-OTH-B) Radar....23
D. FRANCE....24
1. Valensole Skywave HF Radar....24
2. Nostradamus....25
E. ITALY (CONDO-R)....27
F. JAPAN....29
G. THE RUSSIAN FEDERATION....29
1. IRIDA Over-the-Horizon Surface Wave (OTH-SW) Radar....29
2. Over-the-Horizon Backscatter (OTH-B) Radar....30
H. UKRAINE....33
1. Transportable Over-the-Horizon Surface Wave (OTH-SW) Radar....33
2. Shipboard Over-the-Horizon Surface Wave (OTH-SW) Radar....34
3. Transportable SkyWave Over-the-Horizon (SkW-OTH) Radar....34
I. UNITED KINGDOM....35
1. Alenia Marconi Over-the-Horizon (OTH) Radar....35
2. Overseer....36
J. UNITED STATES....37
1. Magnetic-Drum Radar Equipment (MADRE)....37
2. Wide Aperture Research Facility (WARF)....38

3. AN/FPS-95, Cobra Mist 38
4. AN/FPS-112 Over-The-Horizon (OTH) Radar....39
5. AN/FPS-118 Over-The-Horizon Backscatter (OTH-B) Radar....39
6. AN/TPS-71 Relocatable Over-The-Horizon Backscatter (OTH-B) Radar (ROTHR) 41
K. CHAPTER SUMMARY....42
IV. CHARACTERISTICS OF THE OTHR SYSTEMS 45
A. WAVEFORMS....45
B. TARGET DETECTION....46
C. OTHR DETECTION RANGE 47
D. INTERCEPT RECEIVER INTERCEPTION RANGE....51
V. MATHEMATICAL MODELS OF THE OTHR SYSTEM 55
A. SIMULATION TOOLS - PROPLAB-PRO VERSION 2.0 55
B. CHINESE OTH-B RADAR MODEL 55
1. Location, Azimuth, Distance of the Transmitter/Receiver [7]....58
2. UTC Time, Frequency [7] 58
3. CUR Lat, CUR Lon [7]....59
4. Air Dist [7] 59
5. CUR Angle [7] 59
6. The Electron Density Graph and Numeric Density [7] 59
7. Estimated Signal Strength Bar Graph [7] 60
8. Signal Quality Bar Graph and "Sig Qual" [7] 60
9. Mag LAT, Mag LON [7] 61
10. Solar Elevation Angle, "Sol Elv" [7] 61
11. Height or Altitude of the Ray [7]....61
12. Plasma Frequency at the Ray Height [7] 61
13. Signal Elevation Angle, "Sig Elv" [7]....61
14. Auroral Zone, "Aur LAT", "Aur LON", "Aur Dist" [7]....61
15. Ionospheric Distance Traveled, "Iono Dst" [7] 62
16. The Receiver Location [7] 62
17. The Simulation Results....62
C. MAXIMUM SURVEILLANCE RANGE SIMULATION....74
D. CHAPTER SUMMARY....84
VI. CONCLUSION 87
A. SUMMARY OF RESULTS 87
B. FUTURE WORK....87
APPENDIX....89
LIST OF REFERENCES....99
INITIAL DISTRIBUTION LIST 103

LIST OF FIGURES

Figure 1. Thesis Flow Concept....4
Figure 2. Structure of the Atmosphere and the Ionosphere (After [8]).....5
Figure 3. Distribution of Layers in the Ionosphere (After [5]). 7
Figure 4. Skywave Propagation Concept of the OTHR System (After [6])....7
Figure 5. Graphical User Input Panel.....8
Figure 6. Electron Density in Winter Day (January 2007)....9
Figure 7. Electron Density in Winter Night (January 2007). 9
Figure 8. Electron Density in Summer Day (July 2007).....10
Figure 9. Electron Density in Summer Night (July 2007). 10
Figure 10. Ray Path Geometry (From [14]).....12
Figure 11. Geographic Location of JORN. 16
Figure 12. The JORN Transmission Antenna Array (From [15]).....17
Figure 13. A Close View of the Antenna Array (From [16]).....17
Figure 14. An Interior View of the JORN Coordination Center (From [16]).....18
Figure 15. Shore-based SWR System (From [18]). 19
Figure 16. Chinese Type-110 OTHR (From [22]). 21
Figure 17. OTH-B Radar in the East China Sea Fleet (From [22])....21
Figure 18. The Transmitter Antenna Element of Surface Wave OTHR (From [20]).....23
Figure 19. A View of One Receiving Antenna (From [26]). 24
Figure 20. The Receiving Antennas of Nostradamus OTHR (From [27]).....25
Figure 21. A Close View of the Receiving Antennas (From [27]). 26
Figure 22. Command Room of Nostradamus OTHR (From [27]).....26
Figure 23. Underground Network of Nostradamus OTHR System (From [27]). 26
Figure 24. Locations of French OTHRs.....27
Figure 25. The Antenna Unit of the CONDO-R Naval OTHR (From [29]).....28
Figure 26. TPS-828 Mobile Coastal Radar System (From [30]). 28
Figure 27. Location of OTHR Transmitter and Receiver. 29
Figure 28. Geographic Location of Four OTH-B Systems in the Russian Federation. 31
Figure 29. The Antenna Element of OTHR Radar (From [34])....32
Figure 30. Coverage of Russian OTHR (From [34]). 32
Figure 31. Transmission Array Used in the Transportable OTH-SW Radar (2002) (From [35])....33
Figure 32. Typical Coverage of Overseer Radar (1998) (From [38]).....36
Figure 33. MADRE Over-the-Horizon Radar (From [39]).....37
Figure 34. Wide Aperture Research Facility (From [41]).....38
Figure 35. The Transmitter Dipole Elements used in the East Coast OTH-B System (From [40])....40
Figure 36. The Receiver Elements used in the East Coast OTH-B System (From [40]). 40
Figure 37. The AN/TPS-71 ROTHR Transmission Array (From [42]).....41
Figure 38. Target Detection Diagram of OTHR System....47

Figure 39. FMCW OTH-B Maximum Detection Range ($R_{R\max}$) for $\sigma = 1$, 10, and 100 m^2. 49
Figure 40. Geometry Diagram of the Detection Range Calculation. 50
Figure 41. FMCW OTH-B Maximum Detection Range ($R_{\text{footprint}}$) for $\sigma = 1$, 10, and 100 m^2. 50
Figure 42. Intercept Receiver Maximum Interception Range (R_{Imax}) with Square Law / Linear Detector Bandwidth when $f_c = 14.5$ MHz. 53
Figure 43. Intercept Receiver Maximum Interception Range ($R_{\text{interception}}$) with Square Law and Linear Detector Bandwidth. 54
Figure 44. General Location of Chinese OTH-B Radar Transmitter and Receiver. 55
Figure 45. Transmitter Antenna Radiation Pattern of the Chinese OTH-B Radar System. 56
Figure 46. Ionospheric Electron Density Profile for the Chinese OTH-B Radar Analysis for SSN = 30 and AI = 5 at 00:00 UTC 2007/7/31. 57
Figure 47. Ray Path for the Elevation Angle of 0° at 16 MHz Frequency for SSN = 30 and AI = 5 at 00:00 UTC 2007/7/31. 58
Figure 48. Maximum Usable Frequency Profile at the Location of 32.725° N, 241.22° W for SSN = 30 and AI = 5 on 2007/7/31. 63
Figure 49. Global Map of E-layer Critical Frequencies for SSN = 30 and AI = 5 at 00:00 UTC 2007/7/31. 64
Figure 50. Global Map of F2-layer Critical Frequencies for SSN = 30 and AI = 5 at 00:00 UTC 2007/7/31. 65
Figure 51. Maximum Usable Frequency at 700 km Distance for SSN = 30 and AI = 5 at 00:00 UTC 2007/7/31. 66
Figure 52. Maximum Usable Frequency at 3500 km Distance for SSN = 30 and AI = 5 at 00:00 UTC 2007/7/31. 66
Figure 53. Rays in an Elevation Angle from 0° to 20° at 6 MHz Frequency for SSN = 30 and AI = 5 at 00:00 UTC 2007/7/31. 67
Figure 54. Rays in an Elevation Angle from 0° to 20° at 8 MHz Frequency for SSN = 30 and AI = 5 at 00:00 UTC 2007/7/31. 67
Figure 55. Rays in an Elevation Angle from 0° to 20° at 10 MHz Frequency for SSN = 30 and AI = 5 at 00:00 UTC 2007/7/31. 68
Figure 56. Rays in an Elevation Angle from 0° to 20° at 12 MHz Frequency for SSN = 30 and AI = 5 at 00:00 UTC 2007/7/31. 68
Figure 57. Rays in an Elevation Angle from 0° to 20° at 14 MHz Frequency for SSN = 30 and AI = 5 at 00:00 UTC 2007/7/31. 69
Figure 58. Rays in an Elevation Angle from 0° to 20° at 16 MHz Frequency for SSN = 30 and AI = 5 at 00:00 UTC 2007/7/31. 69
Figure 59. Rays in an Elevation Angle from 0° to 20° at 18 MHz Frequency for SSN = 30 and AI = 5 at 00:00 UTC 2007/7/31. 70
Figure 60. Rays in an Elevation Angle from 0° to 20° at 20 MHz Frequency for SSN = 30 and AI = 5 at 00:00 UTC 2007/7/31. 70
Figure 61. Rays in an Elevation Angle from 0° to 20° at 22 MHz Frequency for SSN = 30 and AI = 5 at 00:00 UTC 2007/7/31. 71

Figure 62. Footprint Coverage from 6 to 22 MHz Frequencies with Elevation Angles of 0 to 20 degrees. 71
Figure 63. An Overview of the Generation Processes of the Electron Density Profiles, the MUF Profiles and the Ray Tracing Screens 75
Figure 64. Ionospheric Electron Density Profile for the Chinese OTH-B Radar Analysis for SSN = 30 and AI = 5 at 00:00 UTC 2006/12/21 (winter time)... 76
Figure 65. Ionospheric Electron Density Profile for the Chinese OTH-B Radar Analysis for SSN = 200 and AI = 5 at 00:00 UTC 2006/12/21 (winter time). 76
Figure 66. Ionospheric Electron Density Profile for the Chinese OTH-B Radar Analysis with SSN = 30 and AI = 5 at 00:00 UTC 2007/6/21 (summer time). 77
Figure 67. Ionospheric Electron Density Profile for the Chinese OTH-B Radar Analysis for SSN = 200 and AI = 5 at 00:00 UTC 2007/6/21 (summer time). 77
Figure 68. Maximum Usable Frequency for SSN = 30 and AI = 5 on 2006/12/21 (winter time) 78
Figure 69. Maximum Usable Frequency for SSN = 200 and AI = 5 on 2006/12/21 (winter time) 79
Figure 70. Maximum Usable Frequency for SSN = 30 and AI = 5 on 2007/6/21 (summer time). 79
Figure 71. Maximum Usable Frequency for SSN = 200 and AI = 5 on 2007/6/21 (summer time). 80
Figure 72. Ray Tracing Screen at High FOT = 25 MHz for SSN = 30 and AI = 5 at 01:00 UTC 2006/12/21. 80
Figure 73. Ray Tracing Screen at Low FOT = 6.8 MHz for SSN = 30 and AI = 5 at 14:00 UTC 2006/12/21. 81
Figure 74. Ray Tracing Screen at High FOT = 38 MHz for SSN = 200 and AI = 5 at 01:00 UTC 2006/12/21. 81
Figure 75. Ray Tracing Screen at Low FOT = 9.5 MHz for SSN = 200 and AI = 5 at 19:00 UTC 2006/12/21. 82
Figure 76. Ray Tracing Screen at High FOT = 22.5 MHz for SSN = 30 and AI = 5 at 08:00 UTC 2007/6/21. 82
Figure 77. Ray Tracing Screen at Low FOT = 12.8 MHz for SSN = 30 and AI = 5 at 18:00 UTC 2007/6/21. 83
Figure 78. Ray Tracing Screen at High FOT = 28 MHz for SSN = 200 and AI = 5 at 08:00 UTC 2007/6/21. 83
Figure 79. Ray Tracing Screen at Low FOT = 20 MHz for SSN = 200 and AI = 5 at 19:00 UTC 2007/6/21. 84
Figure 80. Signal Quality at 6 MHz Frequency for SSN = 30 and AI = 5 at 00:00 UTC 31 July 2007. 90
Figure 81. Signal Quality at 8 MHz Frequency for SSN = 30 and AI = 5 at 00:00 UTC 31 July 2007. 90
Figure 82. Signal Quality at 10 MHz Frequency for SSN = 30 and AI = 5 at 00:00 UTC 31 July 2007. 91

Figure 83. Signal Quality at 12 MHz Frequency for SSN = 30 and AI = 5 at 00:00 UTC 31 July 2007. 91
Figure 84. Signal Quality at 14 MHz Frequency for SSN = 30 and AI = 5 at 00:00 UTC 31 July 2007. 92
Figure 85. Signal Quality at 16 MHz Frequency for SSN = 30 and AI = 5 at 00:00 UTC 31 July 2007. 92
Figure 86. Signal Quality at 18 MHz Frequency for SSN = 30 and AI = 5 at 00:00 UTC 31 July 2007. 93
Figure 87. Signal Quality at High FOT = 25 MHz for SSN = 30 and AI = 5 at 01:00 UTC 2006/12/21. 94
Figure 88. Signal Quality at Low FOT = 6.8 MHz for SSN = 30 and AI = 5 at 14:00 UTC 2006/12/21. 94
Figure 89. Signal Quality at High FOT = 38 MHz for SSN = 200 and AI = 5 at 01:00 UTC 2006/12/21. 95
Figure 90. Signal Quality at Low FOT = 9.5 MHz for SSN = 200 and AI = 5 at 19:00 UTC 2006/12/21. 95
Figure 91. Signal Quality at High FOT = 22.5 MHz for SSN = 30 and AI = 5 at 08:00 UTC 2007/6/21. 96
Figure 92. Signal Quality at Low FOT = 12.8 MHz for SSN = 30 and AI = 5 at 18:00 UTC 2007/6/21. 96
Figure 93. Signal Quality at High FOT = 28 MHz for SSN = 200 and AI = 5 at 08:00 UTC 2007/6/21. 97
Figure 94. Signal Quality at Low FOT = 20 MHz for SSN = 200 and AI = 5 at 19:00 UTC 2007/6/21. 97

LIST OF TABLES

Table 1. Chinese Skywave OTH-B Radar System Specifications (After [23]).....22
Table 2. Basic Characteristics of Ukraine Transportable OTH-SW Radar System.....34
Table 3. Basic Characteristics of Ukraine Shipboard OTH-SW and Transportable SkW-OTH Radar System.....35
Table 4. Basic Characteristics of Best Known OTHR.....43
Table 5. Basic Characteristics of Best Known OTHR (Cont'd).....43
Table 6. Basic Characteristics of Best Known OTHR (Cont'd).....44
Table 7. Basic Characteristics of Best Known OTHR (Cont'd).....44
Table 8. Minimum Required Input SNR at 3,500 km Footprint Range.....51
Table 9. Numerical Value of Range and Signal Quality at 6, 8, 10, 12, and 14 MHz with Elevation Angles of 0 to 20 Degrees for SSN = 30 and AI = 5 at 00:00 UTC 2007/7/31.....72
Table 10. Numerical Value of Range and Signal Quality at 16, 18, 20, and 22 MHz with Elevation Angles of 0 to 20 Degrees for SSN = 30 and AI = 5 at 00:00 UTC 2007/7/31.....73
Table 11. Data with Elevation Angles from 0 to 10 Degrees at 16 MHz Frequency for SSN = 30 and AI = 5 at 00:00 UTC 2007/7/31.....73
Table 12. Data with Elevation Angles from 12 to 20 Degrees at 16 MHz Frequency for SSN = 30 and AI = 5 at 00:00 UTC 2007/7/31.....74

THIS PAGE INTENTIONALLY LEFT BLANK

ACKNOWLEDGMENTS

I would like to thank the Headquarters of Navy and Ministry of National Defense (MND) Taiwan R.O.C. for providing me this outstanding opportunity to accomplish postgraduate study and a master's degree here at the Naval Postgraduate School.

I would like to give my appreciation to Professor Phillip E. Pace and Professor Jeffrey B. Knorr for their valuable contributions, experienced guidance and great efforts and also mush thanks to the Missile Defense Agency for their support.

Furthermore, I would like to thank my mother, Tsui-Hua Lin, who devoted herself for our family and brought up my sister and me by herself. I would not have completed this work without her encouragement and her time taking care of my baby, James Hsu.

Lastly, I would like to give my thanks to my beloved husband, Chih-Yung Hsu, for his company which helped me has a good time during my studying and researching. Thanks to all my families for their endless love, support, encouragement, and understanding in completing my Master's Degree and this thesis.

THIS PAGE INTENTIONALLY LEFT BLANK

I. INTRODUCTION

A. OVER-THE-HORIZON RADAR SYSTEMS

Over-the-horizon radar (OTHR), which works in the high-frequency (HF) band, performs wide area surveillance by reflecting the radio wave off of the ionosphere. A significant problem is the phenomenon of multi-path propagation, which arises from the presence of many layers of relatively high electron density in the ionosphere [1]. Besides defense-related and ocean surface monitoring applications, OTHR is also currently being used to detect and localize aircraft suspected of carrying illegal drugs [2].

1. The Beginning of OTHR

Starting in the 1950s, a number of HF emitters, operating between 3 and 30 MHz, were developed to greatly extend the detection ranges by bouncing the signal off of the ionosphere. These are sometimes known as skywave radar systems. The maximum detection range of a skywave radar system is not limited by the curvature of the Earth and the systems can see beyond a direct line of sight. Therefore, HF radars which can detect targets completely obscured by the horizon are of great interest [3].

The OTHR propagation is classified into two categories: surface wave and skywave propagation. Surface wave systems were considered first and operated in the early 1950s with effective skywave systems coming along a little later. The OTHR transmitter emits radio waves which are reflected by the target and detected by a receiver. The receiver is usually separated several hundred kilometers from the transmitter. Surface wave radar also operates in the HF band and makes use of electromagnetic coupling of the HF waves to the sea surface [4]. This coupling provides a means to detect targets over the horizon beyond the line-of-sight limit experienced by conventional microwave radar systems. Surface wave systems usually have a surveillance range no more than 400 km. Therefore, they are mostly used for local area defense against low-flying missiles and also for some monitoring of ship traffic. Although the detection ranges only look over the

immediate horizon, surface wave radars with relatively inexpensive cost are widely used for collecting good quality wave, current and tidal information over a restricted area of ocean.

Skywave radar operating in the HF band presents a means to survey large areas of land and sea for air and maritime targets such as air targets, ballistic missiles during launch phase, and some types of surface targets [4]. They also have remote sensing capabilities, especially storm tracking and ocean wave monitoring. These radars are large, powerful, expensive, and require sophisticated frequency management systems in order to operate via the ever-changing ionosphere [2].

The significant difference between the skywave and surface wave radars is that the skywave radars have large detection ranges (up to 1000-4000 km) which results in the ability to see a considerable distance beyond the horizon. The reason for the extended detection range for the skywave propagation is that the losses caused by the collision and absorption of the D-layer are much less than the surface wave propagation loss. The surface wave propagates mostly around 10 to 400 km due to higher attenuation. Surface wave propagation equipment is always chosen to be vertical polarized to avoid the higher attenuation associated with horizontal propagation.

2. Problems of the OTHR System

It is difficult to find a sufficiently wide bandwidth to clearly distinguish between the interference and the radar return signals. Dynamic range is also a problem for surface wave radar since it is hard to detect a small target at a long range against the sea clutter background. In order to retain the linearity, dynamic range and wideband requirements needed for the OTHR system, good quality propagation technology in the HF band is important [2].

Besides the propagation difficulties, there are other problems encountered when operating both surface wave and skywave HF radars. First, there are problems associated with licensing issues and getting the frequency allocations clear of other radar signals that are wide enough to give good range resolution. In addition, there are often position

difficulties. It can be difficult to find a sufficiently large area to place the radar that meets the requirements of being radio-quiet at the receiving end as well as presenting no environmental problems at the transmitter location. Both surface wave and skywave radars experience ionospheric clutter (unwanted backscatter from the moving ionosphere) and meteor clutter, which can sometimes hide the presence of the desired target echoes [2]. Skywave radars can also suffer significant polarization losses and focusing/defocusing problems due to ionospheric effects. Military HF radars are susceptible to deliberate jamming; however, they fulfill their early warning role to some extent if they can identify the presence and provide protection against any electronic warfare measures.

Another significant problem in OTHR is robust high-resolution Doppler processing of accelerating or decelerating targets. The ionosphere often modulates the return signals and spreads the Doppler, which makes it difficult to detect targets. This Doppler effect arises during aircraft and ship target maneuvers and during observations of rockets in boost phase and mid-course phase flight. Most OTHR systems use classical Doppler processing, where one Doppler spectrum is computed using one full coherent integration time (CIT). Typically, the CIT is on the order of 1-100 seconds in OTHR systems. Some systems use overlapped Doppler processing to provide a spectrogram analysis of time-varying Doppler [6]. Today, more than ever, the prediction of OTHR performance is important especially for naval systems that are trying to avoid being detected at a long-range distance.

B. PRINCIPAL CONTRIBUTIONS

The first step in this thesis involved an investigation of the ionosphere effects on OTHR systems. This was followed by a literature search of currently fielded OTHR systems including their history and some characteristics. The data collection and relative graphs of the best known OTHR systems used around the world were also carried out. Characteristics such as waveforms, target detection techniques, and the skywave radar equation were investigated. The available HF propagation simulation tools were

evaluated for their feasibility in modeling the OTHR systems. Some mathematical HF propagation models, VOCAP, PROPLAB, SWIM and an ionospheric model, IRI-2001, were investigated. The PROPLAB model was chosen for the ray tracing simulation and footprint prediction capability [7]. Simulations run in PROPLAB model focused on the Chinese OTHR system using a general location. Results include ray tracing through the ionosphere, calculation of the maximum usable frequency (MUF), and footprint prediction. Also, radar equation analysis was done in MATLAB to study the signal-to-noise ratio (SNR) requirements.

C. THESIS OUTLINE

Chapter II describes the ionosphere structure and the effects on the OTHR systems. Chapter III discusses the current OTHR systems in use, including a characteristics summary of best known OTHR systems used in Australia, Canada, China, France, Italy, Japan, Ukraine, United Kingdom, the Russian Federation, and the United States. In Chapter IV, the characteristics of OTHR systems such as waveforms, target detection technique and radar equations are applied. Chapter V uses PROPLAB model simulation to bring in the principle of raytracing and footprint prediction techniques of the Chinese OTHR system. In Chapter VI, the conclusions and suggestions for further studies are discussed. Figure 1 illustrates the flow concept of this thesis as described above.

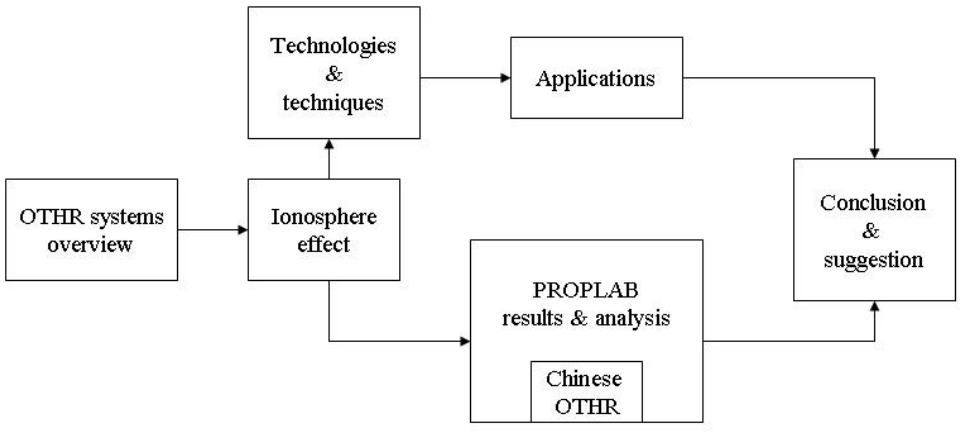

Figure 1. Thesis Flow Concept.

II. IONOSPHERE EFFECTS ON OTHR SYSTEM

The ionosphere has a major effect for HF wave propagation and the factors vary with seasons, months, days, hours, and even minutes. The basic structure of the atmosphere, especially the ionosphere, including D, E, F, F1, and F2-layers are discussed in this section. The concept of how skywave transmission propagates through the ionosphere is also described.

A. IONOSPHERE STRUCTURE

The structure of the neutral atmosphere and the ionosphere containing ionized gas is shown in Figure 2 below [8]. The left side (neutral gas) of the figure shows the altitude (in units of kilometers) as a function of temperature (in units of °K). The layer right

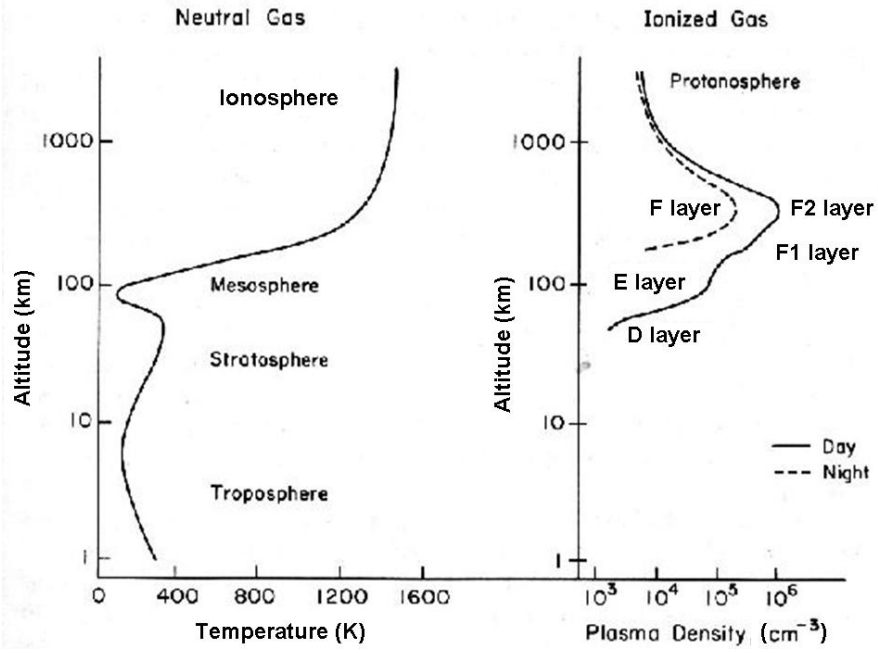

Figure 2. Structure of the Atmosphere and the Ionosphere (After [8]).

above the Earth's surface up to 10 km is troposphere and all weather phenomena occur here. The layer above the troposphere is stratosphere and the air flow is horizontal. Long-

distance (usually across countries) passenger plane traffic uses this layer. The layer above the stratosphere is mesosphere where temperature decreases when altitude increases. The layer above the mesosphere is the ionosphere. The right side (ionized gas) of Figure 2 shows the altitude (km) as a function of plasma density (in units of cm^{-3}). It also shows the layers structure in both daytime (solid line) and night time (dashed line). The plasma is typically the ionized gas and the plasma density actually refers to electron density.

The ionosphere is the region at heights of above 80 km and is also the most outlying area from the center of the Earth [8]. The ionosphere consists of ionized atoms. It directly absorbs the radiation from the Sun and causes the aurora to take place. It makes long-distance propagation possible by reflecting the radio waves off of the ionosphere. The ionospheric medium typically supports reflection of these radio waves at the height between 90 and 350 km above the Earth's surface [6]. The free electron density, an indicator of the degree of ionization, is used to measure the structure of the ionosphere. There are D, E, F1 and F2 -layers in daytime. There is always F-layer at night, sometimes E-layer is distinguished as well.

The wave which propagates through the troposphere is called a surface wave or ground wave. The radio wave refracted from the ionosphere is called a skywave. The D-layer below the ionosphere is between the height of 48 and 80 km above the Earth's surface. This layer only exists in daytime and its absorption usually causes the shorter propagation distance for the radio waves. The distribution of layers in the ionosphere, except the D-layer, is shown in Figure 3. The E-layer exists between 88 and 145 km above the Earth's surface. The maximum electron density in this layer is 1.5×10^5 electrons/cm^3 at the height of about 110 km. The E-layer can refract the HF radio wave inducing propagation distance up to 2,000 km in the daytime. The F-layer splits into the F1 and F2-layers in the daytime and remains only F-layer at night. The F-layer exists between 271 and 321 km. The F1-layer usually exists between 160 and 240 km and sometimes the electron density in this layer is not great enough to distinguish it as a separate layer. The F2-layer exists between 257 and 402 km and most HF radar signal is refracted from this layer to maximize the propagation range [5]. Usually, the nominal

height of layers peak is 90 km for D-layer, 110 km for E-layer, 200 km for F1-layer, and 300 km for F2-layer [8]. Figure 4 illustrates how a skywave is refracted from the ionosphere and propagates over the Earth.

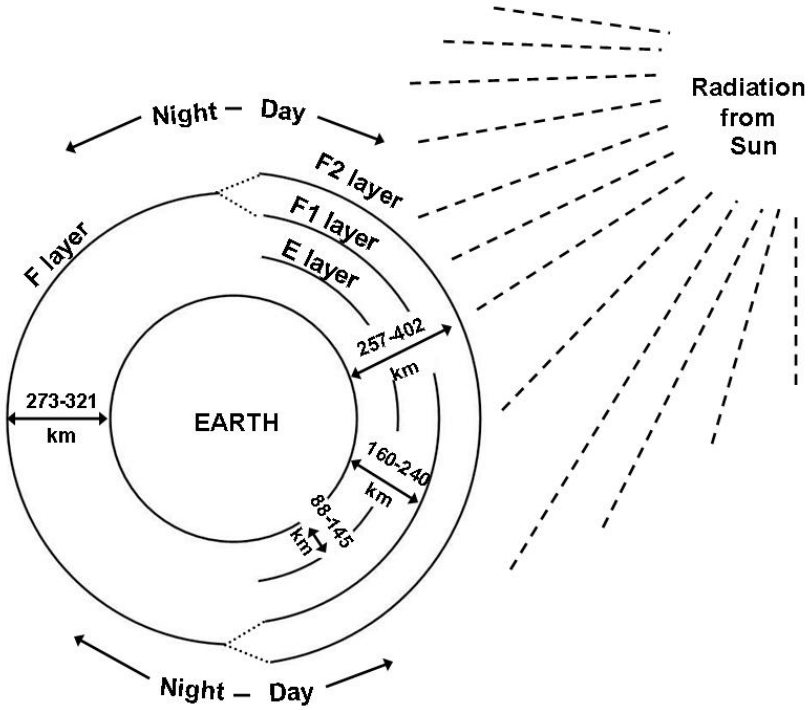

Figure 3. Distribution of Layers in the Ionosphere (After [5]).

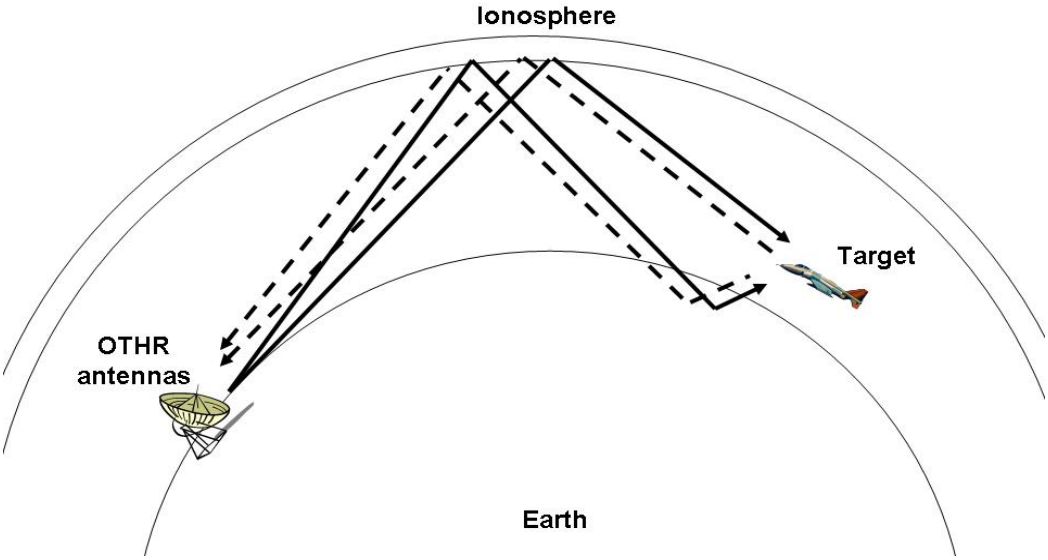

Figure 4. Skywave Propagation Concept of the OTHR System (After [6]).

B. IONOSPHERIC MODEL

The International Reference Ionosphere (IRI) is a joint project of the Committee of Space Research (COSPAR) and the International Union of Radio Science (URSI) [9]. An ionospheric model, IRI-2001 model is investigated by IRI and named after it. The input data for the IRI model, includes the time (universal or local time), date and year, the latitude and longitude of the desired location, the profile type (height, latitude, longitude, year, month, day of month, day of year and hour profile), and the parameters of the profile itself. The optional input includes the sunspot number (SSN) and ionosphere index (IG) [10]. The graphical user input of IRI model is demonstrated in Figure 5.

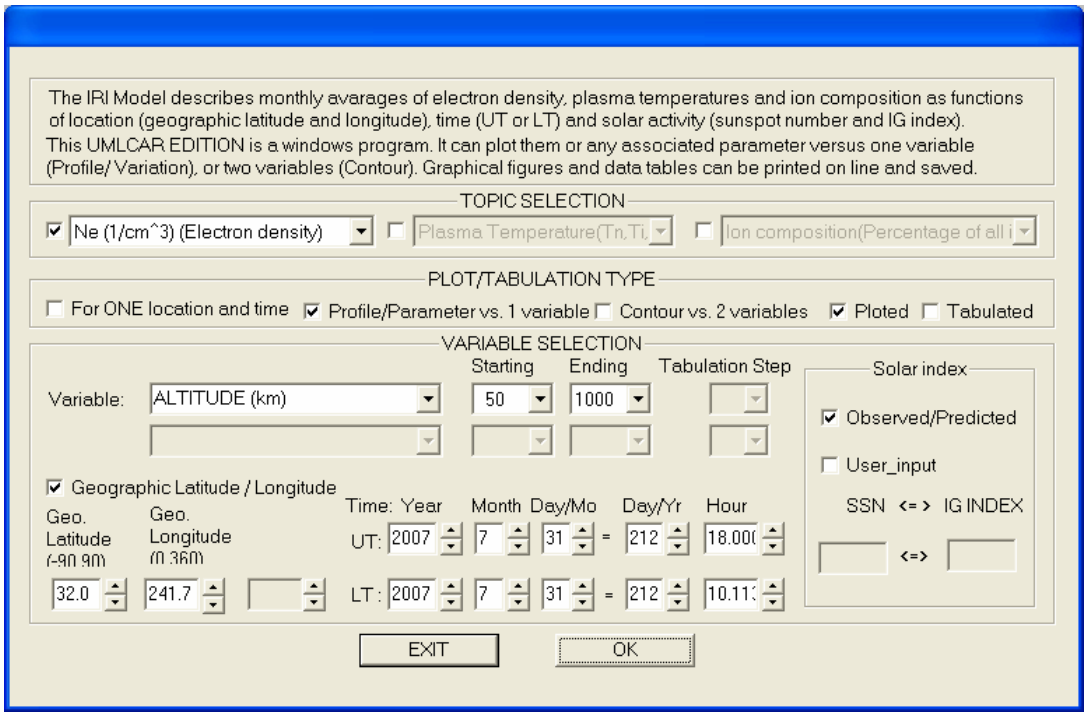

Figure 5. Graphical User Input Panel.

Figures 6 through 9, produced by the IRI model, illustrate diagrams of the electron density profile versus altitude at Nanjing, China for daytime and night time in the winter and summer respectively. The location, Nanjing, is a general location used for the Chinese OTHR system at coordinates of 32.05°N and 118.3°E shown on the left

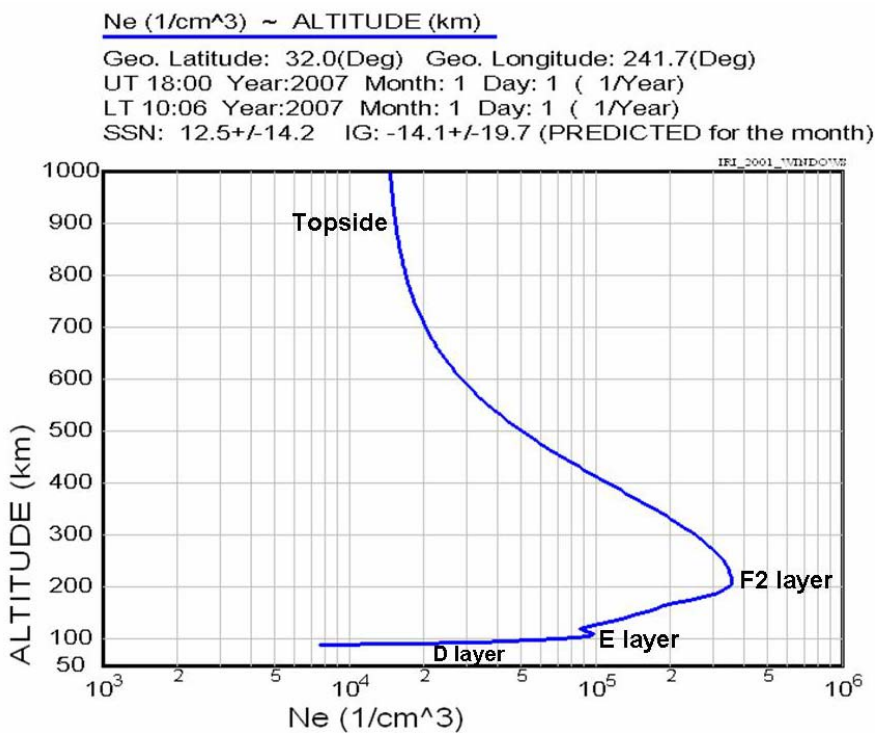

Figure 6. Electron Density in Winter Day (January 2007).

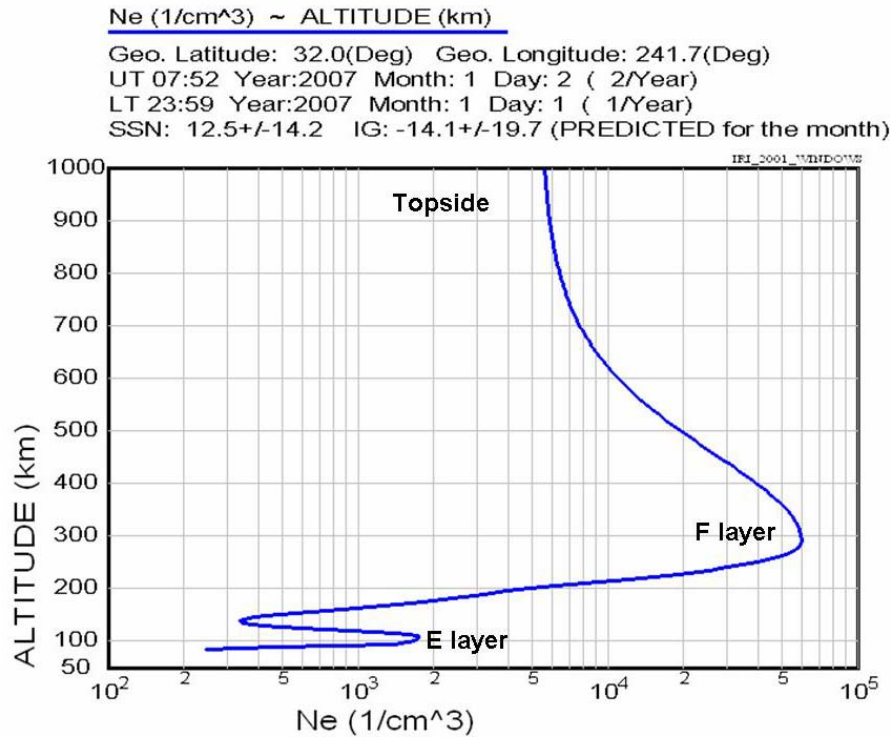

Figure 7. Electron Density in Winter Night (January 2007).

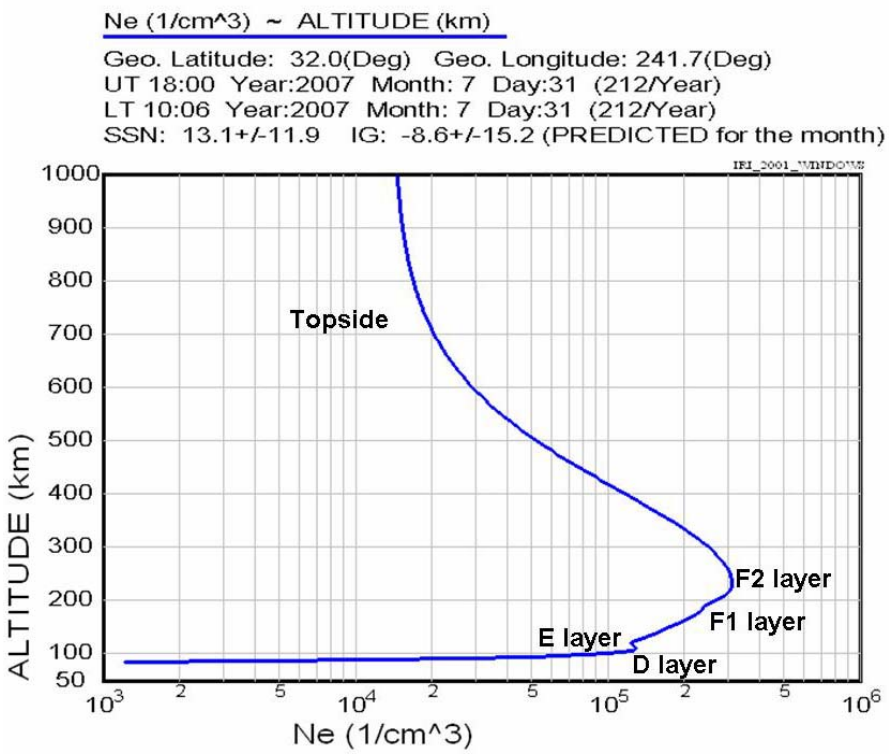

Figure 8. Electron Density in Summer Day (July 2007).

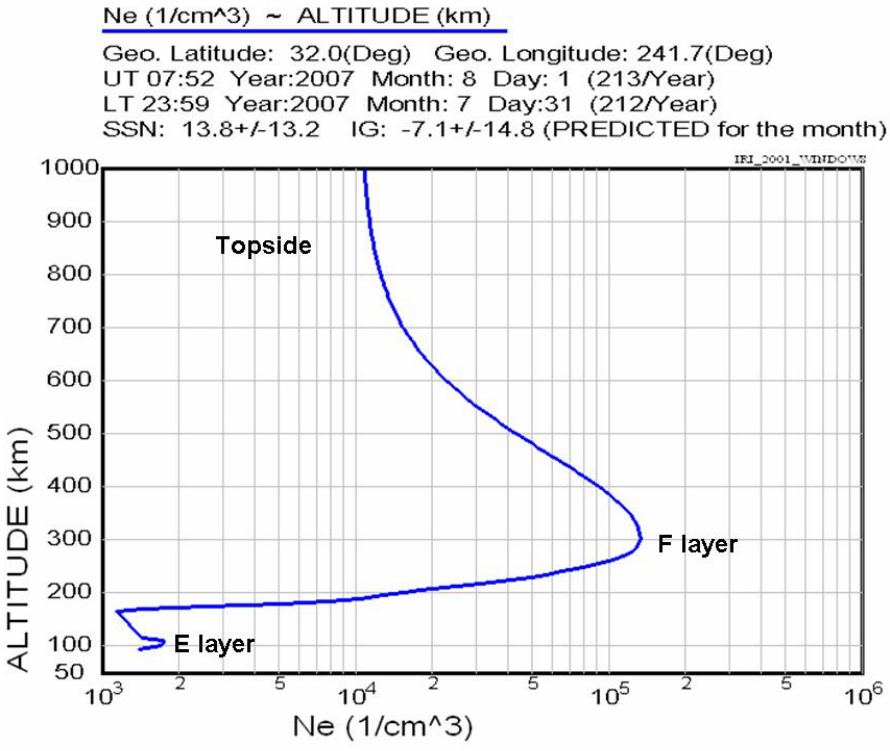

Figure 9. Electron Density in Summer Night (July 2007).

bottom part of the panel in the figures as 32.0° N and 241.7° W. In Figure 6 and 7, the time was set to be 1000 and 2400 (Local Time) in January and the same time set in July in Figure 8 and 9. Both months are in the year of 2007. In these four figures, the value along the abscissa (from left to right) represents the electron density for each altitude. The scale begins at 10^3 electrons/cm^3 and increases up to10^6 electrons/cm^3. The electron density is generated by semi-log calculation method. The numbers along the ordinate of the figure correspond to the altitude above the ground in units of kilometers. The first three lines on the top of the graph represent the information of the geographic coordinates, time, day, and month. The forth line shows the optional inputs, SSN and IG index, which is generated by the model itself unless input by the user. In day time (Figure 6 and 8), the D, E and F2-layers are easily defined, but the F1-layer is not well defined. In night time (Figure 7 and 9), both E and F-layer are well defined. Detailed description of electron density profile can be found in [11].

Modeling the ionosphere gives the electron density and analytical solutions for ray path parameters and is useful for HF propagation studies and OTHR system planning. Equation (1) and (2) expressed below are the methods to calculate the electron density N_e and refraction index μ of the ionosphere [12-14].

$$N_e = N_m \left\{ 1 - \left(\frac{r - r_m}{y_m} \right)^2 \left(\frac{r_b}{r} \right)^2 \right\}$$

$$\text{for } r_b \le r \le \frac{r_m r_b}{r_b - y_m} \tag{1}$$

and

$$\mu = \left(1 - \frac{81 N_e}{f^2} \right)^{1/2} \tag{2}$$

where r is the radial distance from the Earth center (height + Earth's radius), r_m is the radial distance from the Earth center where the maximum electron density N_m is, r_b is the radial distance from the Earth center to the base of the designated layer, y_m is the

semithickness of the designated layer, N_e is the electron density at a desired height from the Earth center, f is the wave frequency in Hz. The parameters are illustrated in Figure 10.

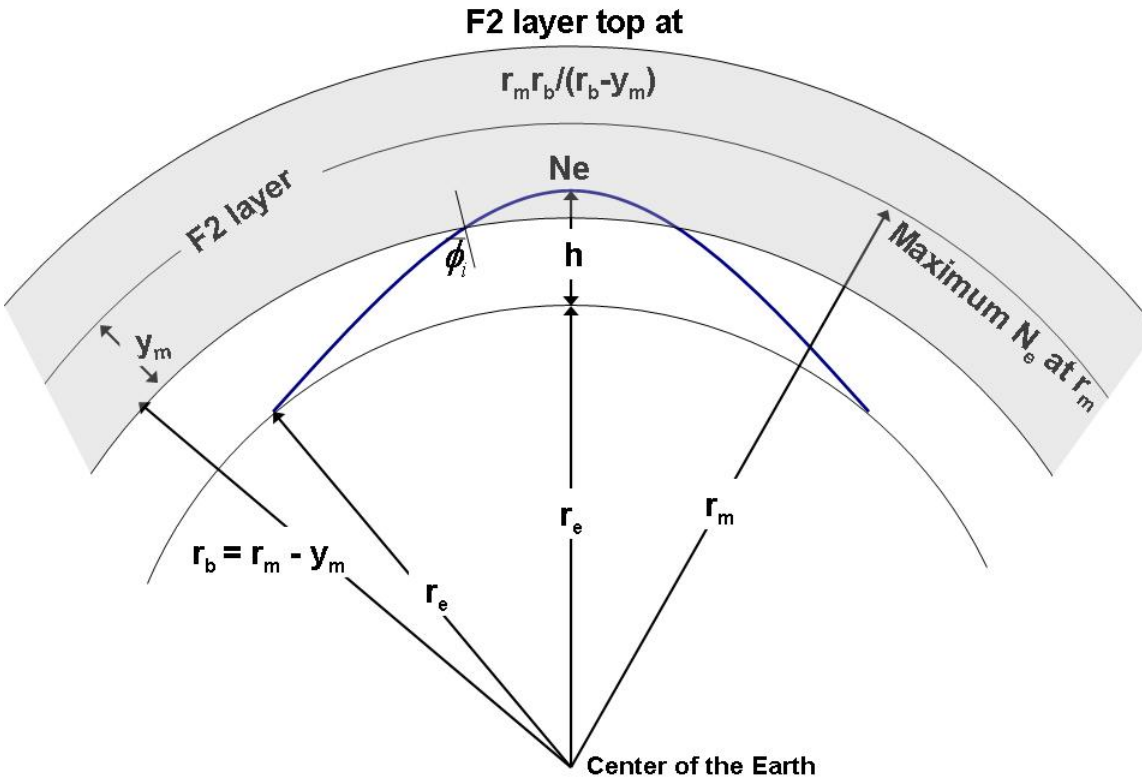

Figure 10. Ray Path Geometry (From [14]).

The Earth's radius is 6378.1 km. For example, in Figure 8, the electron density profile for the summer daytime, the maximum electron density N_m of the F2-layer is at the height of r_m = 6618.1 km (240+6378.1), with a value of 3×10^5 electrons/cm^3. The F2-layer semithickness y_m is 50 km or 0.5(300-200), and the base height of the F2-layer $r_b = r_m - y_m$ or $r_b = 6568.1$ km which means the base height of the F2-layer is 190 km above the Earth's surface and this corresponds to the graph shown in Figure 8. For example, at a desired height of 200 km above the Earth's surface, the electron density is calculated from (1) and (2) as 2.99839×10^5 electrons/cm^3. Based on (2), the refractive

index μ is function of electron density N_e and operating frequency f. The term $9\sqrt{N_e}$ is the critical frequency f_c or $f_c = 9\sqrt{N_e}$. A negative refractive index occurs when $f < f_c$ and this results in a ray at normal incidence being reflected from the ionosphere to return to the Earth. It can be shown that the maximum usable frequency (MUF) for a skywave path is given by

$$f_{MUF} = f_c \sec \phi_i \tag{3}$$

where $f_c = \sqrt{81 N_{\max}}$ and ϕ_i is the incidence angle.

Thus, at normal incidence ($\phi_i = 0°$), a wave will penetrate the ionosphere if $f > f_c$. At the maximum one hop distance, around 4,000 km and $\phi_i \approx 72°$, a wave will penetrate the ionosphere if $f \geq 3.6 f_c$. Therefore, higher frequencies can be used on longer paths.

THIS PAGE INTENTIONALLY LEFT BLANK

III. CURRENT OTHR SYSTEMS IN USE

In order to see a target without being limited by the curvature of the Earth, OTHR systems have been developed since World War II. The main idea of the design is to secure the national defense with a wide area detection and early warning surveillance. In addition, these radar systems can detect cruise missiles within the launch phase, flying targets, and surface ships far beyond the horizon. In order to defend against cruise missiles being launched by adversaries, several countries such as Australia, Canada, China, France, Italy, Japan, Ukraine, United Kingdom, the Russian Federation, and the United States are still working on developing and upgrading the OTHR systems. Some of these systems are described in this section. Most of the information was obtained from the Jane's database.

A. AUSTRALIA

1. Geographically Strategic Location

Australia is a landmass of under 7.7 million square kilometers with coastline of approximately 37,000 kilometers [15]. One of the several methods to protect its territory against potential hostile interests is to maximize the surveillance and reconnaissance capabilities. The Australian radar industry has been increasing its capability over the past 30 years and both the research and development in OTHR systems was carried out in order to monitor vast areas more efficiently and economically.

2. Jindalee Operational Radar Network (JORN)

Jindalee was the first project taken up in the 1960s and it is the original word for "bare bone". Jindalee is a bistatic OTHR system and is controlled from the Jindalee Facility at Alice Spring (JFAS) in central Australia, where two separate transmitter and receiver systems are located. The main OTHR transmitter is located at Harts Range and the receiver is located at Mount Everard. The other system is an ionospheric sounder known as the frequency management system (FMS). On 2 April 2003, Jindalee was

joined with two other OTHR systems and formed what is now known as Jindalee Operational Radar Network (JORN). One site is near Laverton, in Western Australia, and the other is at Longreach, Queensland, in eastern Australia as illustrated in Figure 11. The combination of these three systems, JORN, can detect all sea and air Doppler moving targets in the area between 1,000 and 3,000 km north of the radar sites. It is also the key component of the sea-air gap surveillance system in Australia by ensuring a surveillance area with an arc of almost 180° wide and out to 2,000 km from the Australian coastline [16]. The detailed characteristics of Jindalee and JORN can be found in [15]. Figures 12 and 13 show the transmission antenna array of JORN near Longreach, in Queensland. Figure 14 demonstrates an interior view of the JORN Co-ordination center at RAAF Edinburgh, South Australia.

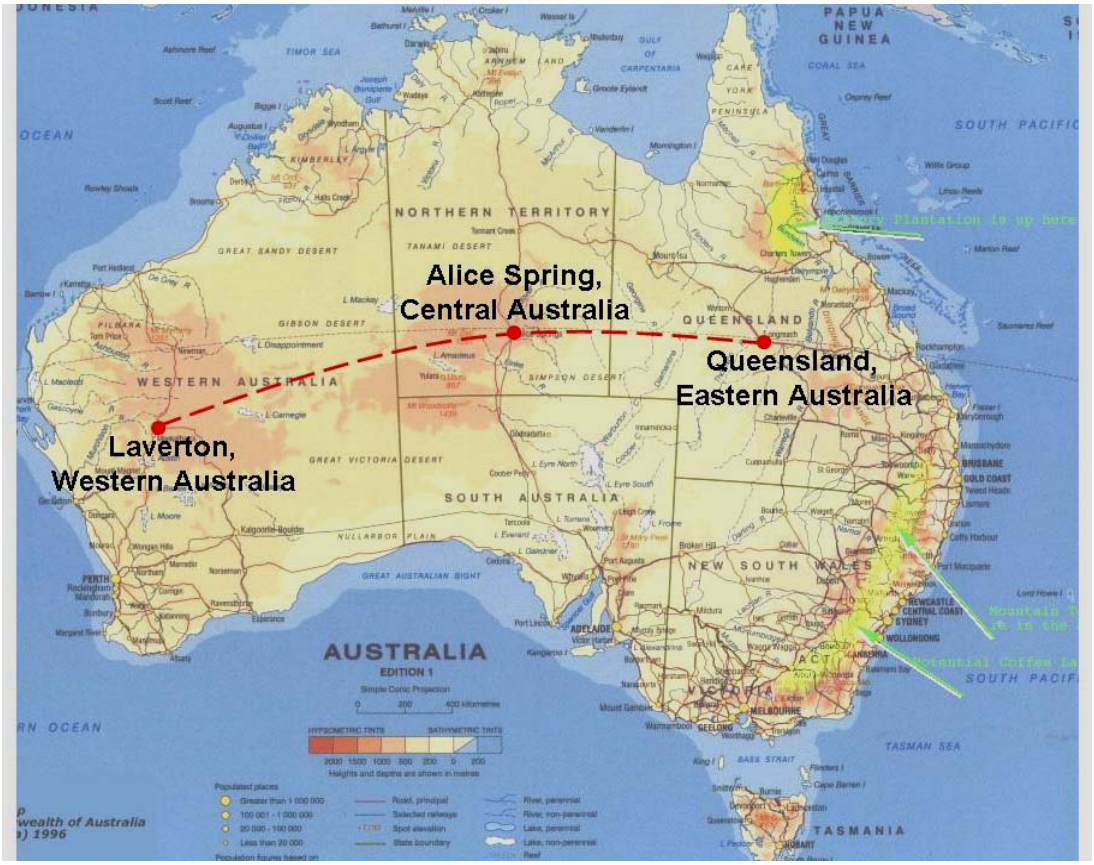

Figure 11. Geographic Location of JORN.

Figure 12. The JORN Transmission Antenna Array (From [15]).

Figure 13. A Close View of the Antenna Array (From [16]).

Figure 14. An Interior View of the JORN Coordination Center (From [16]).

B. CANADA

1. Geographically Strategic Location and Defense Innovation

Comparing to other countries, Canada has one of the longest coastlines of the world. Along the coastline, there are enormous challenges for surveillance against illegal imports, immigration and threats to its fish stocks and national security. A Canadian fleet of Aurora Aircraft can be used for airborne surveillance, but it is too expensive to maintain a persistent surveillance capability. The operating cost of the Aurora is reported to be significant, therefore, a team of Defence Research and Development Canada (DRDC) scientists led by Dr. Hing Chan and Harold Wilson have been working on a project at Shirleys Bay to reduce the cost and improve the effectiveness in monitoring maritime traffic along the coastline [17].

In order to overcome the line-of-sight problem in motoring offshore maritime traffic using conventional ground-based radar, the DRDC uses HF surface wave to make the radar signal follow the curvature of the Earth. The coastal surveillance HF radars can continuously monitor approximately 320 km Economical Exclusion Zone (EEZ) from the

shore [17]. Canada is now developing a cost-effective wide-area coastal surveillance radar network based on the technique of detecting beyond the line of sight and the new surveillance radar network will soon operate for use in maritime defense.

2. SWR Series High-Frequency Surface Wave Radar (HFSWR)

The radar developed by DRDC is known as a Surface Wave Radar (SWR), also known as coastal surveillance radar. Surface vessels and low-altitude aircraft below the radar horizon can now be detected by the method of using shore-based radar, like the SWR, shown in Figure 15. SWR uses the HF band with 3.5 to 10 MHz sub-band to propagate over the visual horizon. High-Frequency Surface Wave Radars (HFSWRs) are developed by the Raytheon Company and were identified as SWR-503 and SWR-610 in July 2002. The SWR series HFSWRs are shore-based systems that are designed to detect and track ships, aircraft and ice formations out to ranges of 400 km and beyond. The SWR-503 operates at a frequency of 3.5 to 5.5 MHz and is optimized for long range surveillance of targets out to an instrumented range of 407 km. The SWR-610 which operates at a higher frequency of 6 to 10 MHz is designed for medium range (instrumented range of 333 km) enhanced detection and tracking capability for smaller targets compared to SWR-503 [18].

Figure 15. Shore-based SWR System (From [18]).

C. CHINA

1. An Overview of Chinese Radar Development

Since 1950s, China has been working on the development of their radar industry. Meter wavelength surveillance radar systems were first designed and then coastal surveillance microwave radar systems. Both types of systems were largely produced in the late 1950s. A technique of linear frequency modulated (FM) pulse expansion and compression was also used in the late 1950s. Continuous wave (CW) radar development was carried out during the 1960s and performed the role of tracking and detection. From the late 1960s to 1970s, many research and development programs such as moving target indicator, monopulse, pulse, compression, and electronic scanning antenna were investigated and carried out [19]. In November 1967, China began to develop HF ground wave (surface wave) OTH sensors. The first surface wave radar was designed to detect targets at 250 km [20].

China is enhancing its battlefield surveillance capability and its marine coverage in order to have stronger armed forces against potential intruders and hostile countries. For this reason, Taiwan Strait has become a very essential part in extending China's marine area. Although Taiwan is not a potential threatening country for China, it still plays an important role on the strategic intention of China.

2. Over-the-Horizon Backscatter (OTH-B) Radar

China is improving its intelligence, surveillance, and reconnaissance (ISR) capabilities to detect, monitor and target naval activities in the Western Pacific Ocean and of course the Taiwan Strait. According to the report in [20], China may have as many as three OTH skywave radar systems used in an early warning capacity and also may have deployed at least one surface wave OTHR. In order to extend the national defense surveillance and make the early warning system more effective, China has more skywave OTHR than surface wave OTHR systems without regard to the high budget. The Chinese OTH backscatter (OTH-B) radar is to provide surveillance of the South China Sea. The precise location of this facility has not been released. It was stated that a full-scale

development program into an OTH-B radar system was being carried out in China during November 1986 [21]. A ground-based OTHR named Type-110 is shown in Figure 16. In Figure 17, an operational drill is being conducted for processing the received signal data from the targets in the East China Sea Fleet OTH-B radar station.

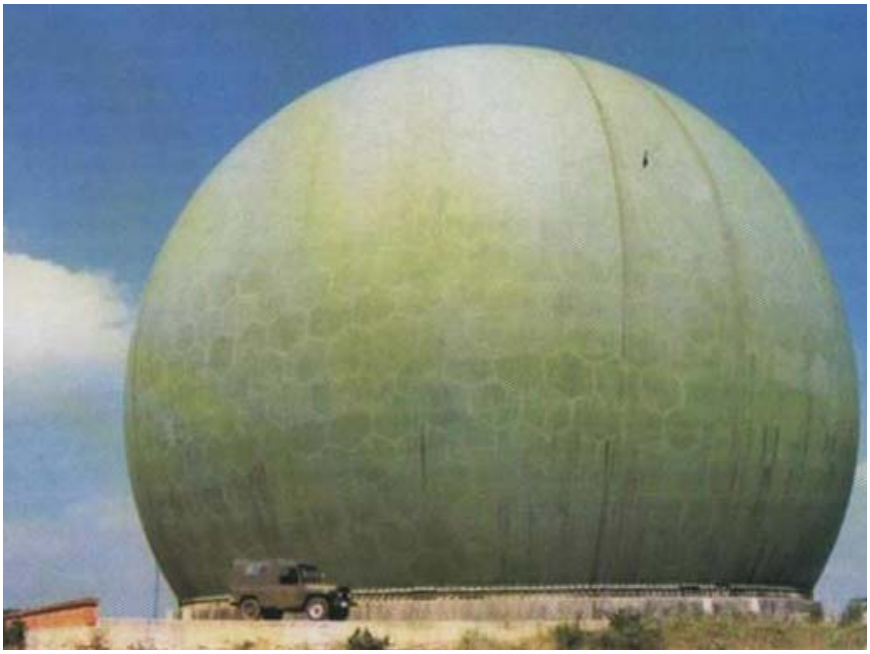

Figure 16. Chinese Type-110 OTHR (From [22]).

Figure 17. OTH-B Radar in the East China Sea Fleet (From [22]).

Operating Frequency	HF (6-22 MHz)
Output Power	50 dBW (from [2]) 1 MW (from [21]) 200-1200 kW (from [24])
Antennas - Transmitting Array - Receiving Array	 8 dipole elements, vertical polarization Directive gain 18dB (at 14.5 MHz) 32 log-periodic elements, vertical polarization Directive gain 26dB (at 14.5 MHz)
Beamwidth - Transmission Beamwidth - Reception Beamwidth	 7.5º horizontal 5-36º vertical 2.5º horizontal 5-36º vertical
Waveform Selection	FM/CW
Polarization	Vertical
Range	700-3500 km

Table 1. Chinese Skywave OTH-B Radar System Specifications (After [23])

The basic characteristics of the Chinese skywave OTH-B radar systems are shown in Table 1.

3. Surface Wave (ground wave) Over-the-Horizon (OTH) Radar

The surface wave radar is another branch of the HF OTH-B radar and has been researched and developed since 1967. It is designed to detect ships and low attitude aircraft outside the coastline. The maximum detection range of the surface wave radar system is no more than 400 km and it is used for local area defense. It also collects good quality clutter and tidal information [25]. The price for this radar system is relatively low compared to HF OTH-B radar system. Based on the geographical location of China, the potential outside threat weapon would be further away compared to the 400 km distance detected by the surface wave OTH radar. Figure 18 illustrates the transmitter antenna array of the surface wave OTHR system.

Figure 18. The Transmitter Antenna Element of Surface Wave OTHR (From [20])

4. Pulse Doppler Over-the-Horizon Backscatter (PD-OTH-B) Radar

Another branch of China OTH-B radar is Pulse Doppler OTH-B (PD-OTH-B) radar. In order to fulfill the performance of bistatic OTHR, the synchronization is a critical issue to deal with. Based on the Pulse Doppler (PD) technique, the system can successfully solve the synchronization problems of time, phase and spatial processing and handle sophisticated two dimensional (2D) signal processing techniques of ranging and speed measuring. The detection range of a single PD-OTH-B radar is between 700 and 3,500 km with coverage up to six million km^2 in a 60° azimuth sector (which is larger than 1% of the Earth's surface). PD-OTH-B radar can counter low altitude penetrating bombers, have early warning ability against intercontinental ballistic missiles and deployed long range surveillance ships. The resolution of the PD-OTH-B radar to detect aircraft is 2.5° in azimuth, 20-40 km in range and 0.3 Hz in Doppler frequency. The transmitter and receiver sites of the experimental radar are both located in the middle of China. The radar beam points to the north-west region of China. A coherent transponding site is set up at the place 1,486 km away from the receiver location for the calibration, the discrimination of ionosphere mode, and the determination of sub-clutter visibility (SCV) of 55 to 60 dB [25].

D. FRANCE

1. Valensole Skywave HF Radar

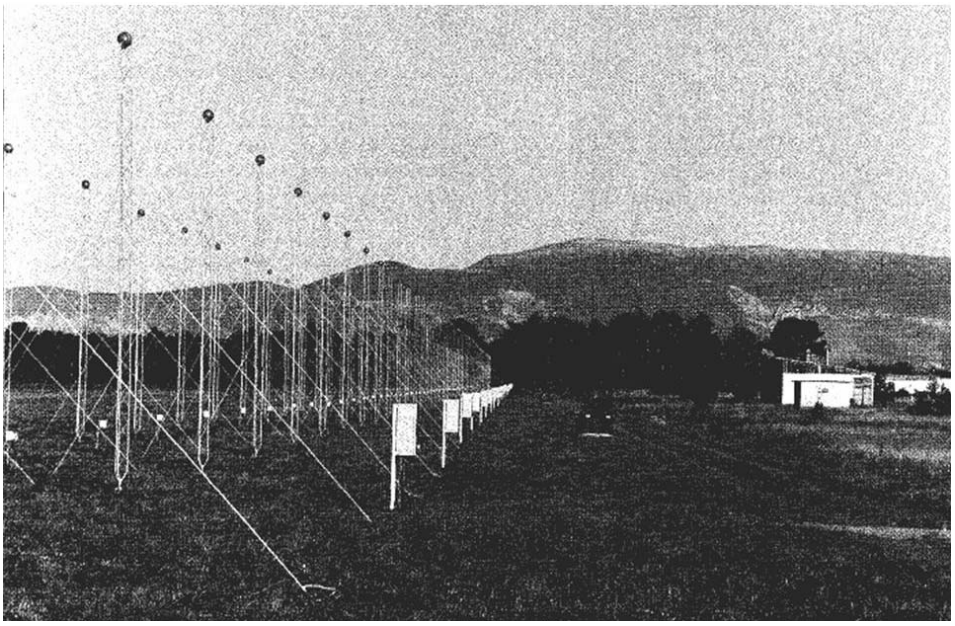

Figure 19. A View of One Receiving Antenna (From [26]).

The Valensole skywave HF radar of the University Pierre et Curie was installed near Valensole in southeastern France (43 ° 48'N, 6 ° 06'E) since 1960 and used for studies in ionosphere research and sea-state remote sensing [26]. This is a monostatic system with 100 kW transmitted peak power and pulse waveform is applied. There are two identical transmitting antennas towards north or west and each antenna consists of 16 wide-band monopole elements. Both transmitting antennas have a main lobe of 7.5 ° wide in azimuth at 15 MHz and antenna beam steered in ± 54 ° sector in 7.5 ° steps. The first receiving array which is 1,100 m long used for westward or eastward propagation and is divided into 23 subarrays. The second receiving used for northward or southward propagation is 550 m long and divided into 11 subarrays. Both the receiving subarrays overlap 50% with each other [M. Six, 1996]. Figure 18 shows the 550 m receiving antenna array with the receiving equipments housed in waterproof box [26].

2. Nostradamus

The French developed OTH radar using the New Transhorizon Decametric System Applying Studio Methods (Nostradamus) during the 1990s and brought this method in service for the French army in 2005 [27]. The Nostradamus OTHR, operates in the HF band (3-30 MHz), is developed by the French ORENA aerospace research establishment and is located close to Dreux, approximately 100 km west of Paris. It consists of 288 emitting and receiving antennas and the antennas are placed in a star pattern with three equally spaced arms as shown in Figures 20 and 21. Based on a star shaped antenna, the Nostradamus OTHR has a detecting range between 800 and 3,000 km. A supercomputer, shown in Figure 22, can coordinate all antennas and the signal can be steered over 360° coverage. Figure 23 illustrates the underground network construction of the Nostradamus OTHR system that uses a database management system. The radar is capable of isolating and tracking multiple targets simultaneously in the area [28].

Figure 20. The Receiving Antennas of Nostradamus OTHR (From [27]).

Figure 21. A Close View of the Receiving Antennas (From [27]).

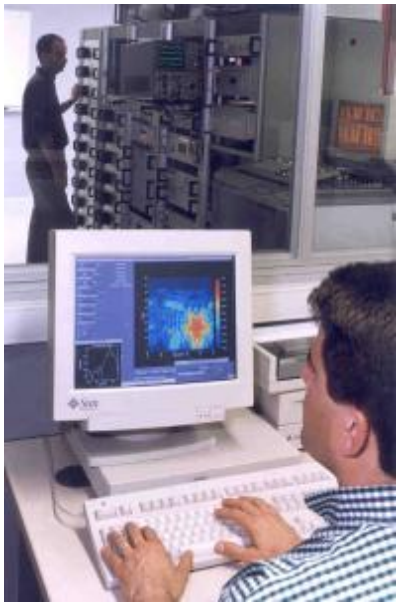

Figure 22. Command Room of Nostradamus OTHR (From [27]).

Figure 23. Underground Network of Nostradamus OTHR System (From [27]).

The French military applied the Nostradamus OTHR in the detection of stealth aircraft and other low observable targets such as cruise missiles with low radar and infrared signature. The Nostradamus OTHR system is relatively inexpensive since it uses commercial off-the-shelf components. The Nostradamus OTHR is the first OTHR system built in France and has at least two distinct advantages. First, it is monostatic and the signal is transmitted and received at the same location. In addition, the star-shaped antenna structure, 360° coverage, and a precise tuning of the elevation of the radar beam provides omnibearing surveillance by collecting the target's ground coordinates including ground range, ground range rate, azimuth angle, and elevation angle. [28] An overview of the geographic location of French skywave HF OTH radars is shown in Figure 24.

Figure 24. Locations of French OTHRs.

E. ITALY (CONDO-R)

The CONDO-R as shown in Figure 25 is a microwave OTH surface surveillance radar system designed to exploit anomalous electromagnetic wave propagation conditions

using atmospheric ducting which extends the propagation distance that would normally be limited to line of sight. CONDO-R provides range performance far beyond the horizon most of the time not only to detect surface ship targets but also low-altitude flying air targets [29]. The system features modern digital processing and automatic control of the beam position inside super-propagation ducts. A variant configured for the coastal surveillance role is designated as the TPS-828, illustrated in Figure 26, which is a mobile coastal radar system capable of covering the needs for long-range surface and OTH surveillance [30]. The CONDO-R is now using I-band (8-10GHz) operating frequency and ready to be upgraded.

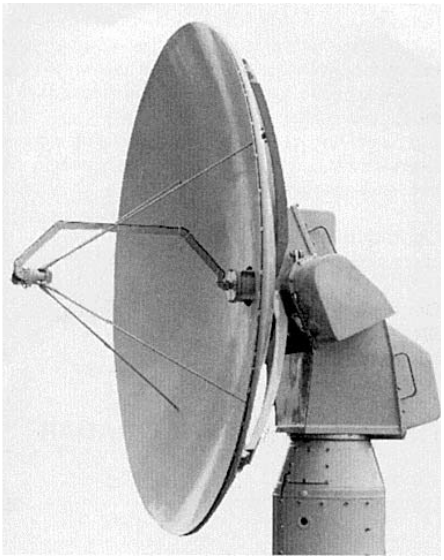

Figure 25. The Antenna Unit of the CONDO-R Naval OTHR (From [29]).

Figure 26. TPS-828 Mobile Coastal Radar System (From [30]).

F. JAPAN

Japan has decided to build an OTHR system primarily as an extension of the United States CONUS-OTH network. It is postulated that the transmitter will be located on Hanajima Island and the receiver with the control center will be located on Iwo Jima Island in order to provide surveillance of the Aleutian Island Chain [31]. The illustration of the transmitter and receiver location is shown in Figure 27 and no further information is available.

Figure 27. Location of OTHR Transmitter and Receiver.

G. THE RUSSIAN FEDERATION

1. IRIDA Over-the-Horizon Surface Wave (OTH-SW) Radar

The Russian OTH-SW radar was developed as a coastal surveillance facility by the NIDAR organization. This is a relocatable HF bistatic system and the transmitter and receiver elements are separated at a distance between 50 and 1,500 km. In order to provide the mobility and flexibility, the system is housed in five standard containers and can be transported by land, sea or air. The system has an operating frequency in HF band

between 7 and 15 MHz, and has a transmitter output peak pulse power of 65 kW and up to 16 kW at average. It can cover $90°$ in azimuth and detect surface targets out to range of about 280-300 km depending on sea conditions and the size of the vessel. It can also monitor low-altitude flying targets at extended range and the aircraft location accuracy is 3-4 km in range and $3-5°$ in bearing [32].

2. Over-the-Horizon Backscatter (OTH-B) Radar

The first development and construction of OTHR system had been reported by former Soviet Union in the late 1950s. The main objective of OTHR development was partially to extend the detection range of conventional early warning radars and partially to overcome the problems with infrared satellites for missile launch detection [33]. The first OTHR functioned in the 1970s using the backscatter principle to detect missile launches by detecting the disturbances in the ionosphere caused by missile exhaust plumes. There were four OTH-B systems deployed for the early warning surveillance. The first one was deployed for experimental purposes at Gomel, Belarus facing towards the United States. A few years later, the second one was added at Komsomolsk-na-Amure in Siberia, also aimed towards the United States. The third one was sited in the early 1980s at Nikolayev near the Black Sea to monitor Chinese missile tests. In the late 1980s, it was reported that a fourth site near Nakhoda, in the coastal region of the Sea of Japan, was under construction to monitor activities of ship, aircraft and ballistic missile movements in the area between the Chinese coast and the island of Guam [33]. A geographic diagram of these systems is shown in Figure 28. These systems were operated between 1976 and 1989 and operated in the frequency band between 4 and 30 MHz with an output power of 20 to 40 MW.

Figure 28. Geographic Location of Four OTH-B Systems in the Russian Federation.

These OTH-B radars in the Russian Federation were nicknamed “Russian Woodpeckers” because they produced continuous clicking sounds with 10 pulses per second. This sound interfered in the entire short wave band. Another nickname given to these systems was “Steel Works” named after their girder-type construction [33]. The antenna elements of the OTH-B radar are shown in Figure 29 and provide net system coverage far beyond the horizon to protect territorial air and space against ballistic missiles. The signal strength transmitted and signal coverage from Belarus (first built radar), Komosomolsk-na-Amure (second built radar), and Nikolayev (third built radar) is illustrated by the green lines in Figure 30. The fourth OTH-B radar was reported under construction and the signal coverage is not shown in Figure 30.

Figure 29. The Antenna Element of OTHR Radar (From [34]).

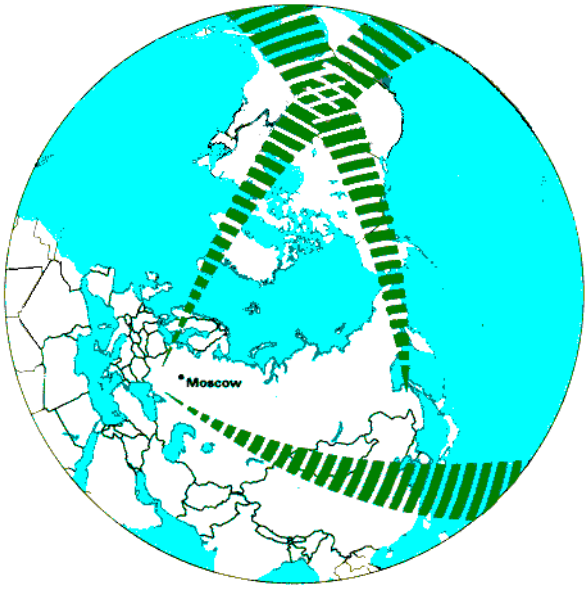

Figure 30. Coverage of Russian OTHR (From [34]).

Today, the OTH-SW and OTH-B radars represented above have come to be used not only for long range coastal surveillance, ballistic missile launch detection, but also for air traffic and current and tide study of the oceans.

H. UKRAINE

1. Transportable Over-the-Horizon Surface Wave (OTH-SW) Radar

Developed by the Ukrainian Radio Technical Institute, the transportable OTH-SW radar operates at frequency of 18 to 25 MHz and it is a removable bistatic set of equipment designed to detect aircraft and ships. The transmitting and receiving antenna array are separated at a distance between 3 and 12 km. According to Jane's sources, there are 200 km and 300 km range variants of the architecture. The operating frequency is 18-25 MHz for the 200 km range configuration and 6-24 MHz for the 300 km range configuration. The 200 km range configurations has a 60° sector coverage. Figure 31 illustrates a general view of part of the transmission array used in the UKRSPETSEXPORT (the Ukraine arms exporter named on Sudanese end use certificates in August 2004) transportable OTH-SW radar [35]. This system can track up to 50 aircraft or 100 surface ships simultaneously and other capabilities are described in Table 2.

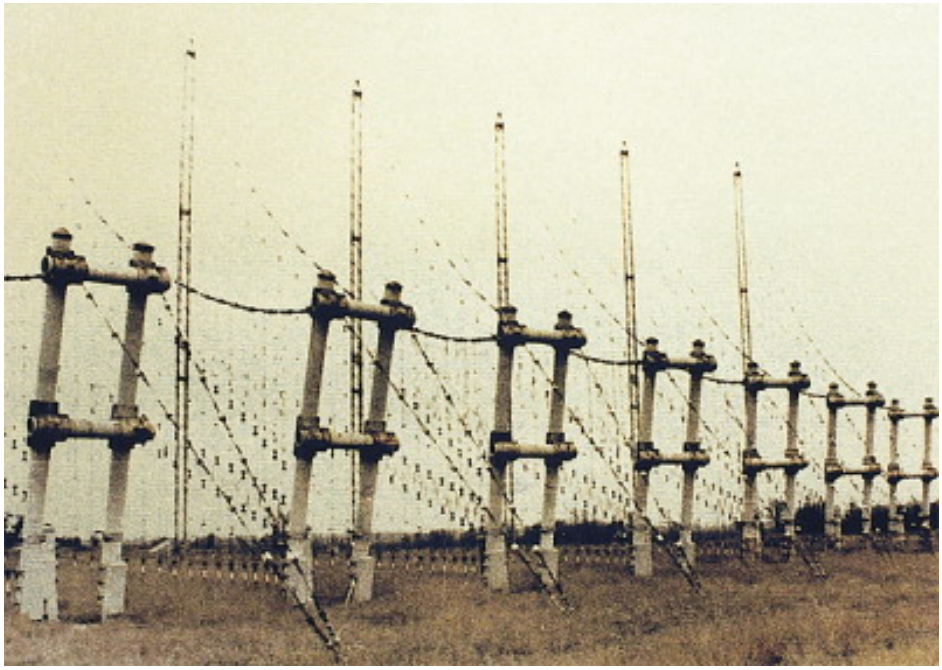

Figure 31. Transmission Array Used in the Transportable OTH-SW Radar (2002) (From [35]).

2. Shipboard Over-the-Horizon Surface Wave (OTH-SW) Radar

The shipboard OTH-SW radar is designed by the Ukrainian Radio Technical Institute to detect and track aircraft targets, anti-ship missiles, and surface targets. It consists of a 60 m vertically polarized receiver array mounted along the sides of the vessel and a two element transmitter array located on the mast of the vessel [36]. Characteristics of this system are shown in Table 4. This shipboard OTH-SW radar system was developed by UKRSPETSEXPORT in 2000 and still plays a role of protecting the territorial waters.

3. Transportable SkyWave Over-the-Horizon (SkW-OTH) Radar

The SkW-OTH radar operates in the 5-28 MHz band and is designed to detect and track air, sea surface and ballistic missile targets. This is a bistatic system and the transmitting and receiving antennas are separated at a distance between 20 and 200 km. The detection range is from 600 to 2,600 km using skywave propagation [37]. Other specifications are shown in Table 3.

Radar Type		Transportable OTH-SW radar	
Operating Frequency		18-25 MHz	6-24 MHz
Receiver element - Antenna array Transmitter element		330 m 64 vibrators 8 vertical log-periodic antennas	640 m 64 vibrators
Detection Coverage		60º arc out to 200 km	60º arc out to 300 km
Detection Range	Aircraft	-	With 1dB/m2 cross section - 60 km (when target height is between 10-100 m) - 120 km (when target height is between 100-100,000 m) - 300 km (when target height is above 100,000 m)
	Ship	-	180 km (with 20dB/m2 cross section) 300 km (with 40dB/m2 cross section)
Detection -to- Tracking Time	Aircraft	-	10-60 sec
	Ship	-	100-300 sec
Target velocity		-	-
Simultaneously Tracking capability		One hundred ships or 50 aircrafts	

Table 2. Basic Characteristics of Ukraine Transportable OTH-SW Radar System.

Radar Type		Shipboard OTH-SW radar	Transportable SkyWave OTH (SkW-OTH) radar
Operating Frequency		15-30 MHz	5-28 MHz - Bistatic system (Tx and Rx antennas are set up at a distance between 20-200 km) - Pt = 180kW (with average Transmitted power of 15 kW at each antenna)
Receiver element - Antenna array Transmitter element		60m	600 m Tx has 12 log-periodic, vertically polarized antenna elements
Detection Coverage		45º arc out to 170 km	60º arc out to 2,000 km
Detection Range	Aircraft	With 1dB/m2 cross section - 80 km (when target height is between 10-100 m) - 130 km (when target height is above 100 m)	For both air targets between 10-60km and ballistic missiles between 5-100 km height are as follows: - 600-2600 km with skywave - Minimum of 15 km with surface wave
	Ship	-	-
Detection-to-Tracking Time	Aircraft	10 sec for missile and aircraft	-
	Ship	500 sec	-
Target velocity		50 km/h (threshold velocity for air target)	40-3,600 m/s (ballistic missile targets at an altitude of 5-100 km) 100-3,600 m/s (air targets at an altitude of 10-60 km) 18 km/h (threshold velocity for sea surface targets)
Simultaneously Tracking capability		Ten missiles and 200 ships	Up to 1,200 air targets. More than 50 missiles within signated controlled areas. More than 300 surface vessels in six periodically controlled zones.

Table 3. Basic Characteristics of Ukraine Shipboard OTH-SW and Transportable SkW-OTH Radar System.

I. UNITED KINGDOM

1. Alenia Marconi Over-the-Horizon (OTH) Radar

Alenia Marconi medium-range HF (3-30 MHz) OTHR system is developed by Alenia Marconi Systems Ltd and deployed for early warning surveillance and for surface and low/high flying air targets detection. The system is shoreline-located equipment and uses surface wave transmission for detection beyond the normal radar horizon. The detection capability is out to 370 km for surface targets and somewhat less for aircraft. It provides 120° sector coverage over the sea for single radar. Multiple radar systems are installed along the coastline and overlap in coverage area to cover the national shoreline

[38]. The peak transmitted output power is at 40 kW and the OTHR system reduces the required peak transmitted power level by applying long pulse widths (100 to 1,000 μs) [38].

2. Overseer

The Overseer is a surface wave radar system used mainly for ship tracking. It gives continuous surveillance with ranges out to 370 km from the coastline. It covers a 120° sector, as shown in Figure 27, with track outputs on 500 surface vessels or an optional 100 aircrafts. It operates in the HF band of 4-12 MHz with a transmitter output power of 40 kW [38].

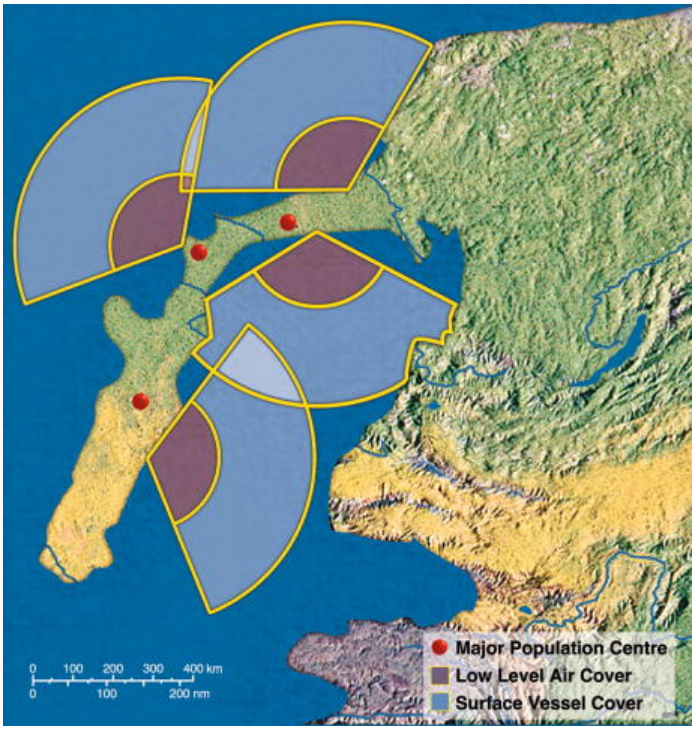

Figure 32. Typical Coverage of Overseer Radar (1998) (From [38]).

J. UNITED STATES

The United States has been developing HF OTHR systems for decades and the successful realization of HF OTHR is one of the more significant radar developments since World War II. The following radars are introduced in the order of development.

1. Magnetic-Drum Radar Equipment (MADRE)

The Naval Research Laboratory (NRL) began to bring their MADRE design into operation in 1961 to monitor the North Atlantic air traffic route. The transmitter and receiver of the MADRE were at the same location using the same horizontal polarized antennas. The MADRE was located at the Chesapeake Bay field site of the NRL. It uses 100 μs, pulse waveform with 25 kW of average power. This experimental radar has been operated with average powers from 5 to 50 kW. The MADRE was even able to detect a rocket launch from Cape Canaveral and atomic tests in Nevada. Figure 33 shows the MADRE site with the two primary antennas. The higher one was a large fixed array steered by changing the length of the feed lines. The other primary antenna was steered by rotating it [39].

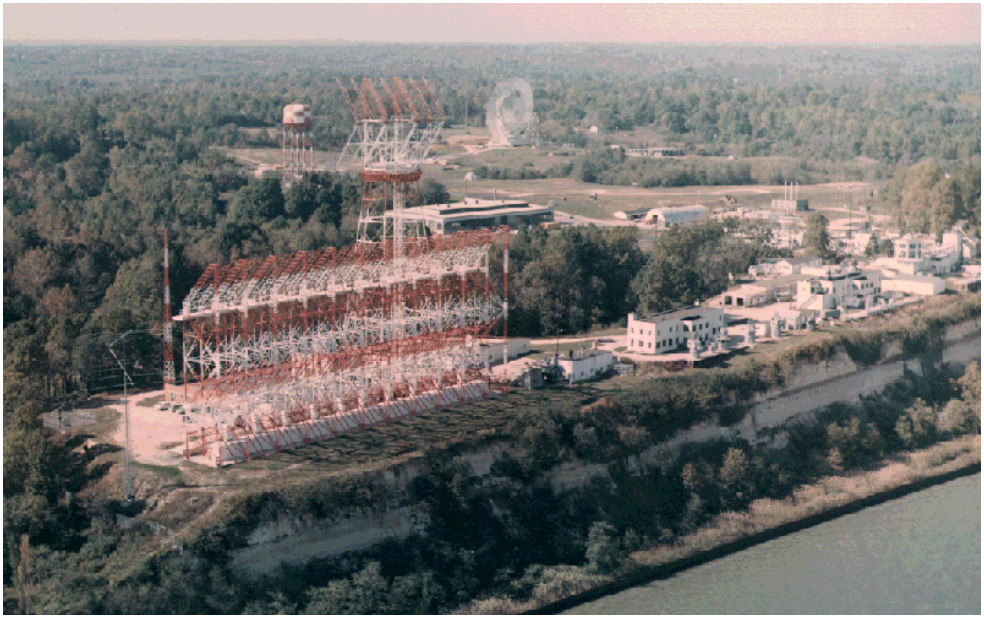

Figure 33. MADRE Over-the-Horizon Radar (From [39]).

2. Wide Aperture Research Facility (WARF)

The WARF was designed and built by Stanford Research Institute International. The WARF is a two site OTHR with the transmitter located near Lost Hills and the receiver near Los Banos, both in California. The WARF has a high-resolution performance and uses a frequency modulated continuous waveform (FMCW). This waveform is more compatible with other users in the HF band than the pulse waveform used by MADRE. The operation center was located at the same site as the receiver, but it was moved to another site for logistical reasons [40]. The other significant difference between MADRE and WARF is the larger receive aperture of WARF that gives better azimuth resolution and better performance against small and slow targets.

The transmitter antenna array is shown in Figure 34a. It includes 16 log-periodic elements operating in the 6-28 MHz frequency range. The receive antenna is shown in Figure 34b which covers a distance of 2.3 km. Figure 34c is a photo of the interior of the WARF Operation and Control Center. [41]

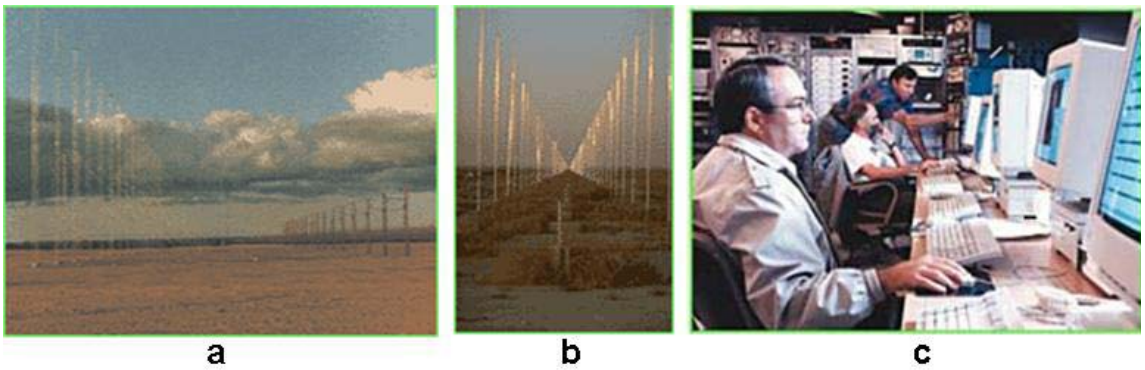

Figure 34. Wide Aperture Research Facility (From [41]).

3. AN/FPS-95, Cobra Mist

The AN/FPS-95 was a ground-based air search radar, also known as Cobra Mist. The Cobra Mist was a joint development of US Air Force and Royal Air Force and located at Orfordness in England and was a single site radar. The Cobra Mist used a simple pulsed waveform which was similar to that used in MADRE but with about 10 dB

higher average power (250 kW) [39]. Due to the poor resolution in range and azimuth, it did not meet its expected performance and was removed from service after two years of operation.

4. AN/FPS-112 Over-The-Horizon (OTH) Radar

The U.S. Navy developed the AN/FPS-112 in mid-1970s with the assistance of the ITT Electro-Physics Laboratory (EPL). The AN/FPS-112 was located near Williamsburg, Virginia and was also a single site radar. EPL used a phased-coded pulse waveform to provide good range resolution with a high duty factor [39]. The AN/FPS-112 was disassembled later to make the room for one of the AN/TPS-71 transmitter.

5. AN/FPS-118 Over-The-Horizon Backscatter (OTH-B) Radar

The AN/FPS-118 was developed by the U.S. Air Force with the assistance of General Electric (GE) in 1970. The first phase was a two site experimental radar located in Maine to demonstrate the technical feasibility. The second phase was to add a separate operation center. Another radar was later added on the west coast. The experimental transmissions from the Maine site covered an arc from 016.5 to 076.5º and from 926 to 3,334 km in range. The radar in Maine was a prototype of the Continental United States OTH Backscatter (CONUS-OTH-B) system [40]. These radars used an FMCW waveform similar to that used in the WARF but with much higher power [39]. Figures 35 and 36 show a close-up view of the canted dipole elements used in the transmission array and the receiver elements of one sector of the U.S.A. East Coast OTH-B system.

The CONUS-OTH-B ground-based early warning system was developed to provide electronic surveillance of aircraft at extended ranges of 800 to 2,880 km. It operates in the HF band (5-28 MHz) and is designed for over-the-horizon detection and tracking of aircraft and cruise missiles flying at any altitude. The radar is a bistatic system with separation of 150-200 km between transmitter and receiver. [40]

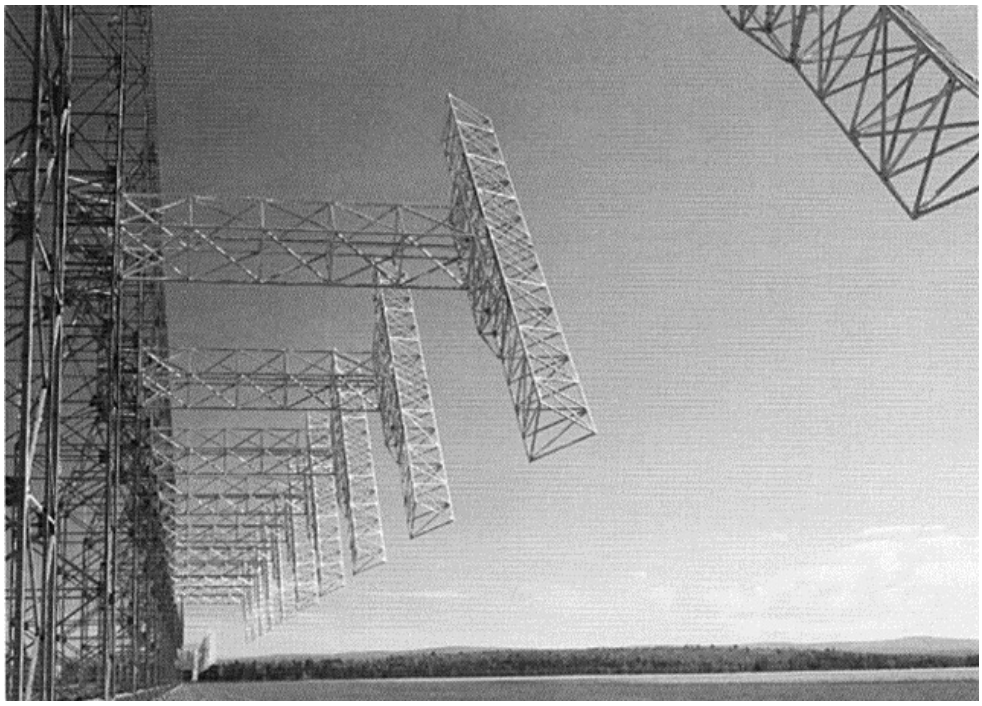

Figure 35. The Transmitter Dipole Elements used in the East Coast OTH-B System (From [40]).

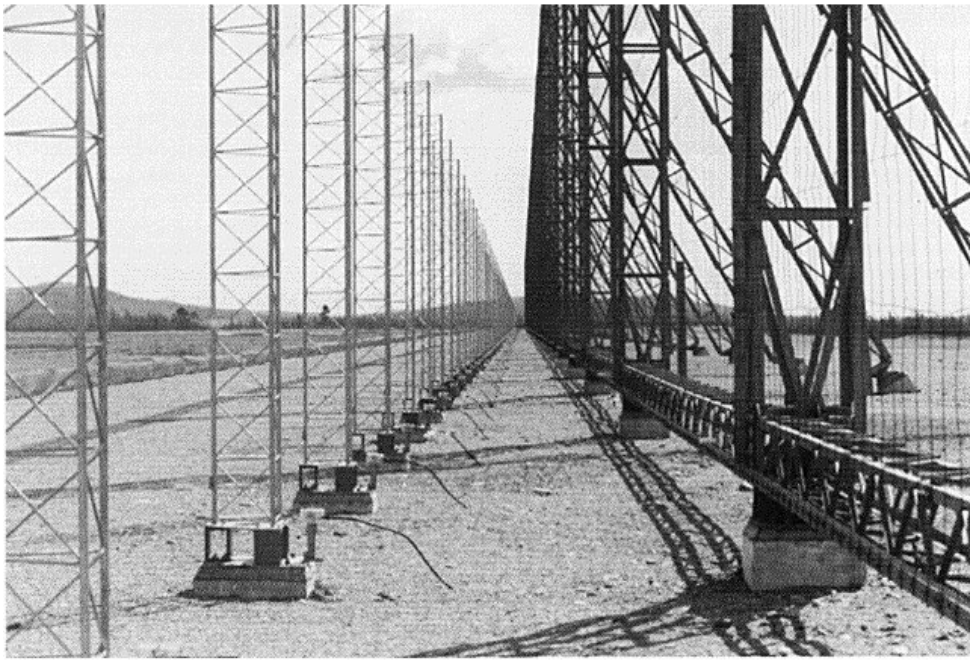

Figure 36. The Receiver Elements used in the East Coast OTH-B System (From [40]).

6. AN/TPS-71 Relocatable Over-The-Horizon Backscatter (OTH-B) Radar (ROTHR)

The AN/TPS-71 ROTHR is also a bistatic system with the transmitter and receiver sites separated by anywhere from 92 to 185 km. The operating frequency is the same as AN/FPS-118 (5-28 MHz) with 200 kW of transmitted power. It covers a 64° wide illuminated sector with a range from 926 to 2,963 km. The ROTHR was originally intended to keep track of ship and aircraft movement over the Atlantic, and thus allow coordinated fleet movements well in advance of an engagement. A prototype ROTHR system was installed on the isolated Aleutian Island of Amchitka, Alaska, monitoring the eastern coast of Russia, in 1991 and used until 1993, but was later moved to Virginia where it is used to counter the illegal drug trade, covering Central America and the Caribbean. A second ROTHR was later set up in Texas, covering many of the same areas in the Atlantic, but also providing coverage over the Pacific down south to Colombia. It also operates in the drug trafficking role [42]. Figure 37 shows the transmission array of the AN/TPS-71 ROTHR system.

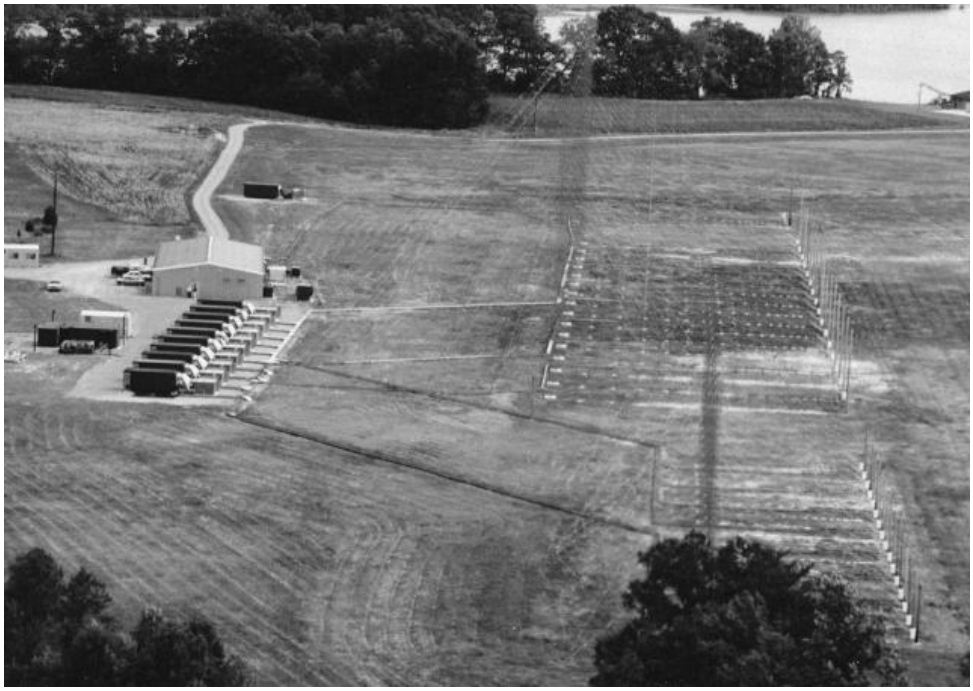

Figure 37. The AN/TPS-71 ROTHR Transmission Array (From [42]).

A project named “terrain mapping” (TMAP) was initiated to improve target positioning accuracy at the AN/TPS-71 systems located in Virginia (ROTHR-VA), Texas (ROTHR-TX), and Puerto Rico (ROTHR-PR). The current application of these ROTHRs is to support counterdrug (CD) aircraft surveillance and interdiction. The immediate operational application of the TMAP research is to improve the accuracy of ground positioning of CD targets of interest. Targets of interest include single-engine private aircraft, larger aircraft, and ocean-going vessels of all sizes. [43]

K. CHAPTER SUMMARY

Use of the HF band (3-30 MHz) provides an extended range beyond the horizon. The detection range is up to 4,000 km for skywave propagation and up to 400 km for surface wave propagation. The development of OTHR has been a great interest for many countries due to the extended range available using HF propagation.

Some characteristics and parameters for the best known OTHR systems discussed in this chapter are listed in Table 4 through 7. The parameters used in Chapter IV are focused on Chinese OTH-B radar system highlightened in Table 4.

Country	Australia	Canada		China		
Name or Type of the System	Jindalee-B	SWR-503	SWR-610	OTH-B	PD-OTH-B	SW-OTH
Operating Frequency	-	HF (3.5-5.5 MHz)	HF (6-10 MHz)	HF (6-22 MHz)		-
Waveform selection	-	-	-	FMCW	Pulse Doppler waveform	-
Monostatic/Bistatic	Bistatic	-	-	-	Bistatic	-
Transmitter Power (PT)	560 kW peak 158 kW (52 dBW)	-	-	200-1200 kW average	-	-
Transmitter Antenna Power Gain (GT)	21 dB	-	-	18 dB	-	-
Receiver Antenna Power Gain (GR)	32 dB	-	-	26 dB	-	-
Coherent Integration Time (tc)	17 dBs	-	-	6 dBs	-	-
Angular Resolution (Δθ, degrees)	0.5	-	-	5	-	-
Range Resolution (ΔR, km)	20	-	-	15	-	-
Detection Range	1000-3000 km	407 km	333 km	700-3500 km	700-3500 km	≤ 400 km
Note	-	-	-	-	-	-

Table 4. Basic Characteristics of Best Known OTHR.

Country	France		Italy	USSA	
Name or Type of the System	Valensole	Nostradamus	CONDO-R	IRIDA OTH-SW	OTH-B Woodpeckers
Operating Frequency	HF	HF skywave (3-30MHz)	I-band (8-10 GHz)	HFsurface wave (7-15MHz)	HF (4-30MHz)
Waveform selection	Pulse waveform	Phased-coded pulse waveform	-	-	-
Monostatic/Bistatic	Monostatic	Monostatic	-	Bistatic	-
Transmitter Power (PT)	100 kW peak (24 dBW)	50 kW	-	65 kW peak 16 kW average	20-40 MW (From [31]) 1.2 MW (61 dBW)
Transmitter Antenna Power Gain (GT)	20 dB	-	-	-	-
Receiver Antenna Power Gain (GR)	26 dB	-	-	-	-
Coherent Integration Time (tc)	25 dBs	-	-	-	-
Angular Resolution (Δθ, degrees)	1	-	-	-	-
Range Resolution (ΔR, km)	22.5	-	-	-	-
Detection Range	-	800-3000 km	-	280-300 km	-
Note	-	-	-	-	-

Table 5. Basic Characteristics of Best Known OTHR (Cont'd).

Country	Ukraine				UK	
Name or Type of the System	Transportable OTH-SW		Shipboard OTH-SW	Transportable SkW_OTH	Alenia Marconi OTHR	Overseer
	200 km	300 km				
Operating Frequency	HF (18-25MHz)	HF (6-24MHz)	HF (18-25MHz)	HF (5-28MHz)	HF surface wave (3-30MHz)	HF surface wave (4-12MHz)
Waveform selection	-	-	-	-	-	-
Monostatic/Bistatic	Bistatic	Bistatic	-	Bistatic	-	-
Transmitter Power (PT)	-	-	-	-	40 kW peak	40 kW peak
Transmitter Antenna Power Gain (GT)	-	-	-	-	-	-
Receiver Antenna Power Gain (GR)	-	-	-	-	-	-
Coherent Integration Time (tc)	-	-	-	-	-	-
Angular Resolution (Δθ, degrees)	-	-	-	-	-	-
Range Resolution (ΔR, km)	-	-	-	-	-	-
Detection Range	~200 km	~300 km	~170 km	600-2600 km	~ 370 km	~ 370 km
Note	-	-	-	-	-	-

Table 6. Basic Characteristics of Best Known OTHR (Cont'd).

Country	USA					
Name or Type of the System	MADRE	WARF	AN/FPS-95 (Cobra Mist)	AN/FPS-112	AN/FPS-118 (CONUS-OTH-B, Maine)	AN/TPS-71 (ROTHR)
Operating Frequency		HF (6-28MHz)	-	-	HF (5-28MHz)	HF (5-28MHz)
Waveform selection	Simple pulse waveform	FMCW	Simple pulse waveform	Phased-coded pulse waveform	FMCW (FMCW)	-
Monostatic/Bistatic	-	-	-	-	Bistatic	Bistatic
Transmitter Power (PT)	25 kW (27 dBW)	43 dBW	250 kW	-	1200 kW	200 kW (53 dBW)
Transmitter Antenna Power Gain (GT)	28 dB	20 dB	-	-	-	21 dB
Receiver Antenna Power Gain (GR)	22 dB	30 dB	-	-	-	34 dB
Coherent Integration Time (tc)	20 dBs	11 dBs	-	-	-	-
Angular Resolution (Δθ, degrees)	1	0.5	-	-	-	0.5
Range Resolution (ΔR, km)	7.5	0.8	-	-	-	-
Detection Range	-	-	-	-	926-3334 km (800-2880 km)	926-2963 km
Note	-	-	Not in current use	Not in current use	-	-

Table 7. Basic Characteristics of Best Known OTHR (Cont'd).

IV. CHARACTERISTICS OF THE OTHR SYSTEMS

The characteristics of OTHR systems are presented in this section and the discussion focuses on the waveform, target detection technique and radar equation analysis.

A. WAVEFORMS

Depending on the mission, different waveforms are used for OTHR systems to perform their designated mission. The waveforms used can be a simple pulse (i.e. MADRE, AN/FPS-95, Cobra Mist [39], Valensole), a pulse Doppler waveform (i.e. PD-OTH-B radar [25]), a phased-coded pulse (i.e. AN/FPS-112 [39] and Nostradamus [44]), FMCW (i.e. WARF and CONUS-OTH-B [40, 45]) or frequency modulated interrupted CW (FMICW) [46]. The most common waveform used in OTHR systems is FMCW.

Pulse Doppler (PD) techniques, such as those used in the Chinese PD-OTH-B radars, provide target location such as bearing, range, and altitude. In addition, it can also measure the target's radial velocity (range rate). The Doppler effect is used to determine the relative velocity of the targets. The returning pulses of signal energy from the target are processed to measure the frequency shift between the carrier cycles in each pulse and the original transmitted frequency [47].

A phased-coded pulse waveform can also be used for long range OTHR systems. The bandwidth of the phased-coded waveform can be used to determine the range resolution and the CIT can be used for the Doppler resolution determination [44]. There are several classes of code sequences commonly used in phased-coded pulse waveforms. These code sequences include Barker sequence and pseudorandom sequence and detailed information can be found in [48].

FMCW radars can determine both range and relative velocity of targets with good accuracy [47]. By using FMCW waveforms, radar systems can be made compatible with simple solid-state transmitters and have extremely high time bandwidth products which

makes the systems very resistant to interception by electronic support (ES) systems [49]. In addition, FMCW radars can operate with good range resolution, can reject external interference, and can recover the range information from the intermediate frequency signal using the fast Fourier transform (FFT). It also easily includes sensitivity time control processing in the frequency domain and can use a reflected power canceller for single antenna operation. The FMCW waveform with a 100% duty cycle is ideal for bistatic or low-power operation and this is the reason the waveform is widely used in OTHR systems [46].

Frequency modulated interrupted CW (FMICW) is simply an FMCW waveform which is gated on and off typically with a pseudorandom sequence. The transmitted and received FMICW waveforms are obtained by multiplying the FMCW waveform with the transmit and receive interrupt sequence respectively. This waveform is used for an experimental OTHR to detect surface targets up to 400 km from shore with a range resolution of 400 m. [46]

B. TARGET DETECTION

In general, target detection for OTHR is commonly classified into two major classes. One is for high-speed flying targets such as aircrafts, and the other one is for low-speed targets such as ships and low-altitude flying targets [50]. The purpose for detecting aircrafts and ships are apparently different and the parameters and factors used differ from each other in order to achieve the great effectiveness of radars in these two conditions respectively.

The objective for aircraft detection is to improve the signal-to-noise ratio (SNR) by selecting the appropriate frequency to generate a strong return signal reflected back from the target through the ionosphere. In addition, a narrow-band transmitter is used to improve detection accuracy, and a high pulse repetition frequency (PRF) is chosen to avoid Doppler aliasing. Ship detection is quite different from aircraft detection. The parameters selected in ship detection are to improve Doppler resolution and signal-to-

clutter ratio (SCR). A long CIT (t_c) is deployed to increase Doppler resolution. A wide-band waveform is used to improve SCR and a lower PRF is used for small Doppler ship detection than that used for aircraft detection. [51]

Usually the detection processes for ships and aircrafts are separate to give the best detection performance. However this is not an issue in OTHR system since it is inefficient and time consuming. OTHR system can combine two detection processes together in order to detect aircraft and ship at the same time. In this case, a wide-band waveform and high PRF might be used. Modern spectral analysis techniques are also used for target detection [45].

C. OTHR DETECTION RANGE

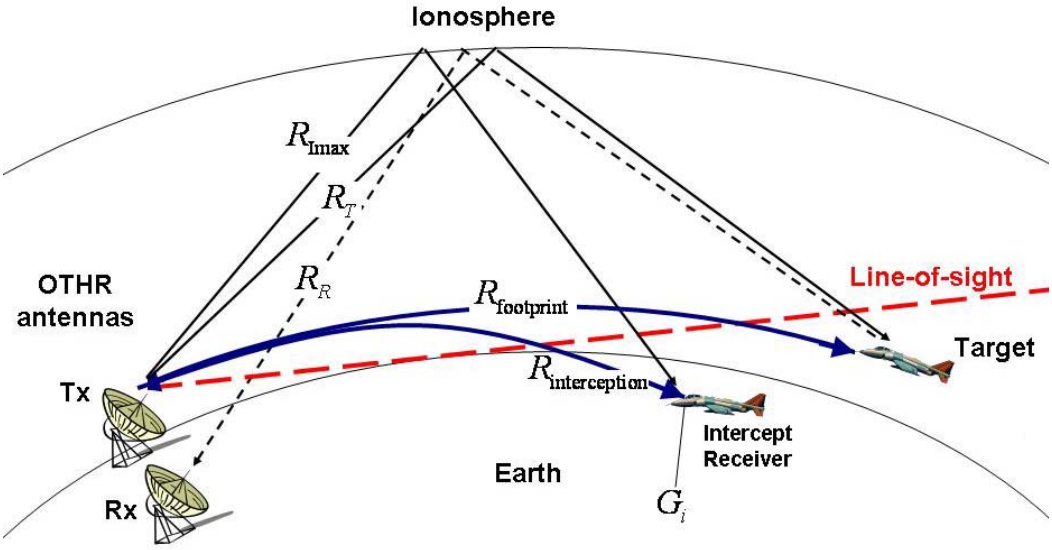

Figure 38. Target Detection Diagram of OTHR System.

For the skywave OTHR, the propagation technique is shown in Figure 38 and the received power at the radar receiver from the target is [2, 3 and 52]

$$P_{RT} = \frac{P_T G_T G_R \lambda_c^{\,2} \sigma L_{P2} L_S L_F}{(4\pi)^3 R_T^{\,2} R_R^{\,2}} \tag{4}$$

where P_T is the average transmitter power in watts, G_T is the transmit antenna gain, G_R is the receive antenna gain, λ_c is the wavelength at the carrier frequency or f_c, σ is the target radar cross section, the term L_{P2} is the two-way transmission path losses in the order of -20 to -10 dB in [24], L_S is the system losses which include the transmitter and receiver subsystem losses which is -15 dB in [2], L_F is the Faraday polarization loss of the ionosphere which is typically -3 dB in [24], R_T is the distance of the ray path traveling from the radar to the target reflecting off of the ionosphere, and R_R is the distance of the ray path traveling from the target to the receiver reflecting off of the ionosphere.

The minimum input SNR, SNR_{Ri} is related to the receiver's sensitivity δ_R. The receiver can detect and process an incoming target signal at this signal level or higher. Substituting of the sensitivity for P_{RT} in (3), the maximum detection range (reflecting off of the ionosphere) of the radar becomes

$$R_{R\max} = \left(\frac{P_T G_T G_R \lambda_c^{\,2} \sigma L_{P2} L_S L_F}{(4\pi)^3 \delta_R} \right)^{\frac{1}{4}} \tag{5}$$

where $R_{R\max}$ is calculated by assuming that the OTHR transmitter and receiver are collocated $R_T = R_R$. The sensitivity δ_R is the product of the minimum SNR required at the input (SNR_{Ri}) times the noise power in the input bandwidth of the receiver which is

$$\delta_R = kT_0 F_R B_{Ri} (SNR_{Ri}) \tag{6}$$

where k is the Boltzmann's constant ($k = 1.3807 \times 10^{-23}$ J/K), T_0 is the standard noise temperature ($T_0 = 290K$), F_R is the receiver noise factor and includes the fact that the additional noise is 20 to 50 dB larger than the receiver thermal noise factor [24], and B_{Ri} is the receiver's input bandwidth in Hz. The maximum detection range (reflecting off of the ionosphere) then can be expressed as

$$R_{R\max} = \left(\frac{P_T G_T G_R \lambda_c^{\,2} \sigma L_{P2} L_S L_F}{(4\pi)^3 k T_0 F_R B_{Ri} (SNR_{Ri})} \right)^{\frac{1}{4}} \tag{7}$$

Consider the Chinese FMCW OTH-B radar characteristics shown in Table 5 in Chapter III with $P_T = 1.2$ MW (61dBW), $G_T = 18$ dB and $G_R = 26$ dB at 14.5 MHz [23], $F_R = 40$ dB, $B_{Ri} = 10$ kHz (calculated from $\Delta R = c/2B_{Ri} = 15$ km), $L_{P2} = -15$ dB, $L_S = -15$ dB, and $L_F = -3$ dB. Figure 39 shows the FMCW OTH-B radar maximum detection range (reflecting off of the ionosphere) as a function of the required input SNR (SNR_{Ri}) for $\sigma = 1$, 10, and 100 m^2 at operating frequencies $f_c = 14.5$ MHz.

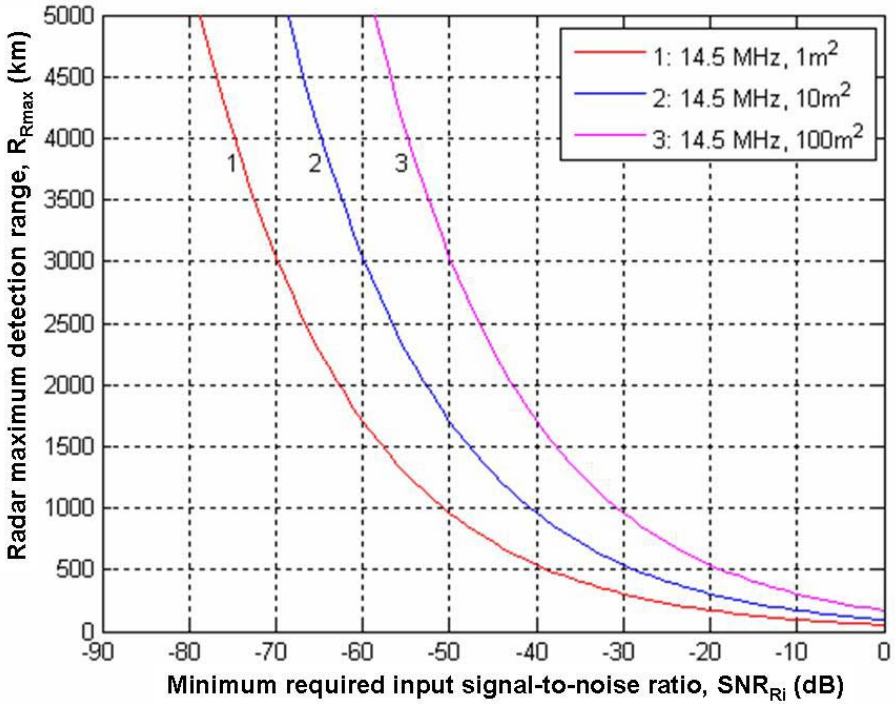

Figure 39. FMCW OTH-B Maximum Detection Range ($R_{R\max}$) for $\sigma = 1$, 10, and 100 m^2.

Assuming a flat Earth situation, the detection range $R_{\text{footprint}}$ along the Earth becomes

$$R_{\text{footprint}} = 2\sqrt{\left(\frac{R_{R\max}}{2}\right)^2 - (h_{F\,2layer})^2} \tag{8}$$

where $h_{F\,2layer}$ is the F2-layer height from the Earth's surface. For this example, an F2-layer height of 240 km is used (Chapter II). The geometry diagram for (7) is shown in Figure 40. The detection distance along the flat Earth ($R_{\text{footprint}}$) is calculated from (6) and (7) shown in Figure 41.

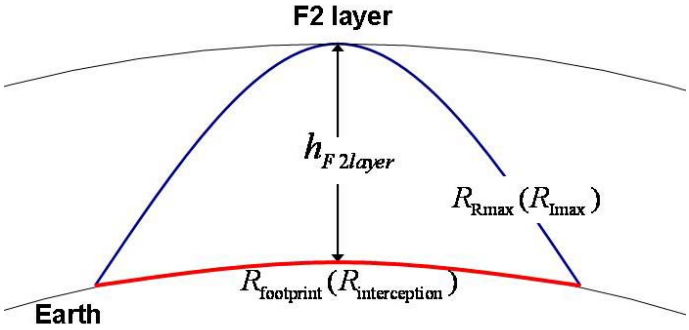

Figure 40. Geometry Diagram of the Detection Range Calculation.

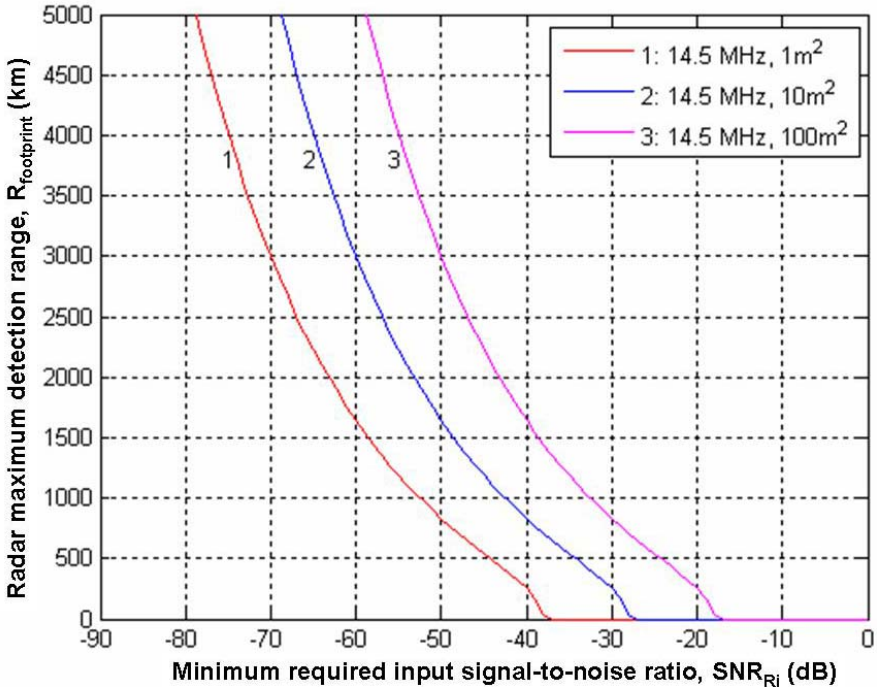

Figure 41. FMCW OTH-B Maximum Detection Range ($R_{\text{footprint}}$) for $\sigma = 1$, 10, and 100 m^2.

From the parameters given in Table 4, the OTH-B radar has a minimum detection range of 700 km and a maximum detection range of 3,500 km. For a maximum detection range along the flat Earth $R_{\text{footprint}}$ = 3,500 km, the $R_{R\max}$ is calculated as 3,532 km from (7). The minimum required input SNR (SNR_{Ri}) for $\sigma = 1$, 10, and 100 m^2 and for f_c =14.5 MHz frequency is shown in Table 8 and Figure 39. Note that these results are first order approximation of the radar performance, a more detailed model is used later to give more accurate results.

Target RCS / Frequency	1m²	10m²	100m²
14.5 MHz	-72.4 dB	-62.4 dB	-52.4 dB

Table 8. Minimum Required Input SNR at 3,500 km Footprint Range.

D. INTERCEPT RECEIVER INTERCEPTION RANGE

From the illustration shown in Figure 38, the signal power available at the intercept receiver from the Chinese FMCW OTHR can be expressed as

$$P_{IR} = \frac{P_T G_T L_{P1} L_{SI}}{4\pi R_I^{\,2}} \left(\frac{G_I \lambda_c^{\,2}}{4\pi} \right) \tag{9}$$

where the term L_{P1} is one-way transmission path loss, L_{SI} is the intercept receiver system loss, G_I is the intercept receiver antenna gain, and R_I is the distance of the ray path traveling from the radar to the interceptor through the atmosphere. Substituting the interceptor receiver's sensitivity δ_I for the signal power P_{IR}, the maximum interception range (reflecting off of the ionosphere) of the intercept receiver can then be written as

$$R_{\text{Imax}} = \sqrt{\frac{P_T G_T G_I L_{P1} L_{SI} \lambda_c^{\,2}}{(4\pi)^2 \delta_I}} \tag{10}$$

where the intercept receiver's sensitivity is defined as

$$\delta_I = kT_0 F_I B_I (SNR_{I_i}) \tag{11}$$

where F_I is the intercept receiver noise factor, B_I is the intercept receiver's bandwidth in Hz, and SNR_{Ii} is the input SNR at the intercept receiver. The maximum interception range (reflecting off of the ionosphere) can be then expressed as

$$R_{\text{Imax}} = \sqrt{\frac{P_T G_T G_I L_{P1} L_{SI} \lambda_c^{\,2}}{(4\pi)^2 k T_0 F_I B_I (SNR_{I_i})}} \tag{12}$$

Different from the radar system receiver design where the bandwidth is matched to the known transmitted signal, the intercept receiver does not know the characteristics of the threat signal. Detail description and approximate expressions can be found in [52]. The bandwidth of the intercept receiver for typical case where $B_{IR} >> B_{IV}$ can be expressed as

$$B_I = \sqrt{2 B_{IR} B_{IV}} \tag{13}$$

for a square law detector and

$$B_I = \frac{1}{2}\sqrt{2 B_{IR} B_{IV}} \tag{14}$$

for a linear detector. In Equations (12) and (13), B_{IR} is the largest coherent radar bandwidth expected or the intercept receiver input RF bandwidth. The intercept receiver input RF bandwidth is assumed to be B_{IR} = 30 MHz. In addition, B_{IV} is the radar receiver video bandwidth or the inverse of the smallest t_c that radar expected which is

$$B_{IV} = \frac{1}{t_c} \tag{15}$$

where t_c is the on the order of 4 sec (6 dBs) from Table 4 in Chapter III. The radar receiver video bandwidth B_{IV} = 0.25 Hz (-6 dBHz) in this case.

In this example, the intercept receiver has an isotropic antenna with gain $G_I = 1$ (0 dB), $L_{P1} = -18$ dB, $L_{SI} = -3$ dB, $F_I = 5$ dB, $B_{IV} = -6$ dBHz, and B_{IR} = 30 MHz (74.8 dBHz). This results in B_I =3,873 Hz for a square law detector and B_I = 1,936 Hz for a linear detector s given by (12) and (13). The intercept receiver maximum interception range along the flat Earth ($R_{\text{interception}}$) can be calculated using the similar formula as (7)

$$R_{\text{interception}} = 2\sqrt{\left(\frac{R_{I\max}}{2}\right)^2 - (h_{F\,2layer})^2} \tag{16}$$

Figure 42 shows the intercept receiver maximum interception range (reflecting off of the ionosphere) and Figure 43 shows the intercept receiver maximum interception range (along the flat Earth) calculated from (11) and (15). Both Figures 42 and 43 are functions of the minimum required input SNR (SNR_{Ii}) and are used in both square law detector and linear detector interception methods to compare the interception capabilities.

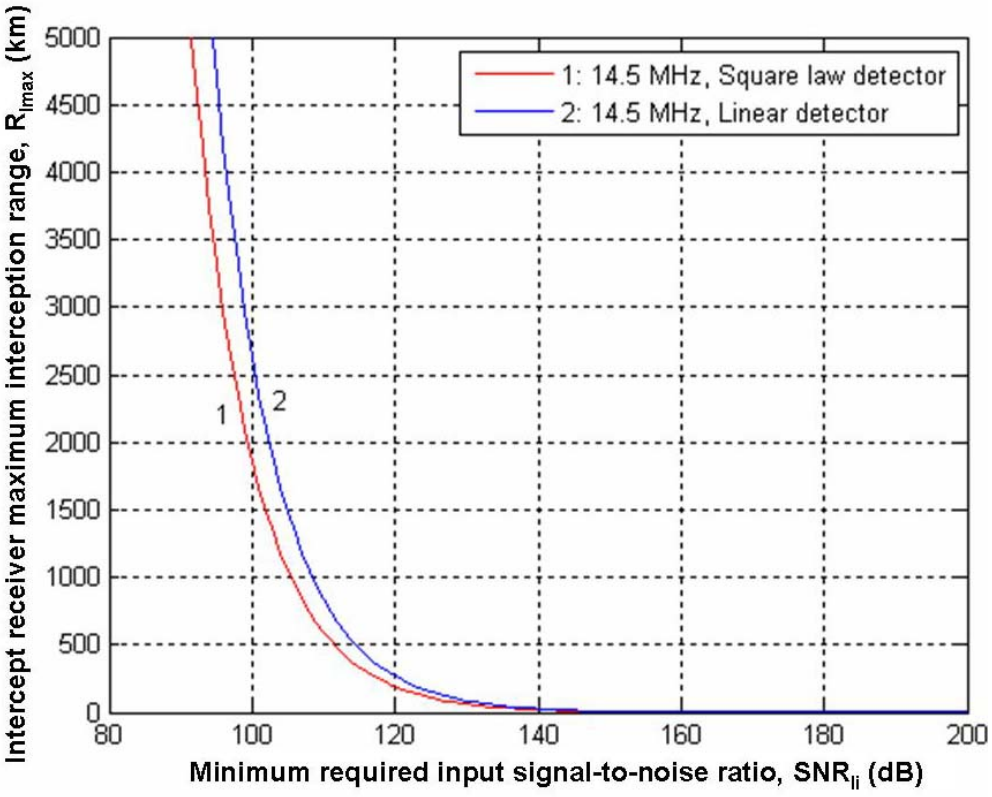

Figure 42. Intercept Receiver Maximum Interception Range (R_{Imax}) with Square Law / Linear Detector Bandwidth when $f_c = 14.5$ MHz.

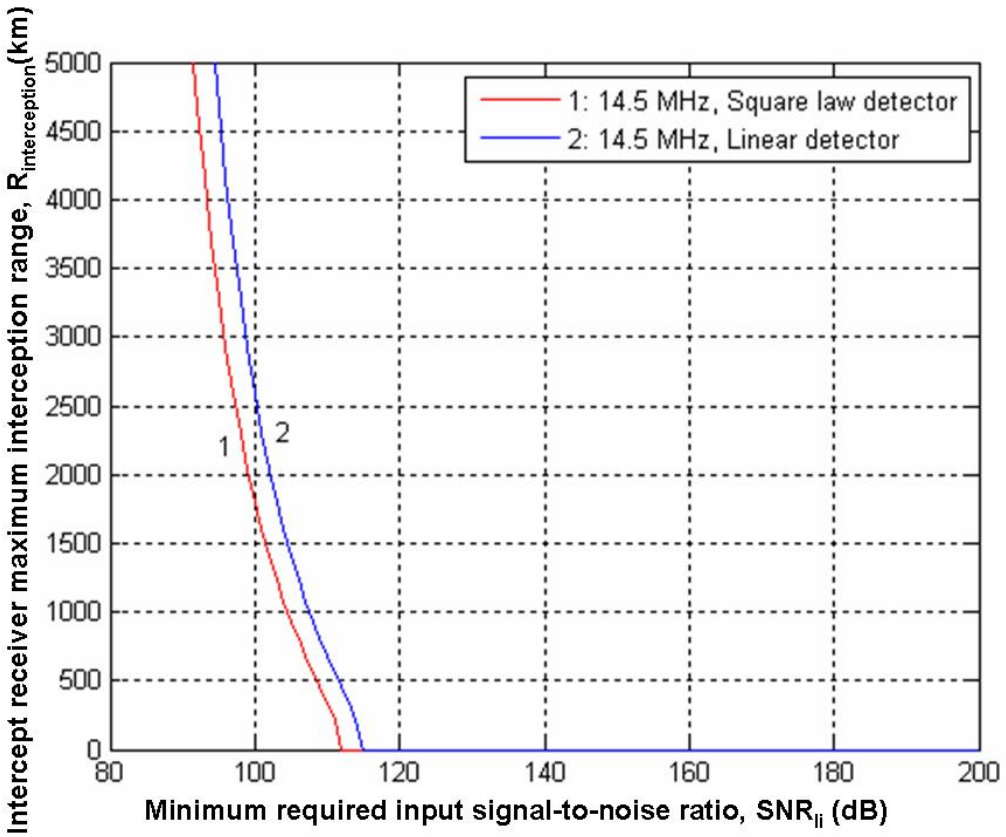

Figure 43. Intercept Receiver Maximum Interception Range ($R_{\text{interception}}$) with Square Law and Linear Detector Bandwidth.

In OTHR equation, the transmission path losses (L_{P1}, L_{P2}), noise factor ($F_{R,} F_I$) and the target cross section (σ) are all functions of frequency. The transmission loss and the noise factor decrease when the frequency increases, and the target cross section increases when the frequency increases. It is beneficial for a small target at a long-range distance since the further the detection range is, the higher the operating frequency that should be used by the radar [24].

Note that the results for both maximum detection range and maximum interception range in this chapter are first order approximation of the radar performance, a more detailed model is used later to give more accurate results.

V. MATHEMATICAL MODELS OF THE OTHR SYSTEM

A. SIMULATION TOOLS - PROPLAB-PRO VERSION 2.0

The PROPLAB-PRO version 2.0 is used for the prediction of the Maximum Usable Frequency (MUF), great-circle paths (or the path traveled by a radio signal from one location to another), and the ability to compute signal quality between two points. It effectively simulates radio transmissions into ionosphere with a high-degree of accuracy by using ionospheric ray tracing techniques [7].

B. CHINESE OTH-B RADAR MODEL

A general transmitter and receiver location for the Chinese FMCW OTH-B radar is shown in Figure 44 and modeled using PROPLAB simulation. The transmitter location is assumed to be at Nanjing ($32.05°$ N, $241.22°$ W) and the receiver is chosen to be at the location of $33.4°$ N, $241.22°$ W which is 150 km north of the transmitter.

Figure 44. General Location of Chinese OTH-B Radar Transmitter and Receiver.

According to [23], the Chinese FMCW OTH-B radar transmit antenna has a directive gain of 18 dB at 14.5 MHz and uses a vertical dipole array in the azimuth at 085° (toward the United States) which is simulated as shown in Figure 45 and applied to the Chinese OTH-B radar system design.

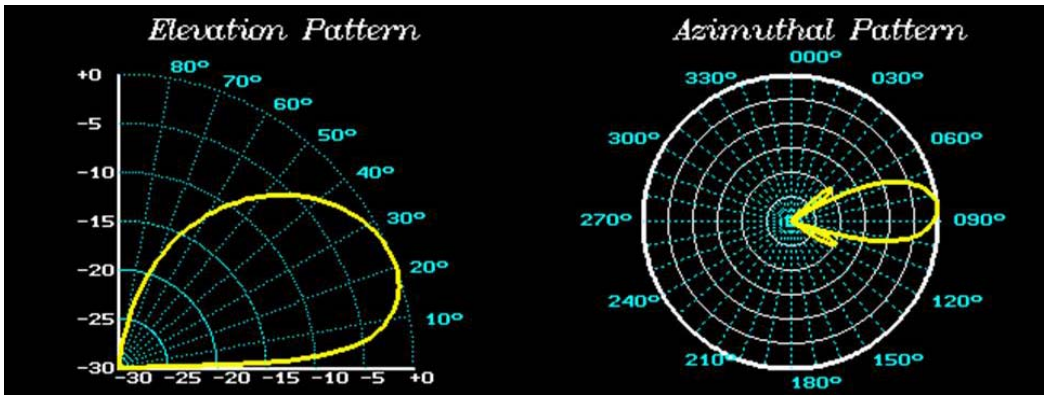

Figure 45. Transmitter Antenna Radiation Pattern of the Chinese OTH-B Radar System.

For the assumed Chinese OTH-B radar location, Figure 46 demonstrates the electron density profile of the ionosphere for SSN = 30 and the level of geomagnetic activity (A- Index, AI) = 5 at 00:00 UTC on 31 July 2007. The bottom of Figure 46 shows the electron density beginning at 1.0×10^{8} electrons/m^3 and increasing up to 6.0×10^{11} electrons/m^3. The left side is the altitude above the Earth's surface in units of kilometers. The electron density profile location ($32.725°$ N, $241.22°$ W) is specified on any single-hop path midpoint. The midpoint is defined as the point lies half-way between the transmitter and the receiver on the great-circle path [7]. Figure 46 also shows the D, E, and F2 –layer characteristics.

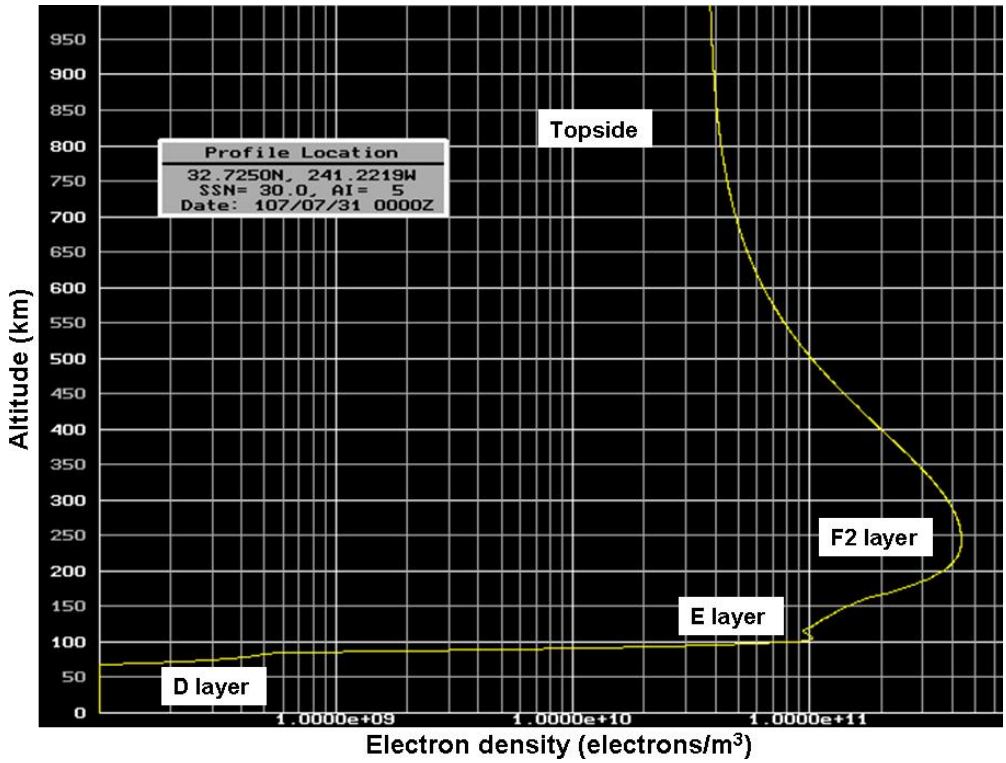

Figure 46. Ionospheric Electron Density Profile for the Chinese OTH-B Radar Analysis for SSN = 30 and AI = 5 at 00:00 UTC 2007/7/31.

A ray with a $f_c = 16$ MHz frequency transmitted through the ionosphere with an elevation angle of 0 degrees is shown in Figure 47. Details regarding the contents of this figure are given later. All of the values at the bottom of the figure (from left to right) are surface distances from the transmitter in units of kilometers. The numbers from top to bottom on the left side of the figure correspond to the altitude above the surface, also in units of kilometers. The bottom panel shows the ray trace with transmission elevation angle of 0 degrees above the horizon. The upper central panel with the logarithmic scale shows the electron density of the ray as it passes through the ionosphere. The vertical tick marks of the upper central panel denote the same distance scale as shown in the larger lower panel [7].

The description of each entry on the ray tracing screen is described as follows. The parameter values for the entries for the ray tracing results in this chapter are tabulated.

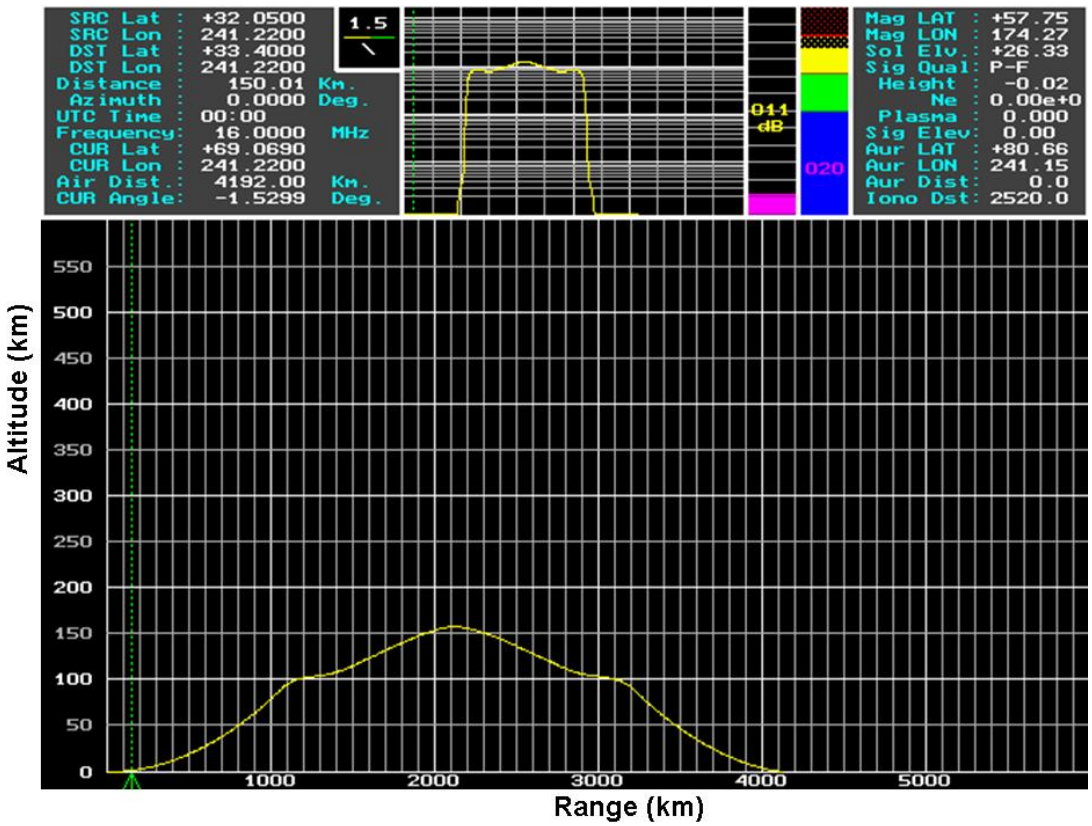

Figure 47. Ray Path for the Elevation Angle of 0° at 16 MHz Frequency for SSN = 30 and AI = 5 at 00:00 UTC 2007/7/31.

1. Location, Azimuth, Distance of the Transmitter/Receiver [7]

The first six lines on the left-top of the panel indicate the geographical positions of the transmitter/source ("SRC Lat", "SRC Lon") and receiver/destination ("DST Lat", "DST Lon"). It also lists the distance from the transmitter to the receiver in kilometers ("Distance"), and the azimuth angle which should be used to transmit from the transmitter to the receiver ("Azimuth").

2. UTC Time, Frequency [7]

The time and frequency of the ray being traced can be found in the seventh and eighth lines of the left-top panel of the ray tracing screen. The time is always universal time and the frequency is in units of MHz.

3. CUR Lat, CUR Lon [7]

The current latitude and current longitude of the signal are donated as “CUR Lat” and “CUR Lon”. They can be used to determine the geographical coordinates where the signal penetrates into the ionosphere, or where it crosses into the auroral zone, or where it loses much of its quality, or the locations of ground-hops.

4. Air Dist [7]

The air distance indicates the distance a signal travels from the transmitter to the receiver by reflecting off of the ionosphere in units of kilometers, not the ground-measured great-circle distance.

5. CUR Angle [7]

As a signal travels from the transmitter to the receiver, the angle of propagation of the signal will change from one instance to another. The “CUR Angle” represents the current elevation angel the signal is headed at. It is measured from the horizontal position. The small box to the left of the geographical coordinates of the transmitter and receiver (in the left-top panel of the ray screen) is a graphical representation of the current angle of the traveling ray. It shows the direction of the traveling ray in numerically, graphically, and textually ways. The numerical value corresponds with the “CUR Angle” value. The graphical method shows the actual angle of the ray by projecting a straight line at the given angle. The textual method is similar to the graphical method except a “／” is used if the signal is traveling upward and a “＼”is used when the signal is traveling downward. If a signal is horizontal, a “－” is used.

6. The Electron Density Graph and Numeric Density [7]

The top-central panel of the screen shows the electron density as the signal passes through the ionosphere. This is not only a diagnostic device, but also an analytical device. (It determines why signals may behave the way they do, or what conditions exist to refract a ray in a certain manner.) A logarithmic display is used in the electron density graph since the electron density behaves in an exponential distribution. The electron

density as a ray is being traced from one point to another in the ionosphere and it is graphed using the same color as is used in ray tracing screen. The base of this graph begins at 1.0×10^{8} electrons/m^3 and increases up to 2.0×10^{12} electrons/m^3. The second logarithmic division is therefore at 1.0×10^{9} electrons/m^3, followed by 1.0×10^{10} electrons/m^3, etc and each subdivision is a tenth of a major division.

The numerical electron density can also be read through the top-right side textual panel of the ray tracing screen. It is the sixth line down from the top and is labeled "Ne" which stands for the electron density. This value is given in scientific notation and represents the electron density per cubic meter. The letter "A" represents 10, the letter "B" represents 11, and the letter "C" represents 12.

7. Estimated Signal Strength Bar Graph [7]

The signal strength bar graph shows the estimated the strength of the signal in units of decibels above one microvolt or dB ($1\ \mu$V). It is partially computed as the ray is being traced through the ionosphere. The final value is determined when the ray actually reaches the ground.

8. Signal Quality Bar Graph and "Sig Qual" [7]

The signal quality is measured as a numerical value between 0 and 100. A value of 100 represents the best possible conditions (extremely good), while a value of 0 represents complete signal loss or radio blackout conditions. The numerical value is converted to a color-coded bar graph. The blue region is associated with very good to good signal propagation. The green area represents signal qualities varying from good to fair. The yellow area corresponds to signal qualities varying from fair to poor. And the signal qualities varying from fair to blackout occur within the red area.

The numerical value of the computed signal quality is also converted into a textual representation. This is displayed on the fourth line down from the top-right panel and is labeled "Sig Qual". The available quality descriptions are as follows: VGOOD (Very Good Quality), VG-G (Very Good to Good), GOOD (Good signal quality), G-F

(Good to Fair quality), FAIR (Fair quality), F-P (Fair to Poor quality), POOR (Poor Quality), P-VP (Poor to Very Poor), and BLKOUT (Radio Black or no signal).

9. Mag LAT, Mag LON [7]

The first two lines of the top-right panel of the screen represent the magnetic coordinates of the ray as it is being traced through the ionosphere.

10. Solar Elevation Angle, "Sol Elv" [7]

The third line of the top-right panel shows the solar elevation, or the elevation angle of the Sun above the horizon, at the current geographical coordinates of the traveling ray. When the sun falls below the horizon (at sunset), this value will become negative, and vice versa.

11. Height or Altitude of the Ray [7]

As a ray travels through the ionosphere, the height of the ray is continually updated beside the acronym "Height" which is located on the fifth line of the top-right panel. The value is in units of kilometers.

12. Plasma Frequency at the Ray Height [7]

The plasma frequency at the ray height is listed beside the "Plasma" on the seventh line of the top-right panel. This value is given in units of MHz.

13. Signal Elevation Angle, "Sig Elv" [7]

The angle of elevation used at the transmitter to broadcast the signal is given in units of degrees above horizon. A zero degree elevation angle corresponds to a transmission directed at the flat horizon. An angle of 90 degrees denotes a vertically propagated signal.

14. Auroral Zone, "Aur LAT", "Aur LON", "Aur Dist" [7]

The three lines on the top-right panel describe the geographical position of that part of the equatorward edge of the auroral zone is the closest to the traveling signal. The

“Aur Dist” variable indicates how far (in kilometers) the signal has spent inside of the auroral zone. Signals that have not (or do not) pass through the auroral zone are associated with the acronym “NoZone”.

15. Ionospheric Distance Traveled, “Iono Dst” [7]

The distance a signal traveled within the ionosphere (in kilometers) is listed on the last line of the top-right panel. This distance does not include the distance required for the signal to travel from the ground to the base of the ionosphere.

16. The Receiver Location [7]

On the ray tracing screen, the receiver location is identified by the dotted green line extending from the base of the distance grid to the top of the ionosphere and a green arrow below the base of the distance grid.

17. The Simulation Results

Figure 48 illustrates the maximum usable frequency (MUF) profile associated to the location shown in Figure 46. The PROPLAB produces the MUF graphs by first collecting the MUF data for the given path for every hour of the day. The F2-layer MUF is the top-most green line. The optimum working frequency (or frequency of optimum transmission, FOT) is the next line down, yellow, and is 85% of the MUF. The thin purple line below the FOT is the numerical average MUF of E-layer and F-layer. The bottom red line is the E-layer MUF which is also known as E-layer penetration (cutoff) frequency. For short-distance transmission, the frequencies should be kept below the E-layer MUF. If the frequencies exceed the E-layer MUF, the signals will penetrate the layer and travel to the F-layer for reflection which results in long-distance propagation [7]. In order to have long-distance propagation, the frequency should be chosen between the E-layer MUF and the F-layer MUF which is the area between the top-most line and the bottom line. This frequency band range allows the rays to be reflected from F-layer and causes an extended long-distance propagation. If the frequency is above the F-layer MUF, the signals will penetrate the ionosphere and be lost to the space.

The FOT in the MUF profile always tends to result in the most reliable propagation. However, there are often a range of frequencies near FOT that can be used reliably and the range is indicated between the FOT and the average MUF of E and F-layer in the MUF profile. Figure 48 is the MUF profile at the midpoint for the path propagates through the transmitter (32.05° N, 241.22° W) and the receiver (33.4° N, 241.22° W) separated by 150 km on 31 July 2007.

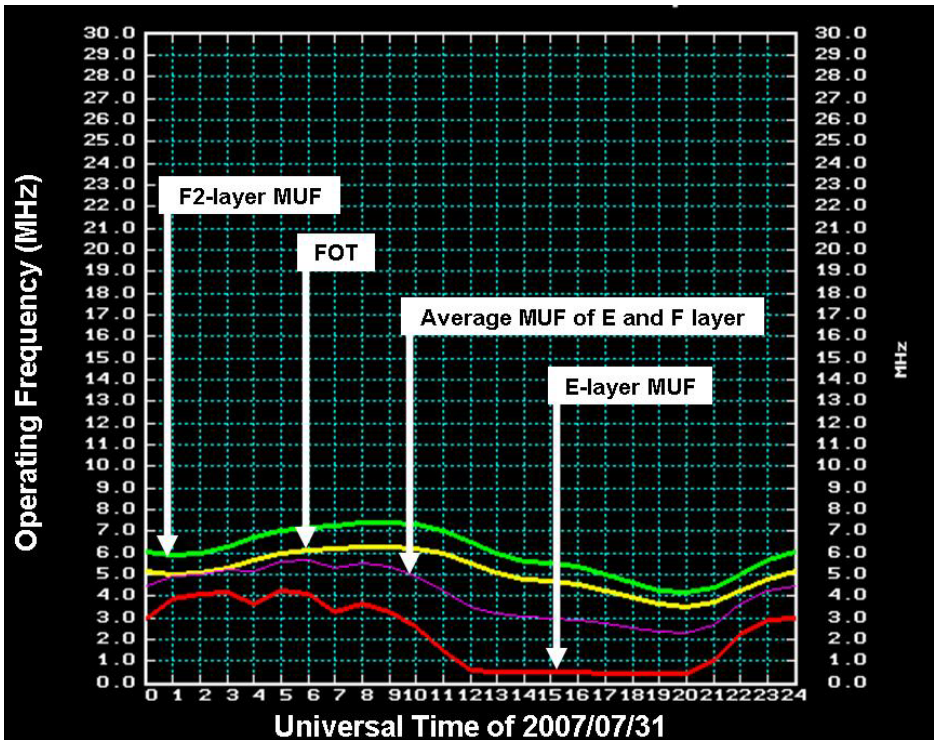

Figure 48. Maximum Usable Frequency Profile at the Location of 32.725° N, 241.22° W for SSN = 30 and AI = 5 on 2007/7/31.

The critical frequency of the E-layer (or foE) is heavily dependent on the location of the Sun. For high solar elevation angles, the critical frequency of the E-layer reaches a maximum of between 3 and 4 MHz. That is, the frequency which would cause a vertically propagated signal to penetrate the E-layer would be between 3 and 4 MHz if the Sun were in the sky. As the Sun drops towards the horizon, the critical frequencies drop. After the Sun sets, the ionization in the E-layer abruptly ends and the critical frequencies fall even further. The minimum critical frequencies are observed around the

local midnight with the values of about 0.4 MHz [7]. Figure 49 is the global map of the critical frequencies of the E-layer throughout the world at 00:00 UTC 31 July 2007 for SSN = 30 and AI = 5. The penetration frequency here is between 2 and 3 MHz at the area around China at the local time of 10:00 at Nanjing.

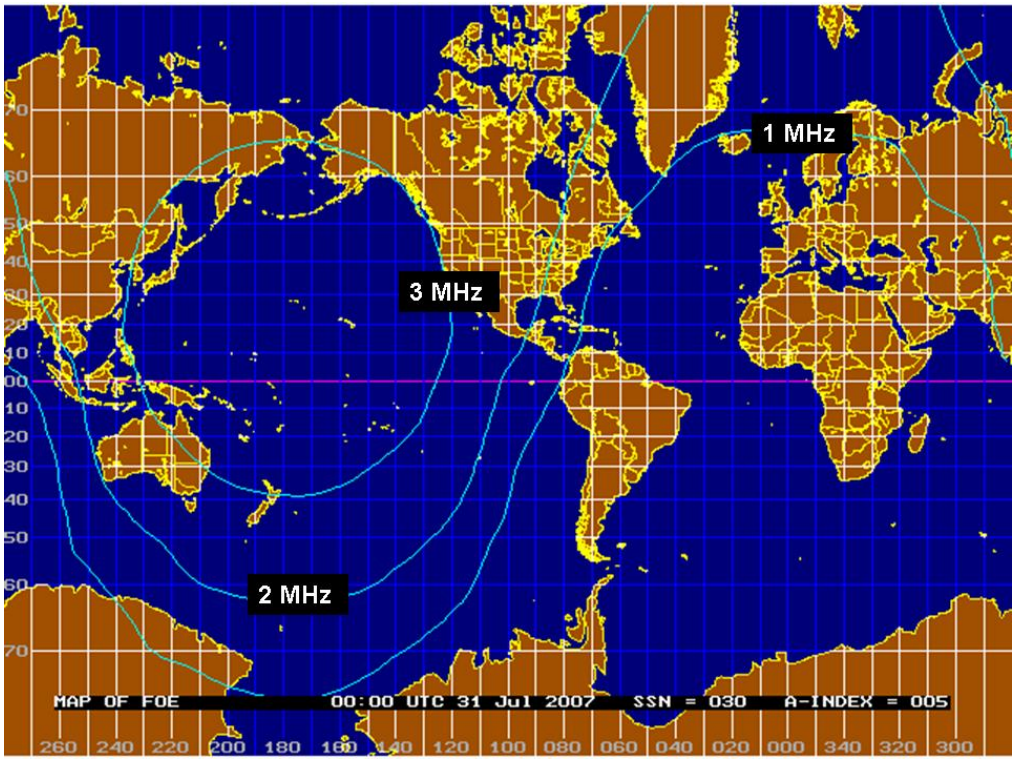

Figure 49. Global Map of E-layer Critical Frequencies for SSN = 30 and AI = 5 at 00:00 UTC 2007/7/31.

Figure 50 shows the world-wide critical frequencies of the F2-layer at 00:00 UTC 31 July 2007 for SSN = 30 and AI = 5. The critical F2-layer frequency is the maximum frequency that can be reflected vertically from the F2-layer. Since the F2-layer is usually the main layer responsible for the ionospheric signal refraction, it is sometimes called the vertical penetration frequency because the vertically propagated signals will penetrate through the ionosphere when the frequencies are higher than the F2-layer critical frequency [7]. In Figure 50, a vertical propagated signal will penetrate to the ionosphere when the frequency is higher than 5 MHz along the region of Nanjing and North America.

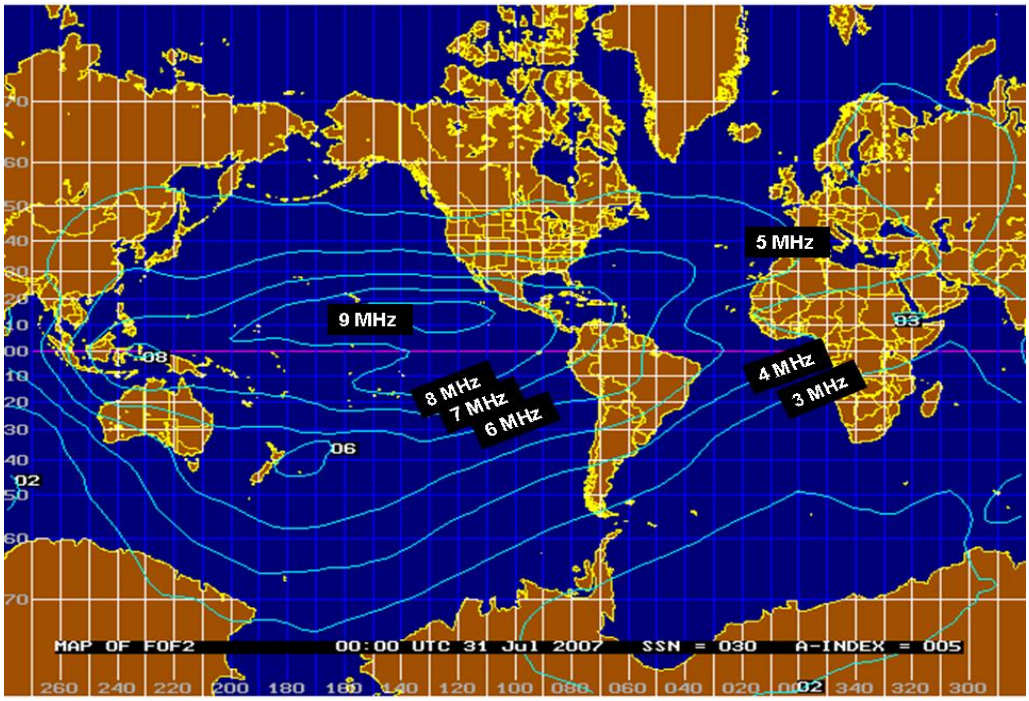

Figure 50. Global Map of F2-layer Critical Frequencies for SSN = 30 and AI = 5 at 00:00 UTC 2007/7/31.

Figures 51 and 52 show the global maps of the MUF profiles at 00:00 UTC 31 July 2007 for SSN = 30 and AI = 5. The MUFs occur in the same regions as the maximum F2-layer frequencies shown in Figure 50. Similarly, the maximum contour gradients occur where the Sun is either rising or setting. The most pronounced and easily defined is the sunrise sector because the F2-layer electron density (and hence the critical frequency) decreases slower during the sunset than it increases during the sunrise. This causes the critical frequency changes more abruptly and systematically during the sunrise than it does during the sunset. Higher F2-layer critical frequencies will produce correspondingly higher MUFs for a given distance since the increased F2-layer ionization will reflect signals with higher frequencies. The map in Figure 51 shows the MUFs in MHz for the path distance of 700 km and each point on the map is the midpoint of a 700 km path. For example, this map shows that North America has an MUF of 7 to 9 MHz for a distance of 700 km. Therefore, it is expected to see an MUF of 7 to 9 MHz when the 700 km signal path passed over North America. This map is only applicable for signals

that travel 700 km in ground distance. The same situation is applied in Figure 52 which shows the MUFs for the path distance of 3,500 km.

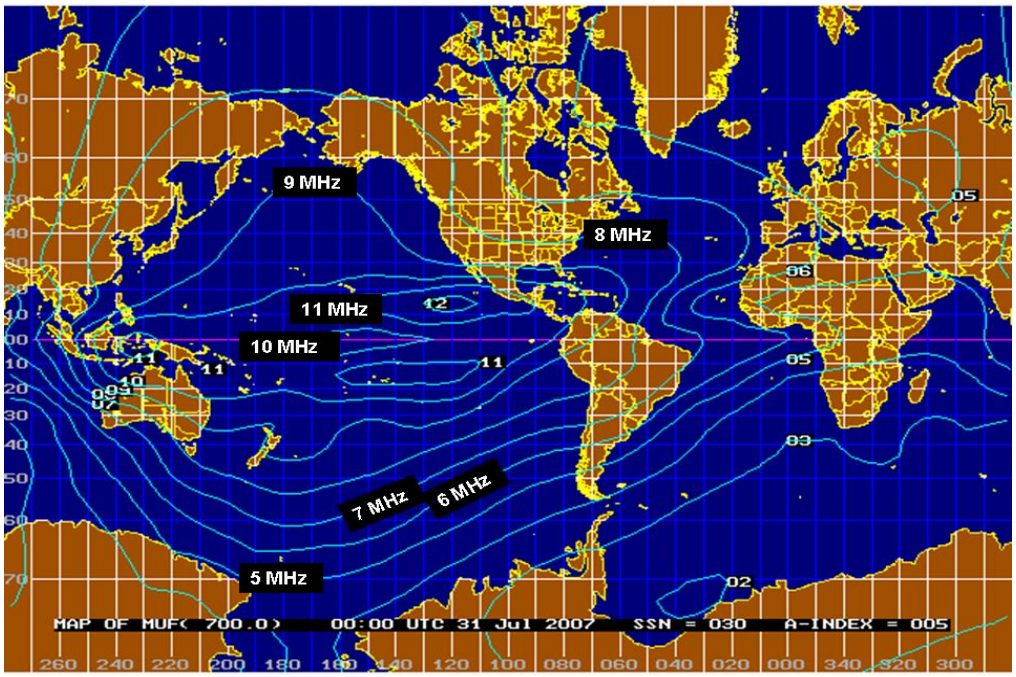

Figure 51. Maximum Usable Frequency at 700 km Distance for SSN = 30 and AI = 5 at 00:00 UTC 2007/7/31.

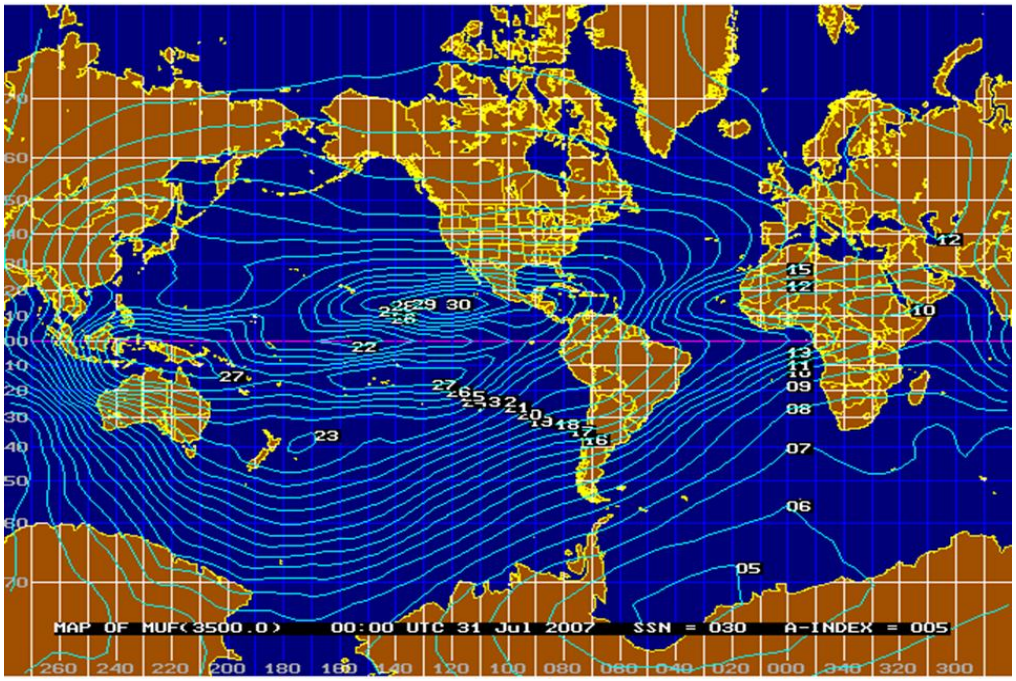

Figure 52. Maximum Usable Frequency at 3500 km Distance for SSN = 30 and AI = 5 at 00:00 UTC 2007/7/31.

Rays in the elevation angles from $0°$ to $20°$ with $f_c = 6$, 8, 10, 12, 14, 16, 18, 20, and 22 MHz frequencies are shown in Figures 53 through 61 respectively. In these ray tracing screens, the skip distance is defined as the minimum distance between the transmitter location and the point where the skywave first turns to the Earth's and there is no signal received within this region.

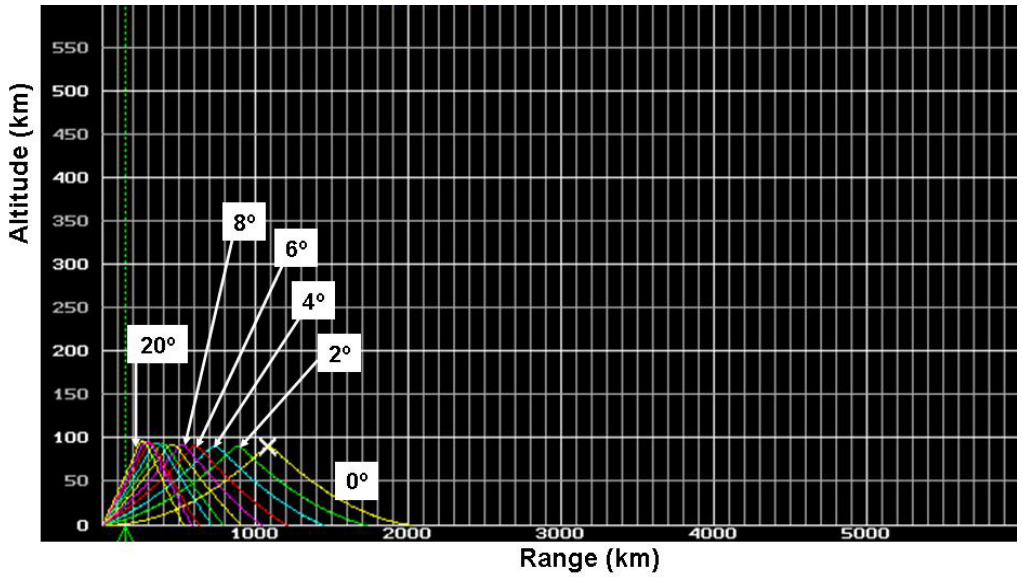

Figure 53. Rays in an Elevation Angle from $0°$ to $20°$ at 6 MHz Frequency for SSN = 30 and AI = 5 at 00:00 UTC 2007/7/31.

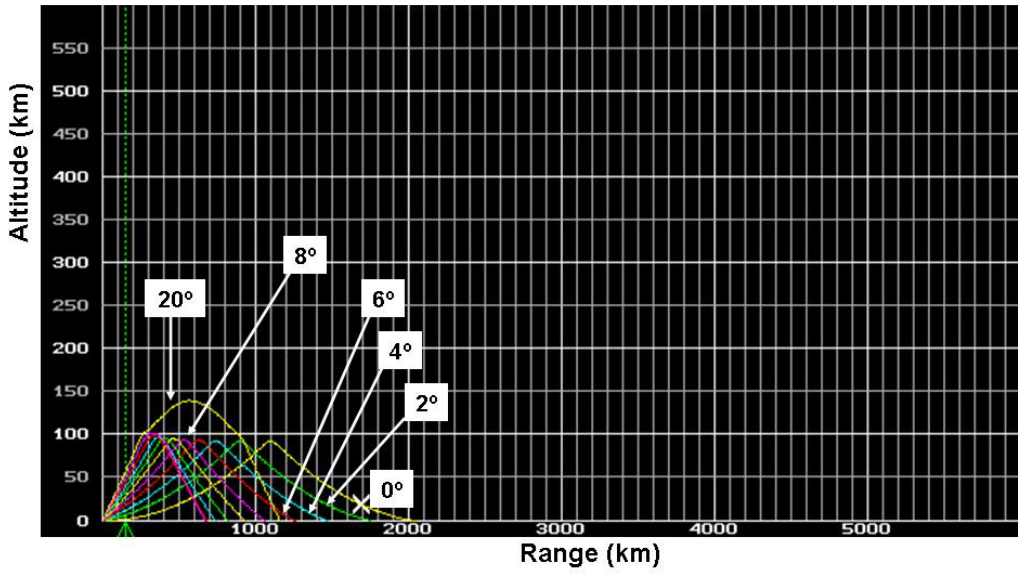

Figure 54. Rays in an Elevation Angle from $0°$ to $20°$ at 8 MHz Frequency for SSN = 30 and AI = 5 at 00:00 UTC 2007/7/31.

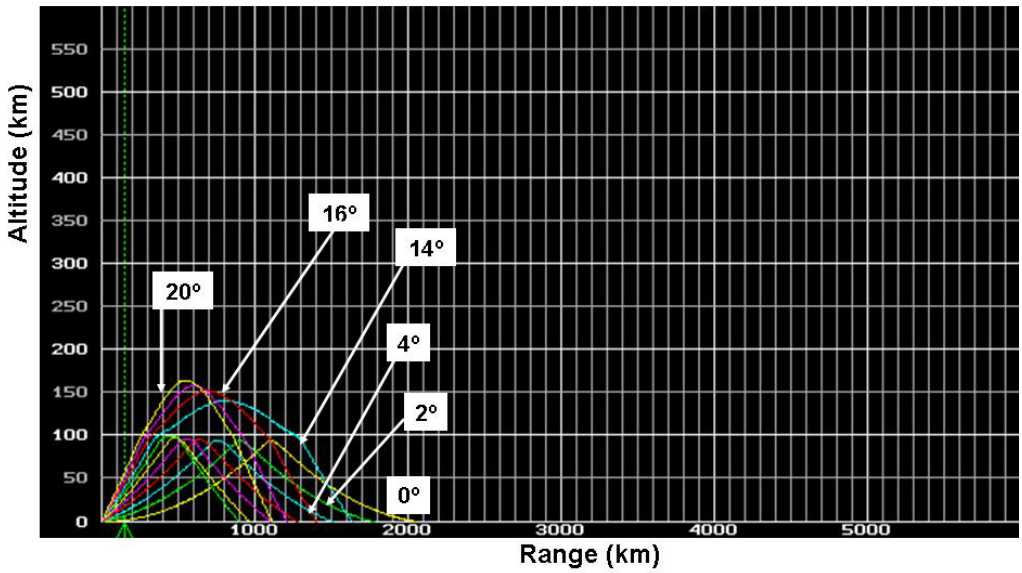

Figure 55. Rays in an Elevation Angle from 0° to 20° at 10 MHz Frequency for SSN = 30 and AI = 5 at 00:00 UTC 2007/7/31.

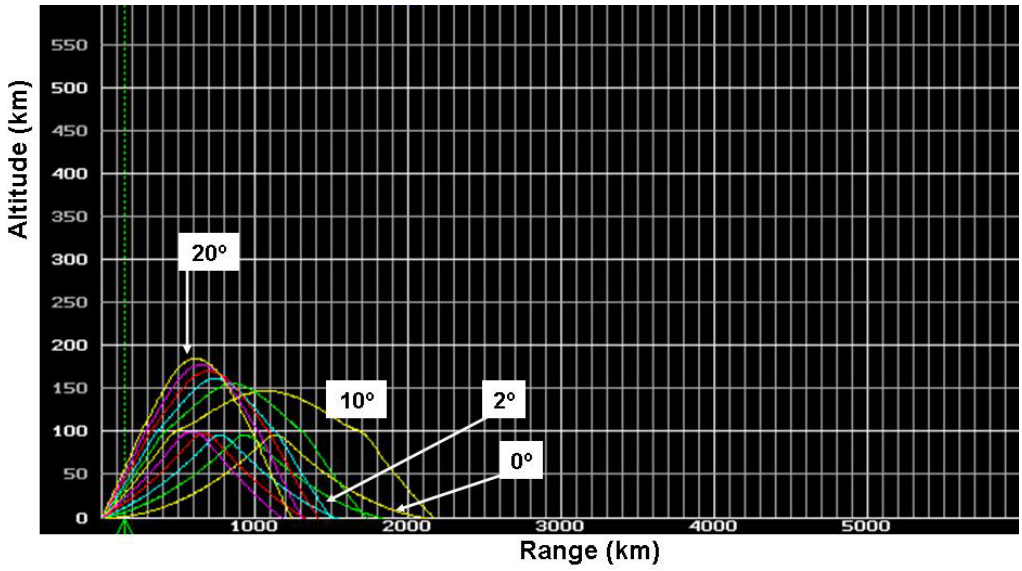

Figure 56. Rays in an Elevation Angle from 0° to 20° at 12 MHz Frequency for SSN = 30 and AI = 5 at 00:00 UTC 2007/7/31.

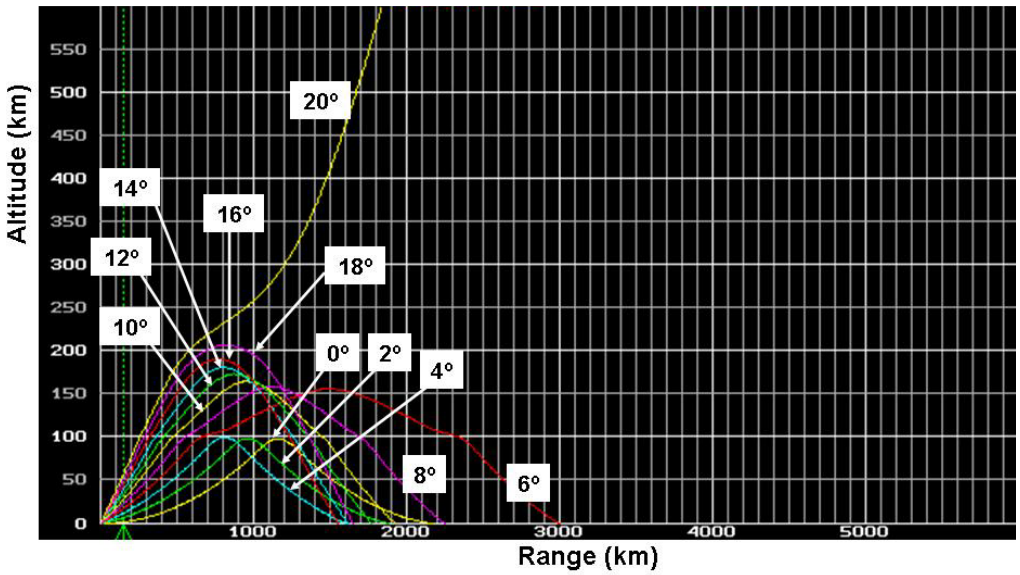

Figure 57. Rays in an Elevation Angle from 0° to 20° at 14 MHz Frequency for SSN = 30 and AI = 5 at 00:00 UTC 2007/7/31.

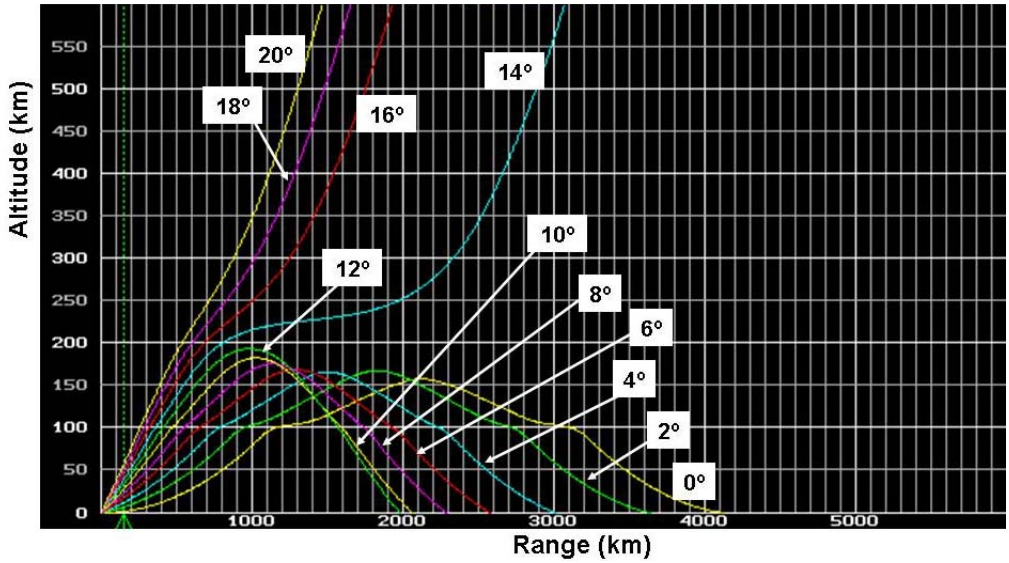

Figure 58. Rays in an Elevation Angle from 0° to 20° at 16 MHz Frequency for SSN = 30 and AI = 5 at 00:00 UTC 2007/7/31.

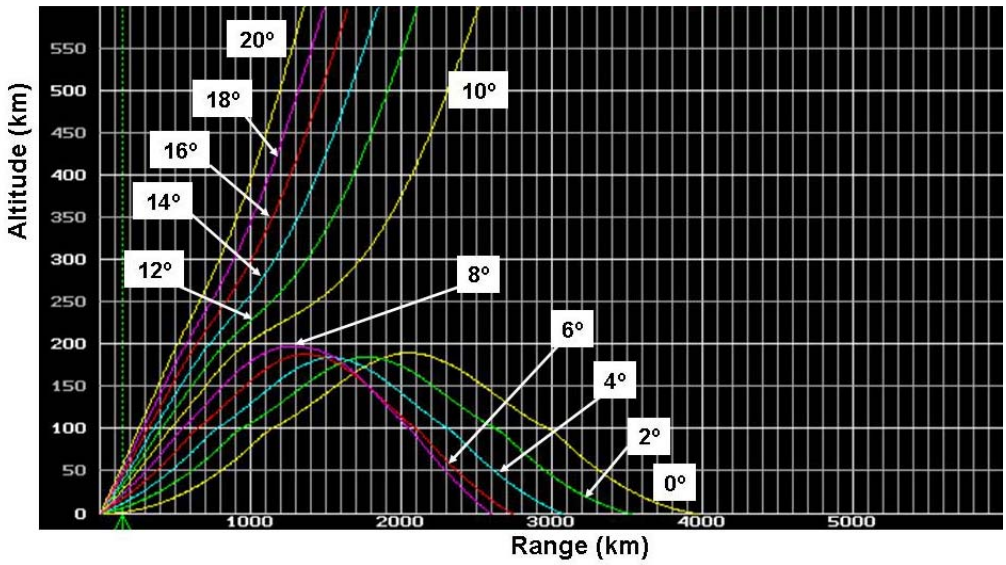

Figure 59. Rays in an Elevation Angle from 0° to 20° at 18 MHz Frequency for SSN = 30 and AI = 5 at 00:00 UTC 2007/7/31.

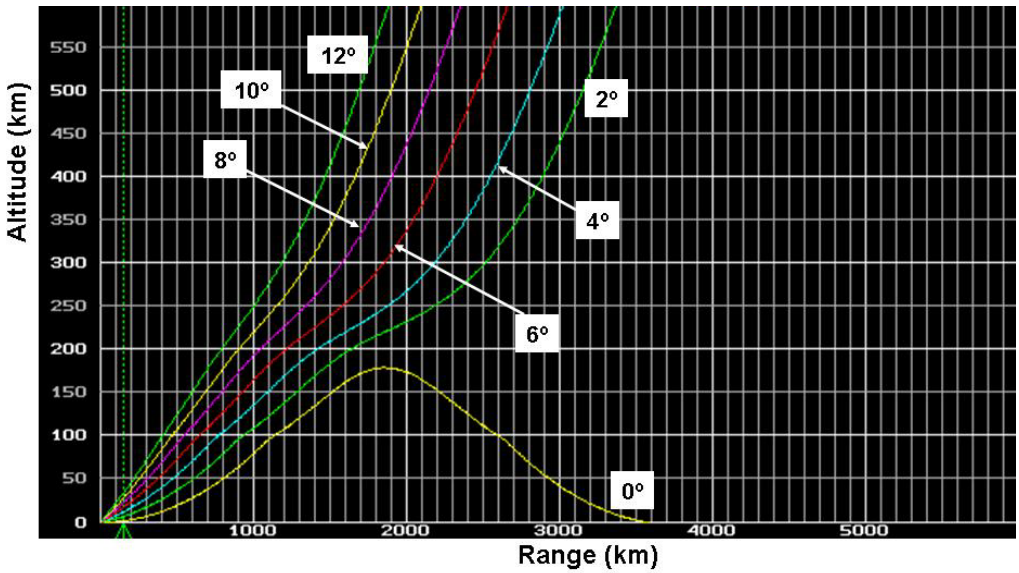

Figure 60. Rays in an Elevation Angle from 0° to 20° at 20 MHz Frequency for SSN = 30 and AI = 5 at 00:00 UTC 2007/7/31.

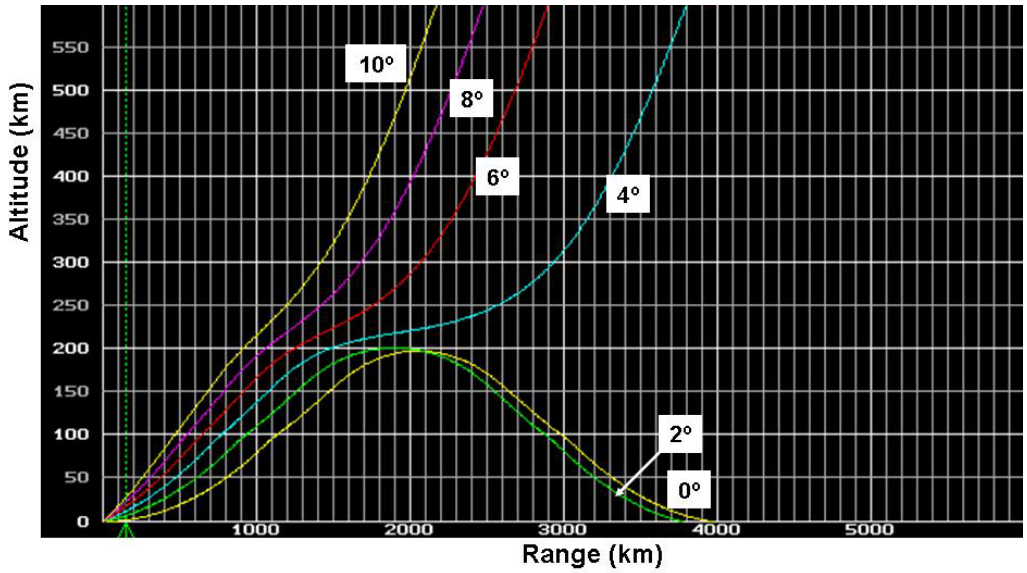

Figure 61. Rays in an Elevation Angle from 0° to 20° at 22 MHz Frequency for SSN = 30 and AI = 5 at 00:00 UTC 2007/7/31.

Based on the simulation results, the longest detection distance is up to 4,000 km when the operating frequency is at approximately 16 MHz with an elevation angle of 0 degrees also shown in Figures 47 and 58. An overview plot of the operating frequencies versus footprint coverage distances is shown in Figure 62 with text summarized in Tables 9 and 10.

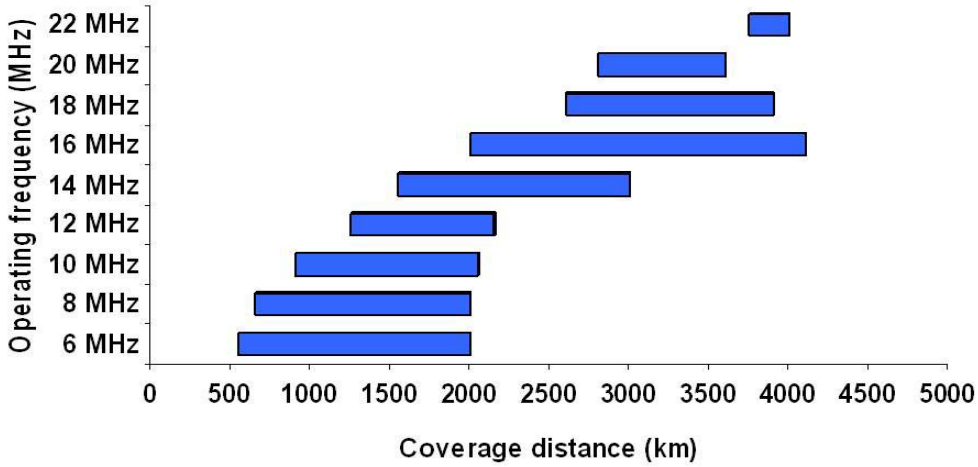

Figure 62. Footprint Coverage from 6 to 22 MHz Frequencies with Elevation Angles of 0 to 20 degrees.

Tables 9 and 10 show a summary of the results including the propagation range along the Earth's surface (in kilometers), the signal quality (in dB and percentage notation) and text code of the signal quality is tabulated from the ray tracing screens of each simulation at $f_c = 6$ to 22 MHz along with elevation angles from 0 to 20 degrees. Based on the results, the maximum detection range is up to 4,100 km at $f_c = 16$ MHz and the maximum footprint coverage distance is up to 2,100 km (from 2,000 to 4,100 km) at $f_c = 16$ MHz as well. Since the maximum detection range occurs when $f_c = 16$ MHz, the detailed ray tracing screen entries are tabulated in Tables 11 and 12 by simulating at $f_c = 16$ MHz with the elevation angles of 0 to 20 degrees.

Degrees / Freq		0	2	4	6	8	10	12	14	16	18	20
6 MHz	Range (km)	2000	1700	1400	1200	1050	900	800	700	650	600	550
	Sig Qual(dB)	0	4	14	21	28	34	38	42	45	48	50
	Signal(%)	0	7	26	42	55	66	75	83	89	94	99
	Sig Qual	BLKOUT	P-VP	F-P	G-F	GOOD	GOOD	GOOD	VGOOD	VGOOD	VGOOD	VGOOD
8 MHz	Range (km)	2000	1750	1450	1250	1050	900	800	750	700	650	1150
	Sig Qual(dB)	1	18	26	33	38	42	46	49	51	53	50
	Signal(%)	0	35	52	64	75	84	91	97	100	100	98
	Sig Qual	BLKOUT	F	GOOD	GOOD	GOOD	VGOOD	VGOOD	VGOOD	VGOOD	VGOOD	VGOOD
10 MHz	Range (km)	2050	1750	1500	1550	1100	950	900	1600	1400	1200	1100
	Sig Qual(dB)	7	25	33	39	43	47	50	47	50	51	52
	Signal(%)	13	50	65	77	86	94	99	93	98	100	100
	Sig Qual	P-VP	GOOD	GOOD	GOOD	VGOOD	VGOOD	VGOOD	VGOOD	VGOOD	VGOOD	VGOOD
12 MHz	Range (km)	2100	1800	1500	1300	1200	2150	1700	1500	1400	1300	1250
	Sig Qual(dB)	11	30	37	43	47	44	47	49	49	50	51
	Signal(%)	22	59	74	84	93	87	93	96	98	100	100
	Sig Qual	P-F	GOOD	GOOD	VGOOD	VGOOD	VGOOD	VGOOD	VGOOD	VGOOD	VGOOD	VGOOD
14 MHz	Range (km)	2100	1900	1600	3000	2250	1900	1750	1600	1550	1650	N
	Sig Qual(dB)	14	33	40	38	43	45	47	48	49	48	45
	Signal(%)	28	64	79	76	84	89	92	95	96	95	89
	Sig Qual	F-P	GOOD	GOOD	GOOD	VGOOD	VGOOD	VGOOD	VGOOD	VGOOD	VGOOD	VGOOD

Table 9. Numerical Value of Range and Signal Quality at 6, 8, 10, 12, and 14 MHz with Elevation Angles of 0 to 20 Degrees for SSN = 30 and AI = 5 at 00:00 UTC 2007/7/31.

Degrees / Freq		0	2	4	6	8	10	12	14	16	18	20
16 MHz	Range (km)	4100	3600	3000	2550	2300	2050	2000	-	-	-	-
	Sig Qual(dB)	11	29	36	40	42	44	46	42	45	48	49
	Signal(%)	20	56	70	78	84	88	90	84	89	94	97
	Sig Qual	P-F	GOOD	GOOD	GOOD	VGOOD	VGOOD	VGOOD	VGOOD	VGOOD	VGOOD	VGOOD
18 MHz	Range (km)	3900	3500	3050	2700	2600	-	-	-	-	-	-
	Sig Qual(dB)	11	29	35	39	41	43	43	45	48	49	49
	Signal(%)	21	57	70	77	82	84	84	89	95	97	97
	Sig Qual	P-F	GOOD	GOOD	GOOD	VGOOD	VGOOD	VGOOD	VGOOD	VGOOD	VGOOD	VGOOD
20 MHz	Range (km)	3600	-	-	2800	3300	-	-	-	-	-	-
	Sig Qual(dB)	12	29	36	39	39	43	45	45	47	49	49
	Signal(%)	23	58	70	77	77	85	89	89	93	97	97
	Sig Qual	P-F	GOOD	GOOD	GOOD	GOOD	VGOOD	VGOOD	VGOOD	VGOOD	VGOOD	VGOOD
22 MHz	Range (km)	4000	3750	-	-	-	-	-	-	-	-	-
	Sig Qual(dB)	41	42	41	44	45	47	48	49	49	49	49
	Signal(%)	81	82	82	86	89	93	95	97	97	97	97
	Sig Qual	VGOOD	VGOOD	VGOOD	VGOOD	VGOOD	VGOOD	VGOOD	VGOOD	VGOOD	VGOOD	VGOOD

Table 10. Numerical Value of Range and Signal Quality at 16, 18, 20, and 22 MHz with Elevation Angles of 0 to 20 Degrees for SSN = 30 and AI = 5 at 00:00 UTC 2007/7/31.

Frequency (MHz)	16	16	16	16	16	16
Degrees	**0**	**2**	**4**	**6**	**8**	**10**
CUR Lat	69.0690	64.7178	59.0827	55.1665	52.5865	50.5700
CUR Lon	241.2200	241.2200	241.2200	241.2200	241.2200	241.2200
Air Dist. (km)	4192.00	3708.00	3076.00	2640.00	2356.00	2136.00
Cur Angle	-1.5299	-2.4996	-4.2756	-6.2340	-8.1578	-10.1433
Signal Qual (dB)	11	29	36	40	42	44
Signal	20%	56%	70%	78%	84%	88%
Mag Lat	+57.75	+53.41	+47.78	+43.85	+41.29	+39.27
Mag Lon	174.27	173.86	173.45	173.21	173.07	172.97
Sol Elv	+26.33	+27.70	+29.22	+30.12	+30.62	+30.97
Sig Qual	P-F	GOOD	GOOD	GOOD	VGOOG	VGOOG
Height	-0.02	-0.16	-0.31	-0.01	-0.66	-0.71
Ne	0e+0	0e+0	0e+0	0e+0	0e+0	0e+0
Plasma	0.000	0.000	0.000	0.000	0.000	0.000
Aur Lat	+80.66	+80.66	+80.66	+80.66	NoZone	NoZone
Aur Lon	241.15	241.15	241.15	241.15	NoZone	NoZone
Aur Dist.	0.0	0.0	0.0	0.0	0.0	0.0
Iono Dist. (km)	2520.0	2316.0	1948.0	1728.0	1588.0	1488.0

Table 11. Data with Elevation Angles from 0 to 10 Degrees at 16 MHz Frequency for SSN = 30 and AI = 5 at 00:00 UTC 2007/7/31.

Frequency (MHz)	16	16	16	16	16
Degrees	**12**	**14**	**16**	**18**	**20**
CUR Lat	49.8096	59.6858	56.7134	47.9338	45.7951
CUR Lon	241.2200	241.2200	241.2200	241.2200	241.2201
Air Dist. (km)	2060.00	3288.00	2492.00	1952.00	1716.00
Cur Angle	-12.1451	+26.8337	+27.5537	+28.6984	+29.9416
Signal Qual (dB)	46	42	45	48	49
Signal	90%	84%	89%	94%	97%
Mag Lat	+38.51	+48.38	+41.42	+36.64	+34.50
Mag Lon	172.93	173.49	173.08	172.84	172.75
Sol Elv	+31.09	+29.07	+30.60	+31.37	+31.64
Sig Qual	VGOOG	VGOOD	VGOOD	VGOOD	VGOOD
Height	-0.50	601.05	601.18	600.92	601.55
Ne	0e+0	4.57e+A	6.42e+A	6.41e+A	6.42e+A
Plasma	0.000	1.920	2.275	2.277	2.275
Aur Lat	NoZone	+80.66	+80.66	NoZone	NoZone
Aur Lon	NoZone	241.15	241.15	NoZone	NoZone
Aur Dist.	0.0	0.0	0.0	0.0	0.0
Iono Dist. (km)	1492.0	3040.0	2276.0	1752.0	1540.0

Table 12. Data with Elevation Angles from 12 to 20 Degrees at 16 MHz Frequency for SSN = 30 and AI = 5 at 00:00 UTC 2007/7/31.

In Tables 11 and 12, the elevation angles are from 0 to 20 degrees with a 2 degrees increment. The definition of each entry can be found earlier in this chapter. An electron density value of zero (at elevation angles of 0 to 12 degrees) means the ray is reflected back to the Earth's surface and its ground distance for each angles is defined as "Range" (in kilometers) in the section of 16 MHz in Tables 10. The 16 MHz ray starts to penetrate into the ionosphere at the elevation angles of 14 degrees with N_e = 4.57e+A where the letter "A" represents 10 which means $N_e = 4.57 \times 10^{10}$ electrons/m^3. The signal quality coverage maps are shown and discussed in the Appendix.

C. MAXIMUM SURVEILLANCE RANGE SIMULATION

The maximum detection range of the Chinese OTH-B radar system is 3,500 km as described earlier. A target is assumed to be located at $30° \text{ N}, \ 204.3° \text{ W}$ which is 3,500 km

from the assumed transmitter location in Nanjing. Figure 63 illustrates the flow chart process in this section based on the 3,500 km detection range. The different seasons, different SSN and different FOT are simulated for the generation of the electron densities, the MUF profiles, the ray trace plots, and the signal quality coverage maps for determining the surveillance capability and performance of the Chinese OTH-B radar system. The electron density (N_e), the MUF profiles, and the ray tracing screens are generated for high/low SSN and winter/summer time.

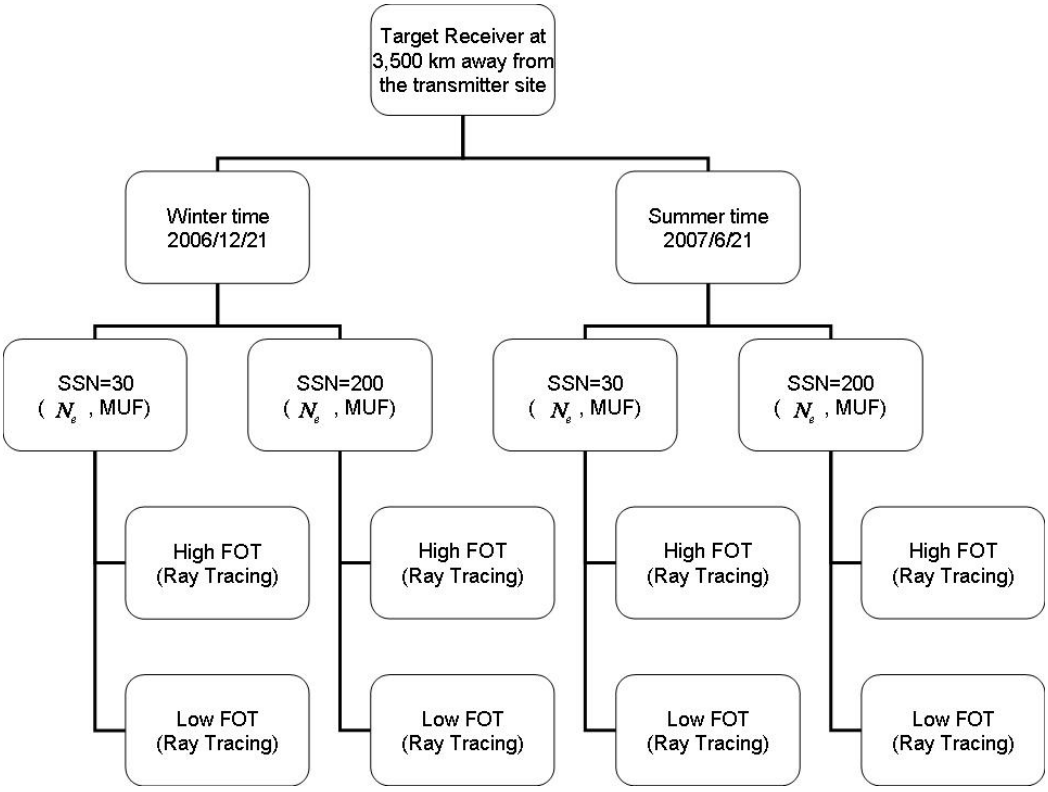

Figure 63. An Overview of the Generation Processes of the Electron Density Profiles, the MUF Profiles and the Ray Tracing Screens.

The electron density profiles at the midway location (32.377° N, 222.554° W) of the 3,500 km propagation path from the transmitter to the target in different input information are shown in Figures 64 through 67. Figures 64 and 65 illustrate the electron densities at 00:00 UTC 21 December 2006 in winter time for low SSN (SSN=30) and high SSN (SSN=200). Figures 66 and 67 illustrate the electron densities at 00:00 UTC 21 June 2007 in summer time for low SSN (SSN=30) and high SSN (SSN=200) as well.

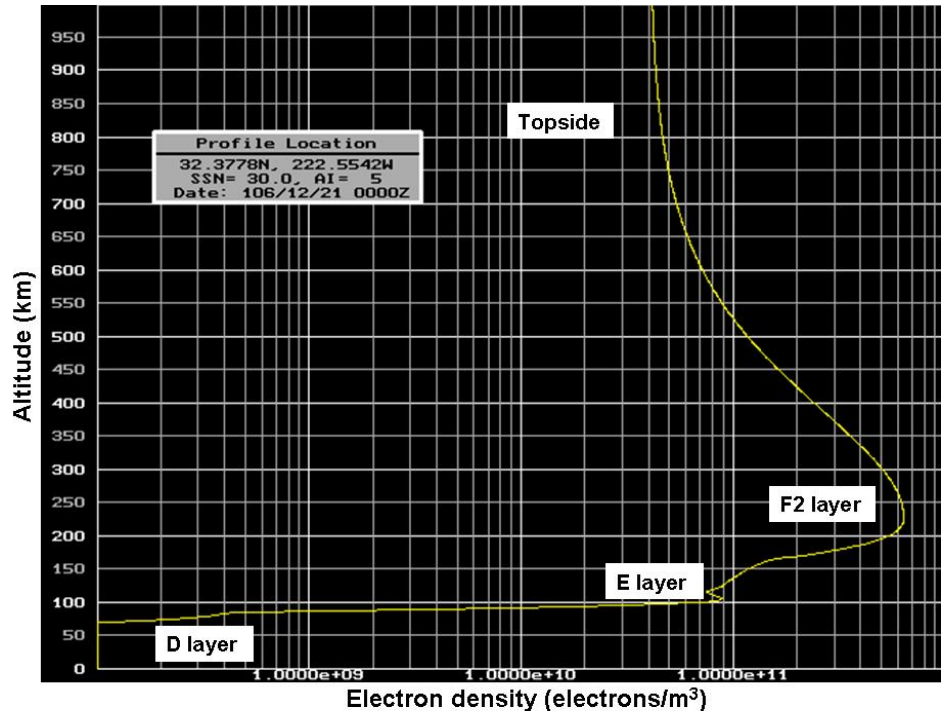

Figure 64. Ionospheric Electron Density Profile for the Chinese OTH-B Radar Analysis for SSN = 30 and AI = 5 at 00:00 UTC 2006/12/21 (winter time).

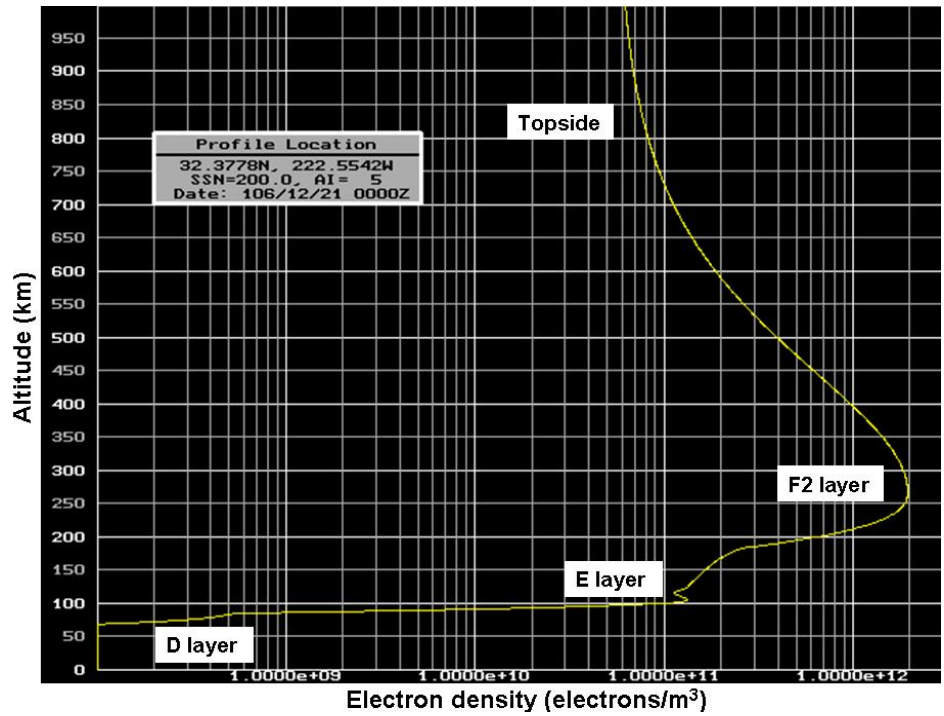

Figure 65. Ionospheric Electron Density Profile for the Chinese OTH-B Radar Analysis for SSN = 200 and AI = 5 at 00:00 UTC 2006/12/21 (winter time).

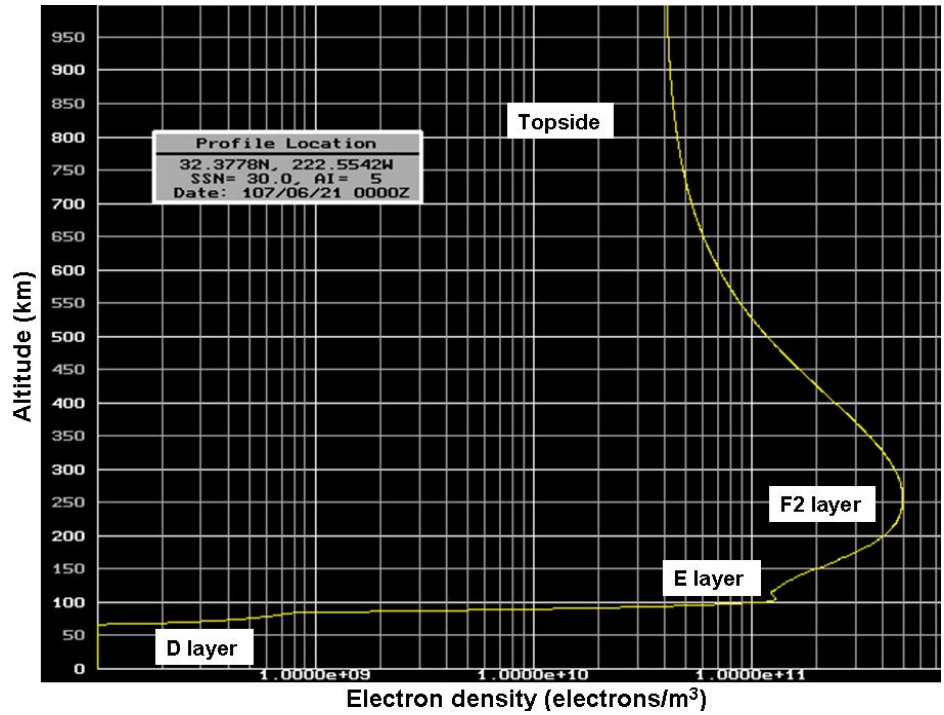

Figure 66. Ionospheric Electron Density Profile for the Chinese OTH-B Radar Analysis with SSN = 30 and AI = 5 at 00:00 UTC 2007/6/21 (summer time).

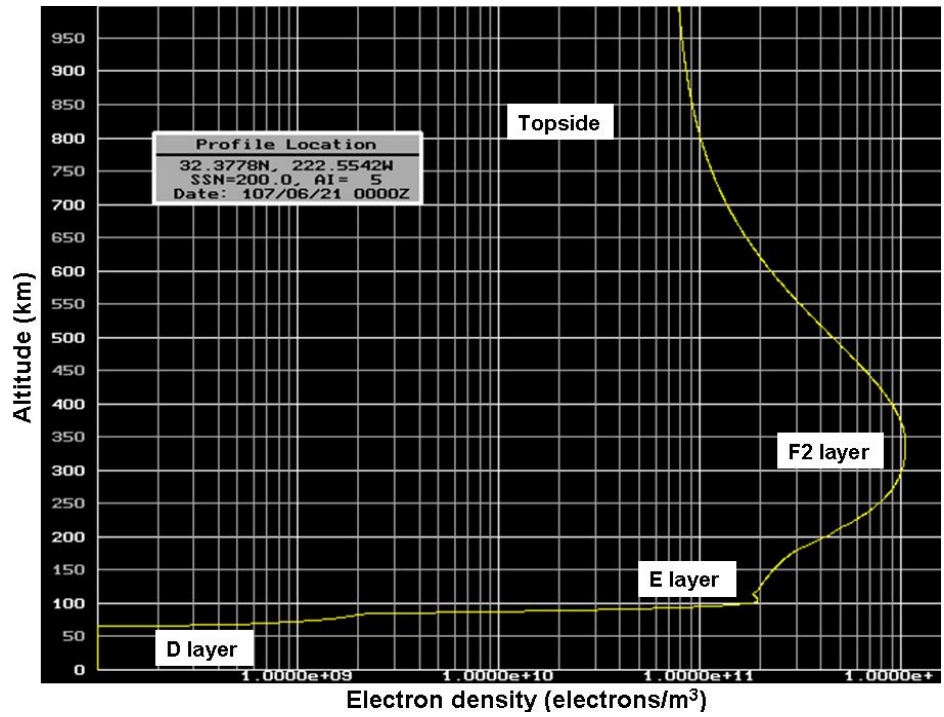

Figure 67. Ionospheric Electron Density Profile for the Chinese OTH-B Radar Analysis for SSN = 200 and AI = 5 at 00:00 UTC 2007/6/21 (summer time).

The MUF profiles corresponding to Figures 64 through 67 are shown in Figures 68 through 71. The maximum and minimum FOTs in Figure 68 are 25 MHz at 01:00 UTC and 6.8 MHz at 14:00 UTC for SSN = 30 and AI = 5 on 21 December 2006. The maximum and minimum FOTs in Figure 69 are 38 MHz at 01:00 UTC and 9.5 MHz at 19:00 UTC for SSN = 200 and AI = 5 on 21 December 2006. The maximum and minimum FOTs in Figure 70 are 22.5 MHz at 08:00 UTC and 12.8 MHz at 18:00 UTC for SSN = 30 and AI = 5 on 21 June 2007. The maximum and minimum FOTs in Figure 71 are 28 MHz at 08:00 UTC and 20 MHz at 19:00 UTC for SSN = 200 and AI = 5 on 21 June 2007. The signal quality coverage maps simulated based on the maximum/minimum FOT from the MUF profiles are discussed in the Appendix.

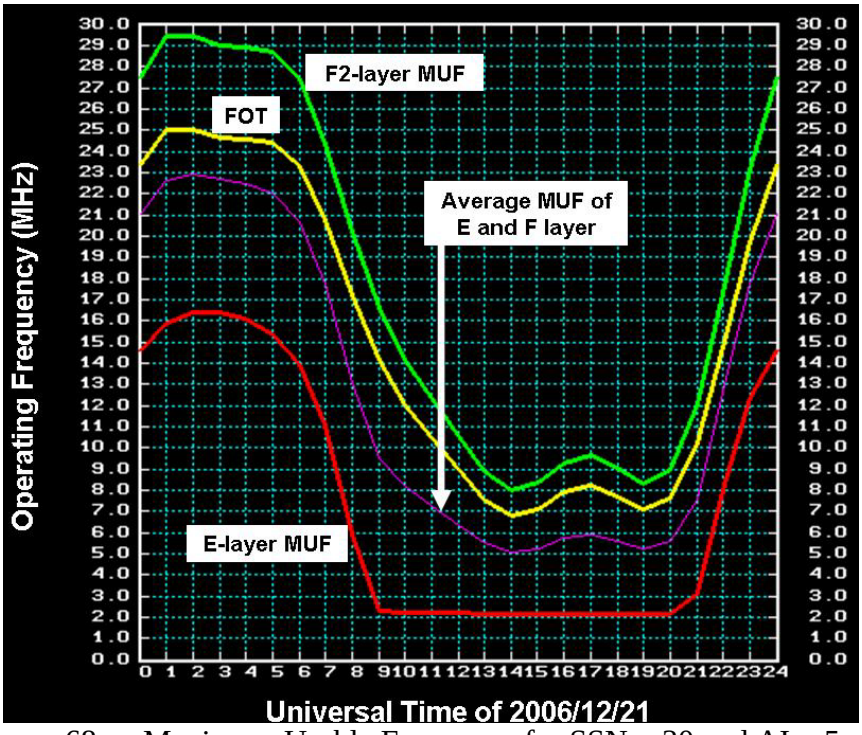

Figure 68. Maximum Usable Frequency for SSN = 30 and AI = 5 on 2006/12/21 (winter time).

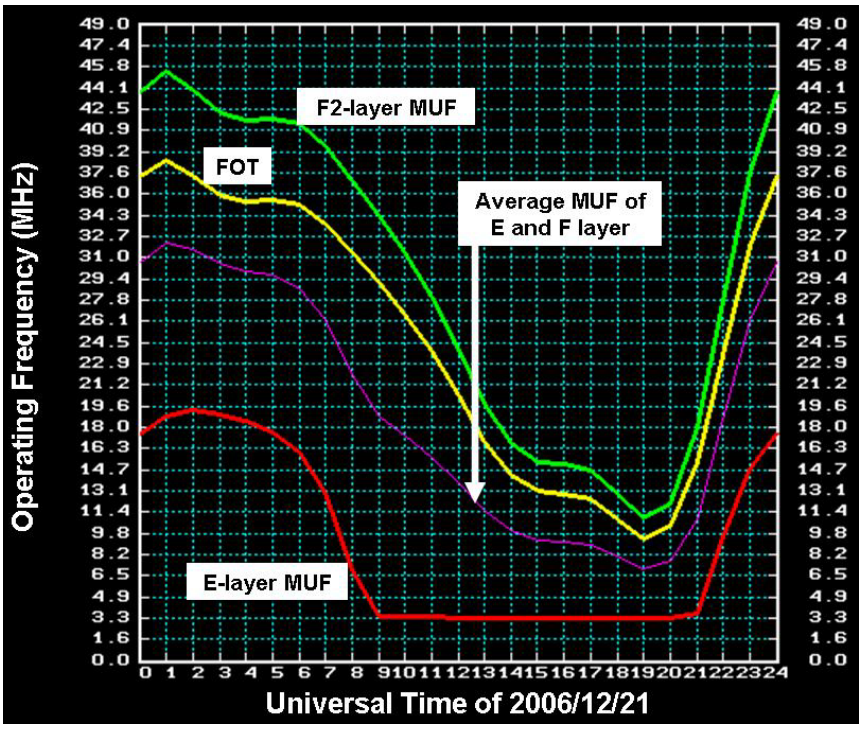

Figure 69. Maximum Usable Frequency for SSN = 200 and AI = 5 on 2006/12/21 (winter time).

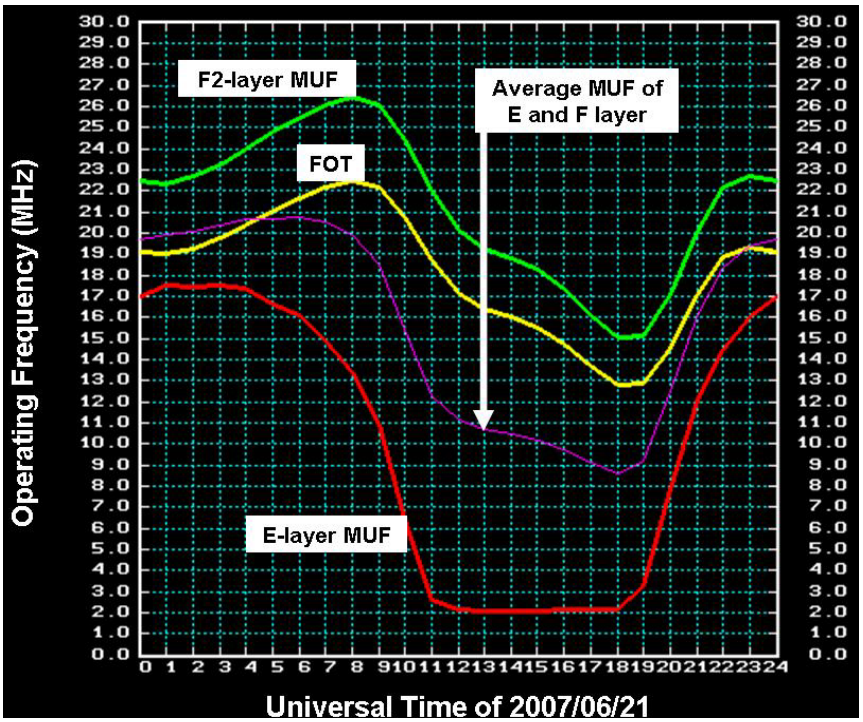

Figure 70. Maximum Usable Frequency for SSN = 30 and AI = 5 on 2007/6/21 (summer time).

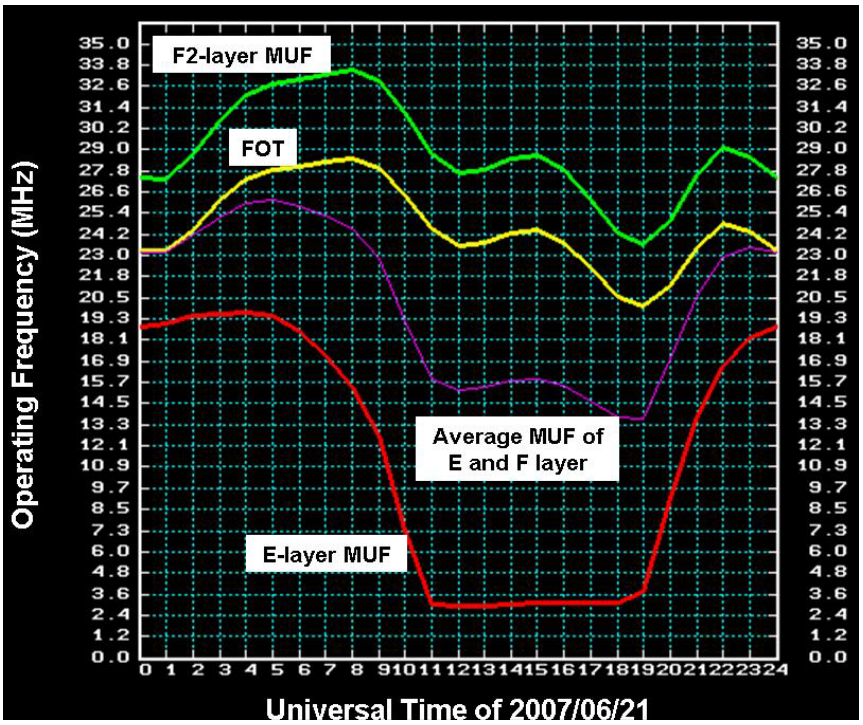

Figure 71. Maximum Usable Frequency for SSN = 200 and AI = 5 on 2007/6/21 (summer time).

The ray tracing screens associated to the high/low FOT for SSN = 30/200 and AI = 5 at specific times are shown in Figures 72 through 79.

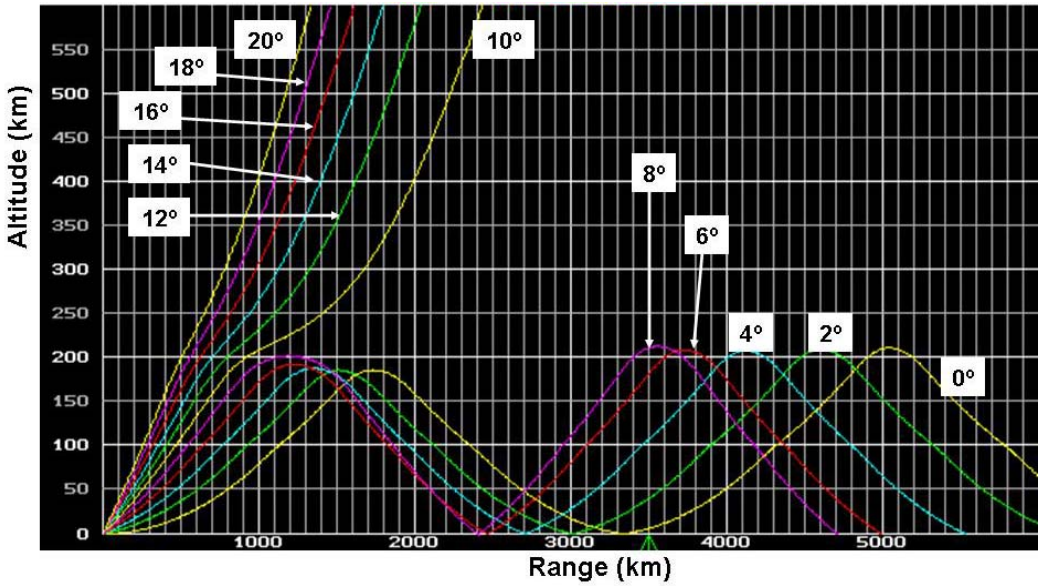

Figure 72. Ray Tracing Screen at High FOT = 25 MHz for SSN = 30 and AI = 5 at 01:00 UTC 2006/12/21.

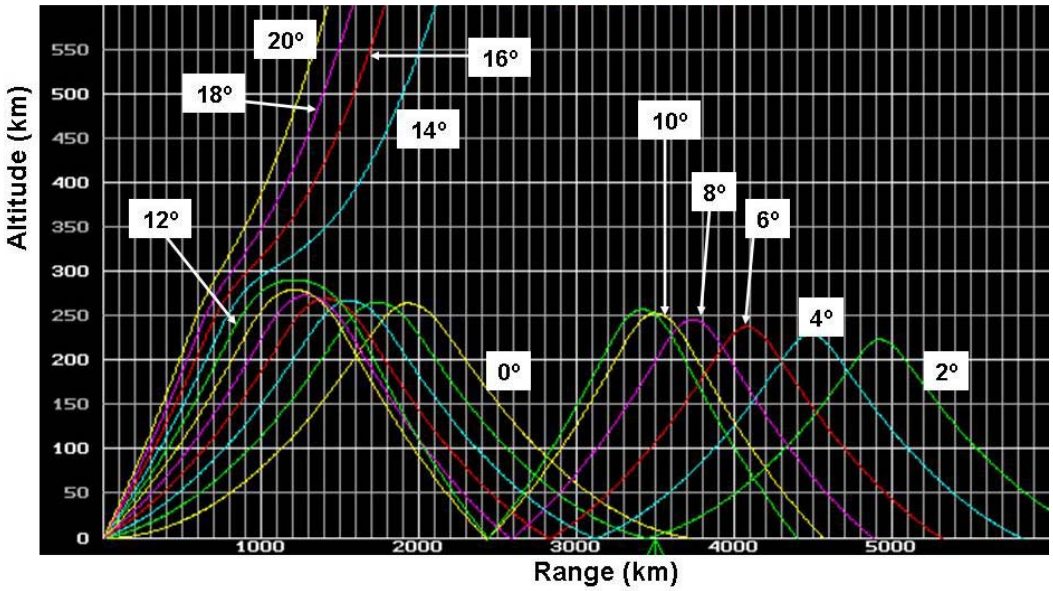

Figure 73. Ray Tracing Screen at Low FOT = 6.8 MHz for SSN = 30 and AI = 5 at 14:00 UTC 2006/12/21.

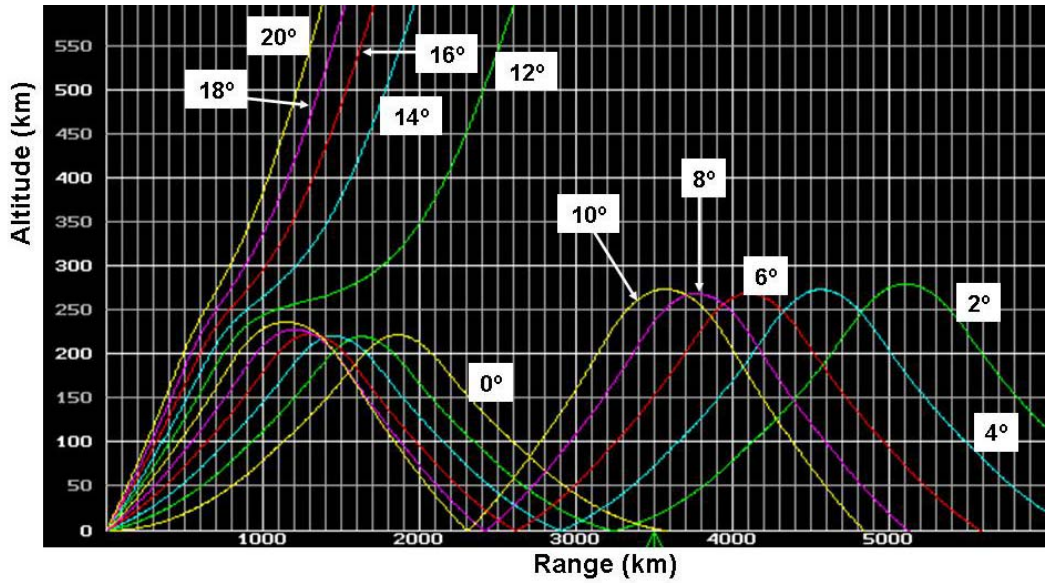

Figure 74. Ray Tracing Screen at High FOT = 38 MHz for SSN = 200 and AI = 5 at 01:00 UTC 2006/12/21.

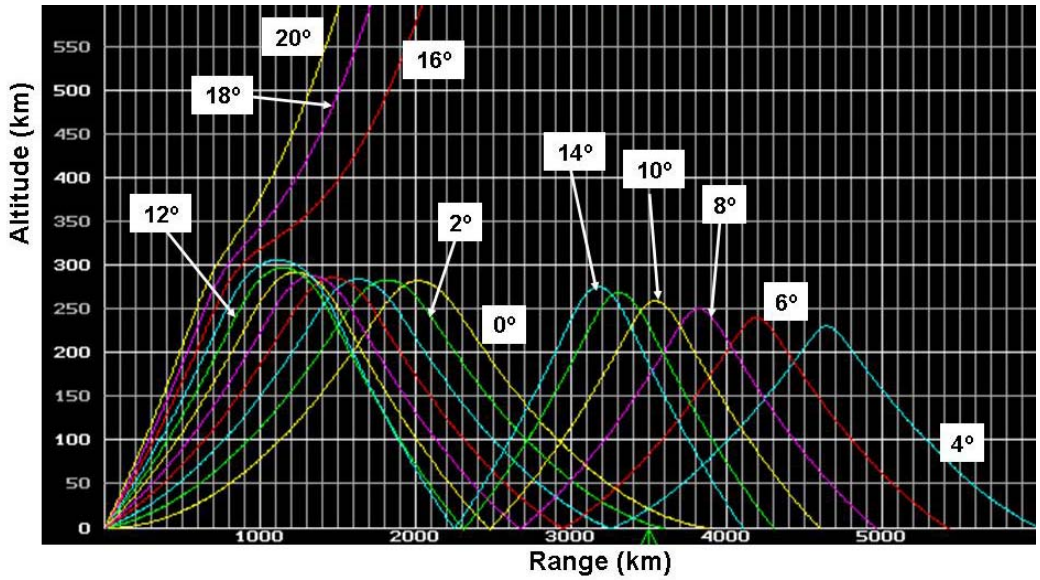

Figure 75. Ray Tracing Screen at Low FOT = 9.5 MHz for SSN = 200 and AI = 5 at 19:00 UTC 2006/12/21.

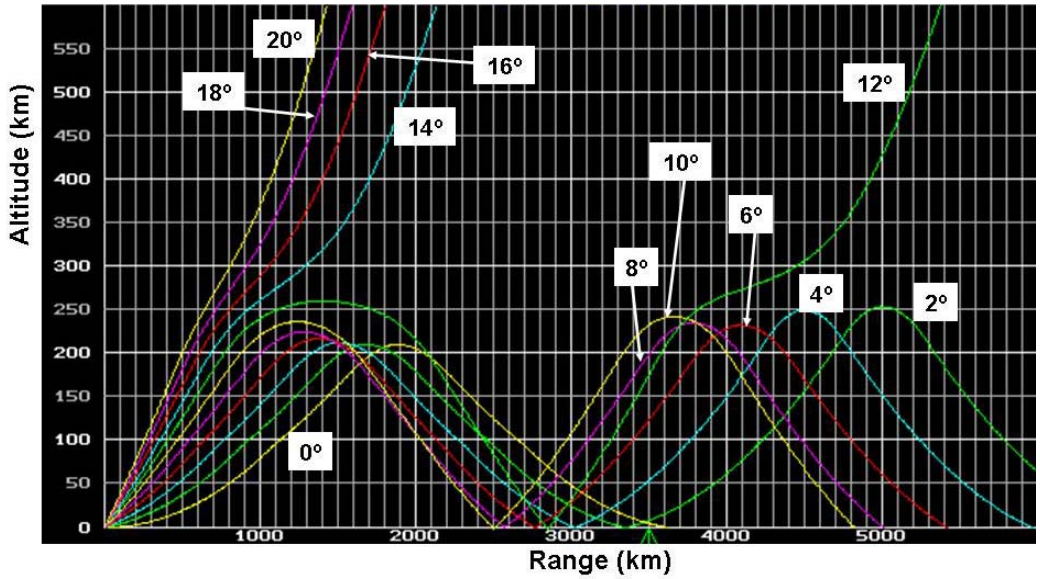

Figure 76. Ray Tracing Screen at High FOT = 22.5 MHz for SSN = 30 and AI = 5 at 08:00 UTC 2007/6/21.

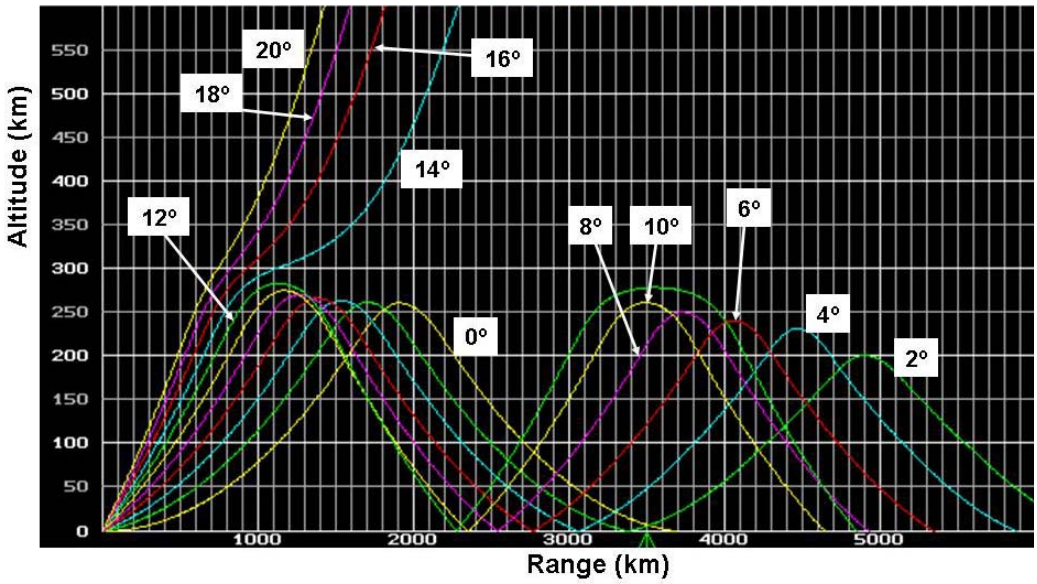

Figure 77. Ray Tracing Screen at Low FOT = 12.8 MHz for SSN = 30 and AI = 5 at 18:00 UTC 2007/6/21.

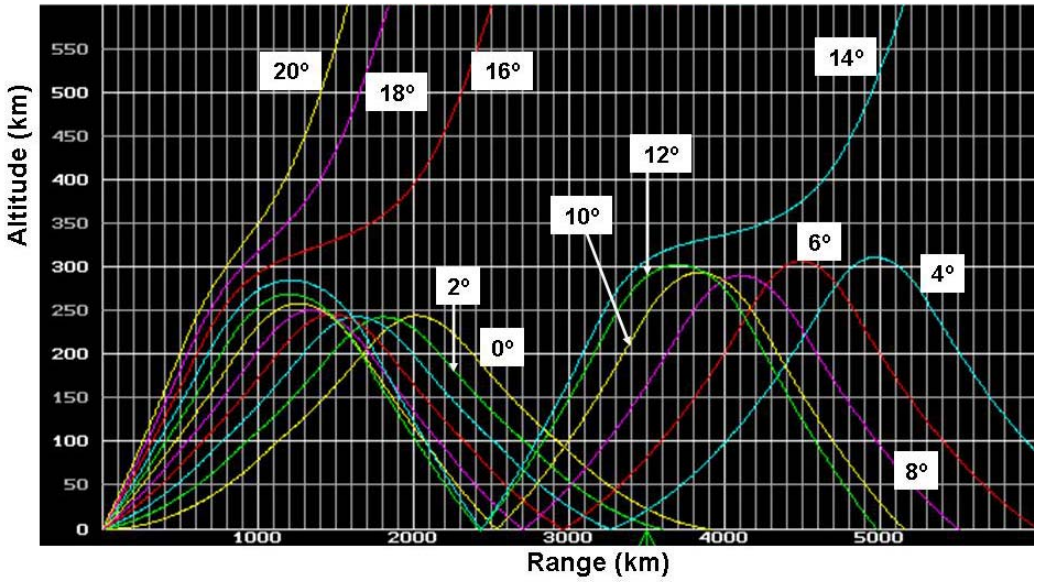

Figure 78. Ray Tracing Screen at High FOT = 28 MHz for SSN = 200 and AI = 5 at 08:00 UTC 2007/6/21.

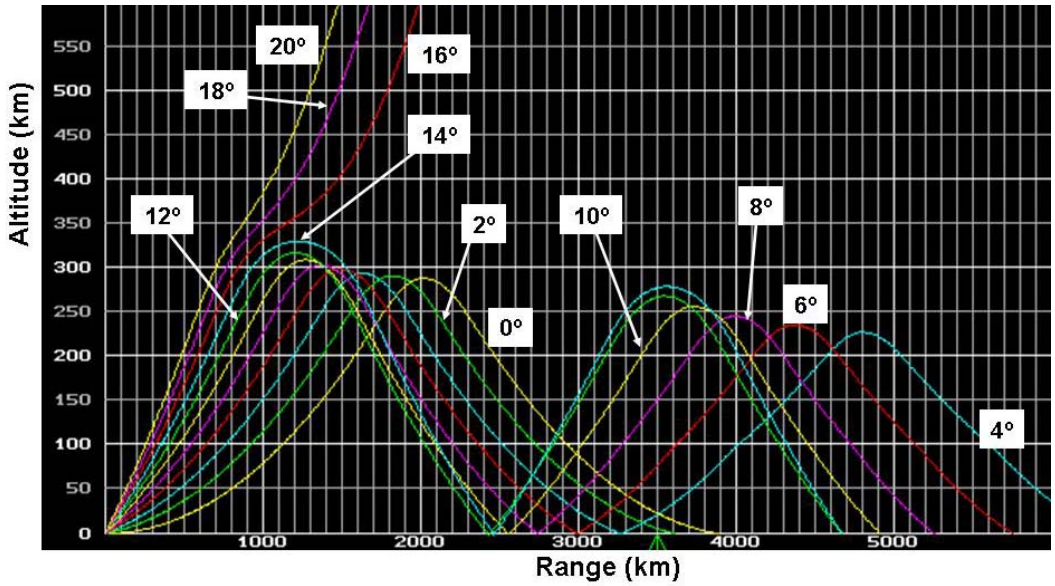

Figure 79. Ray Tracing Screen at Low FOT = 20 MHz for SSN = 200 and AI = 5 at 19:00 UTC 2007/6/21.

The rays in Figures 72 through 79 are generated with elevation angles of 0 to 20 degrees with 2 degrees increment. The footprint coverage is approximately from 2,200 km to 3,900 km from the ray tracing simulation results above. The skip zone varies from 2,200 km (for SSN = 200 at 9.5 MHz at 01:00 UTC 21 December 2006 as shown in Figure 75) to 2,500 km (for SSN = 30 at 22.5 MHz at 08:00 UTC 21 June 2007 as shown in Figure 76). The elevation angles which cause the ray to penetrate into the ionosphere vary from 10 degrees (at 25 MHz as shown in Figure 72) to 16 degrees (at 9.5 MHz as shown in Figure 75, 28 MHz shown in Figure 78, and 20 MHz shown in Figure 79).

D. CHAPTER SUMMARY

This chapter is mainly focused on the simulation of the Chinese OTH-B radar system and performs the PROPLAB capabilities. From the simulation results shown in this chapter, the electron density and the MUF profiles are great references for choosing the appropriate operating frequency used by the radar system to have a better detection performance. The prediction of the footprint can help determine the surveillance coverage area of the radar system. In order to fulfill the detection performance of the

radar system, it is necessary not only to have an effective frequency and antenna elevation angle, but also to have the antenna pointed in the right direction. Depending on the location of the targets, the best resolution would occur when the high gain antenna direction is pointed in the direction of the desired targets. PROPLAB is a good tool to design a radar antenna with an effective azimuth angle and elevation angle to obtain the greatest performance for its designated mission by running through the required simulations. There seems to be a discrepancy concerning the signal quality coverage maps and the ray trace results. Therefore, the signal quality coverage maps are shown and discussed in the Appendix.

THIS PAGE INTENTIONALLY LEFT BLANK

VI. CONCLUSION

A. SUMMARY OF RESULTS

The basic concept of the structure and properties of the ionosphere are discussed to explain how the performance of the OTHR system is affected. An overview of the OTHR system characteristics and performance are presented along with some applications currently used around the world, including their geographic location and historical background. The waveforms used for the OTHR systems include simple pulse, pulse Doppler, phased-coded pulse, FMCW, and FMICW. Other characteristics such as target detection methods and the skywave OTHR range equation are also discussed.

A model of the maximum detection range for the Chinese FMCW OTH-B radar was developed in MATLAB. An intercept receiver maximum interception range was also analyzed. Simulation results indicate that the minimum required input SNR for a target with 100 m^2 cross section at 3,500 km footprint range is -52.4 dB at $f_c = 14.5$ MHz. In addition, a non-cooperative intercept receiver requires a minimum input SNR of 94 dB for a square law detector and 97 dB for a linear detector for interception at a footprint range of 3,500 km at $f_c = 14.5$ MHz. A ray tracing technique was also used in PROPLAB to present a more detailed analysis. The analysis included the electron density profile, the maximum MUF profile, the critical frequency of the layers, the footprint coverage prediction, and the signal quality coverage map (discussed in the Appendix). The simulations focused on the Chinese OTH-B radar system are for the prediction of the Chinese surveillance capabilities. Also, an assumed target set at the location of 3,500 km away from the transmitter is used for simulate the performance at the radar's maximum detection range.

B. FUTURE WORK

The detailed results in this thesis were obtained using the PROPLAB simple ray tracing techniques. A more comprehensive three-dimensional simulation capability can

also be used to increase the accuracy of the results. The signal quality through the day at different ranges can be further simulated for investigating the vulnerability of the desired target area. On the radar operator's point of view, the signal quality coverage should be maximized to have better surveillance and reconnaissance capabilities. On the other hand, the signal strength might need to be minimized to avoid being intercepted. Furthermore, after having the signal quality information at the target, the target signal strength and the target cross section product can be used as the next step input of the transmitted power and then calculate the maximum interception range using the integration time. This can be used to investigate the loss from the transmitter to the target and the reciprocal direction back to the receiver. A minimum required SNR at the receiver site can be then explored. Also, a narrow elevation antenna beam can be investigated to perform the signal quality coverage maps capability and to compare the results with the results in this thesis

It is favorable to modify the PROPLAB code and put the target distance and the receiver SNR together as the input parameters for easier mathematical calculation and prediction. Other OTHR systems can also be analyzed quickly using the tools described in this thesis. In addition, the concepts of the OTHR systems counter-targeting can also be investigated.

APPENDIX

Figures 80 to 86 are simple broadcast coverage maps showing the signal quality of the Chinese OTH-B radar with a maximum detection range of 3,500 km with the transmitter and receiver location separated by 150 km (shown in Figure 44 in Chapter V) at $f_c = 6$, 8, 10, 12, 14, 16, and 18 MHz for SSN = 30 and AI = 5 at 00:00 UTC 31 July 2007. There is no sufficient information for PROPLAB to run the signal quality coverage maps at the frequencies higher than 20 MHz since most of the rays penetrate to the ionosphere and are not reflected back to the Earth at this time.

The signal quality profile is run with an elevation angle of 0 to 20 degrees corresponding to the previous ray trace simulations in Chapter V. The skip distance for 6 MHz frequency is 550 km which is as the inner circle boundary in Figure 80 and the footprint range extends to greater than 2,000 km and corresponds to the ray tracing screen in Figure 53 and Table 9 (Chapter V). The first skip zone is increasing from 500 km (6MHz as shown in Figure 80) to 2,600 km (18 MHz as shown in Figure 86). The distance results, however, have greater footprint coverage compared to the ray tracing screens (Figures 53 to 61). The color code for the signal strength coverage maps is described as follows. The blue area represents the signal qualities varying from very good to good propagation. The red/pink area corresponds to the signal qualities varying from fair to blackout situation. The signal quality becomes very good (blue area) just outside of the skip zone where MUF focusing is occurring [7].

The signal quality broadcast coverage maps give indications of the propagation area and its signal strength which is easier to visualize than the numerical expressions.

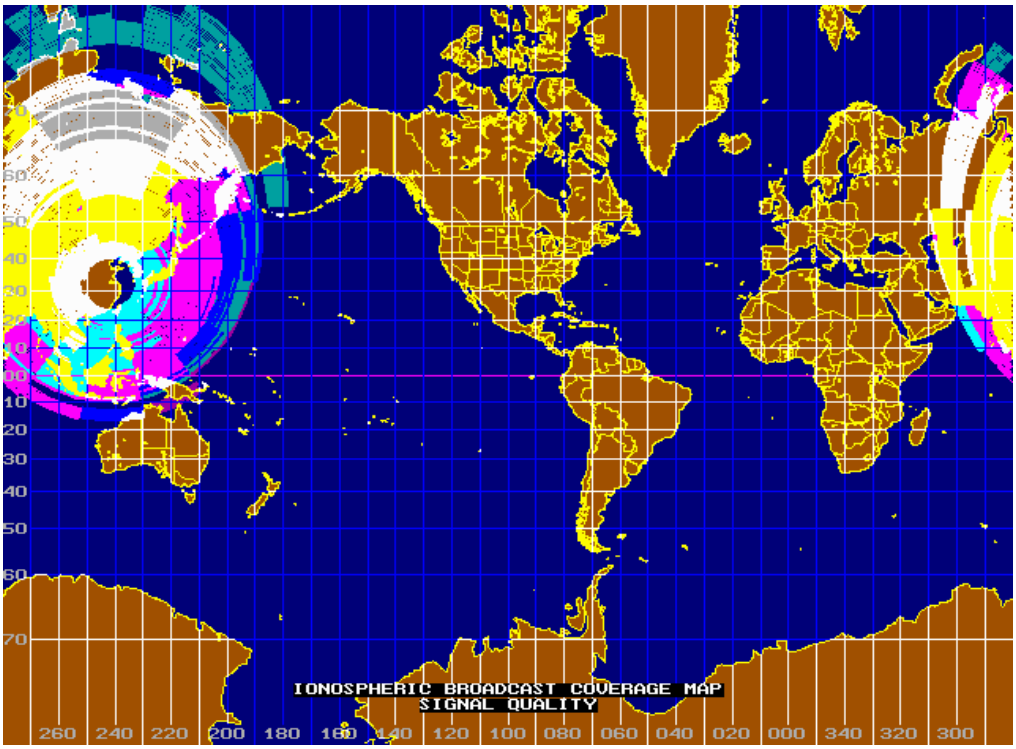

Figure 80. Signal Quality at 6 MHz Frequency for SSN = 30 and AI = 5 at 00:00 UTC 31 July 2007.

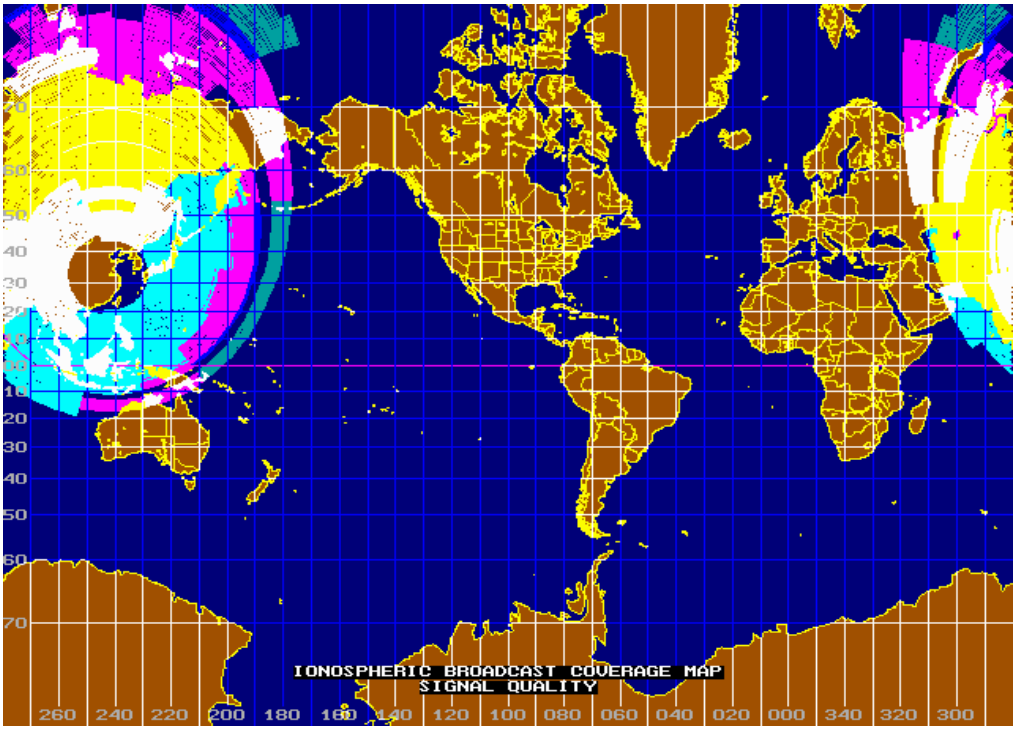

Figure 81. Signal Quality at 8 MHz Frequency for SSN = 30 and AI = 5 at 00:00 UTC 31 July 2007.

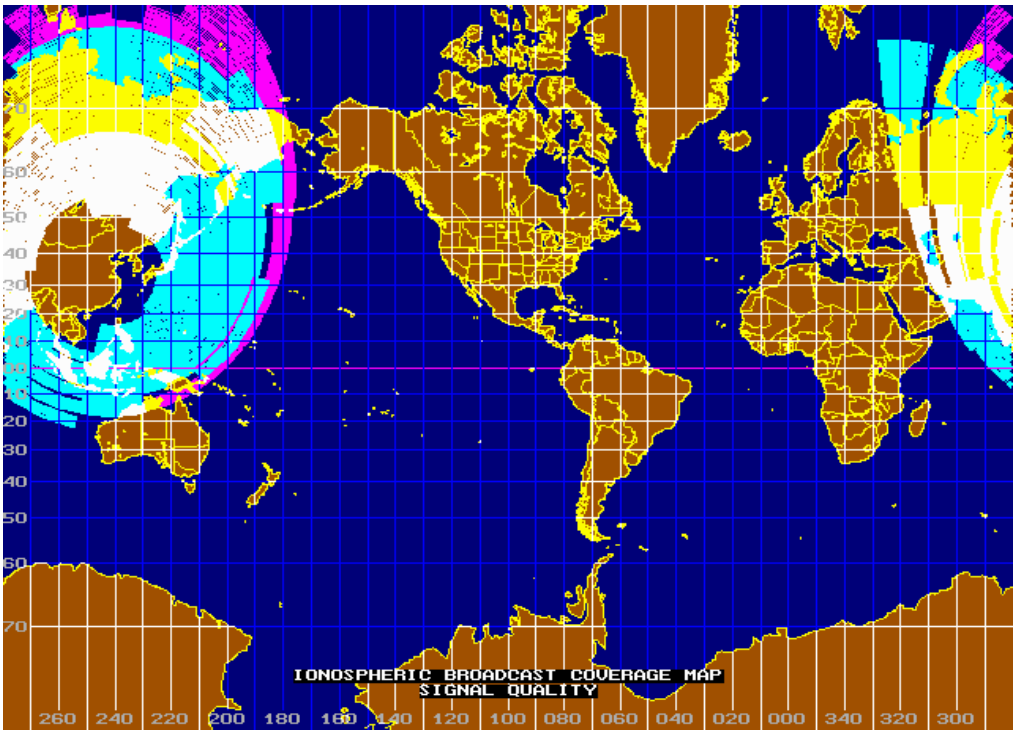

Figure 82. Signal Quality at 10 MHz Frequency for SSN = 30 and AI = 5 at 00:00 UTC 31 July 2007.

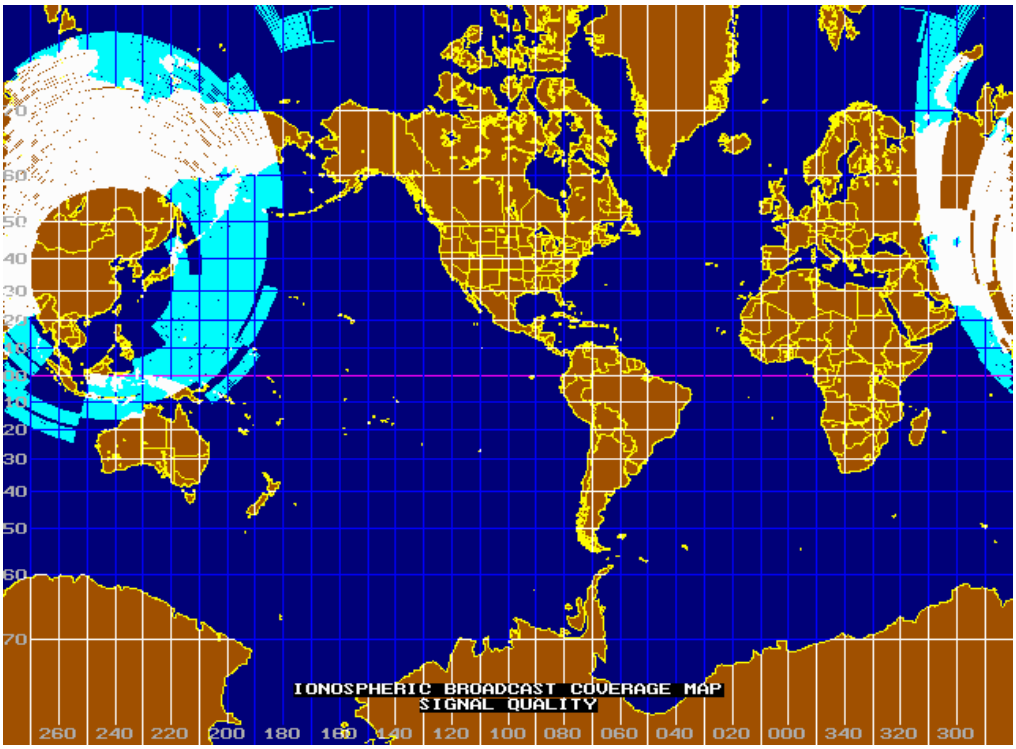

Figure 83. Signal Quality at 12 MHz Frequency for SSN = 30 and AI = 5 at 00:00 UTC 31 July 2007.

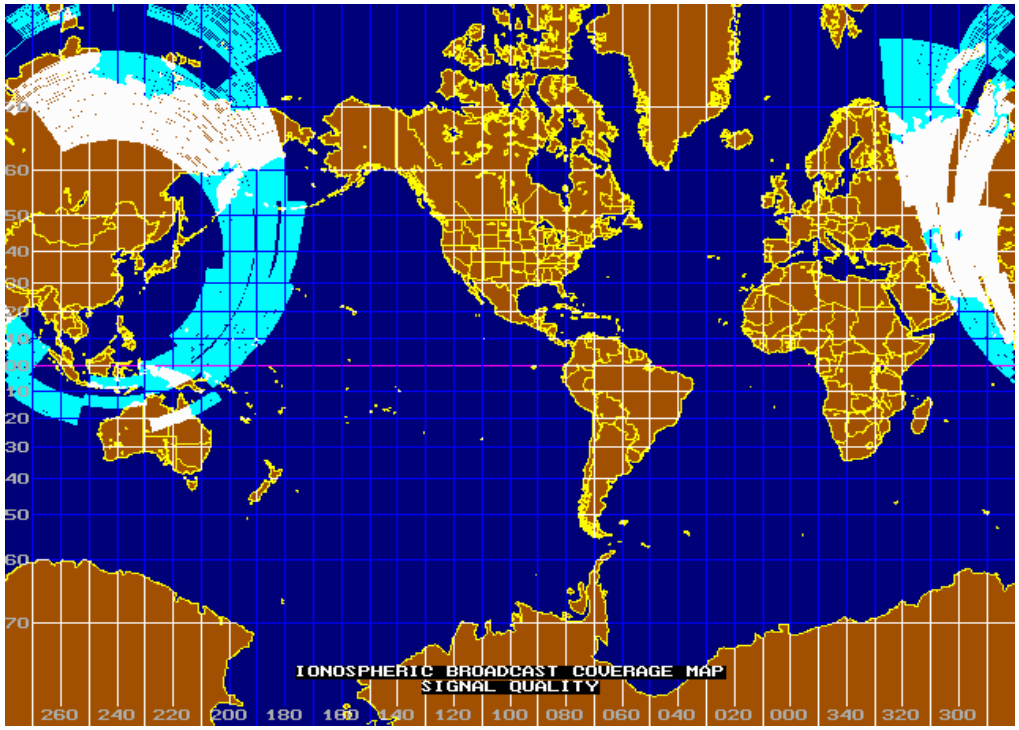

Figure 84. Signal Quality at 14 MHz Frequency for SSN = 30 and AI = 5 at 00:00 UTC 31 July 2007.

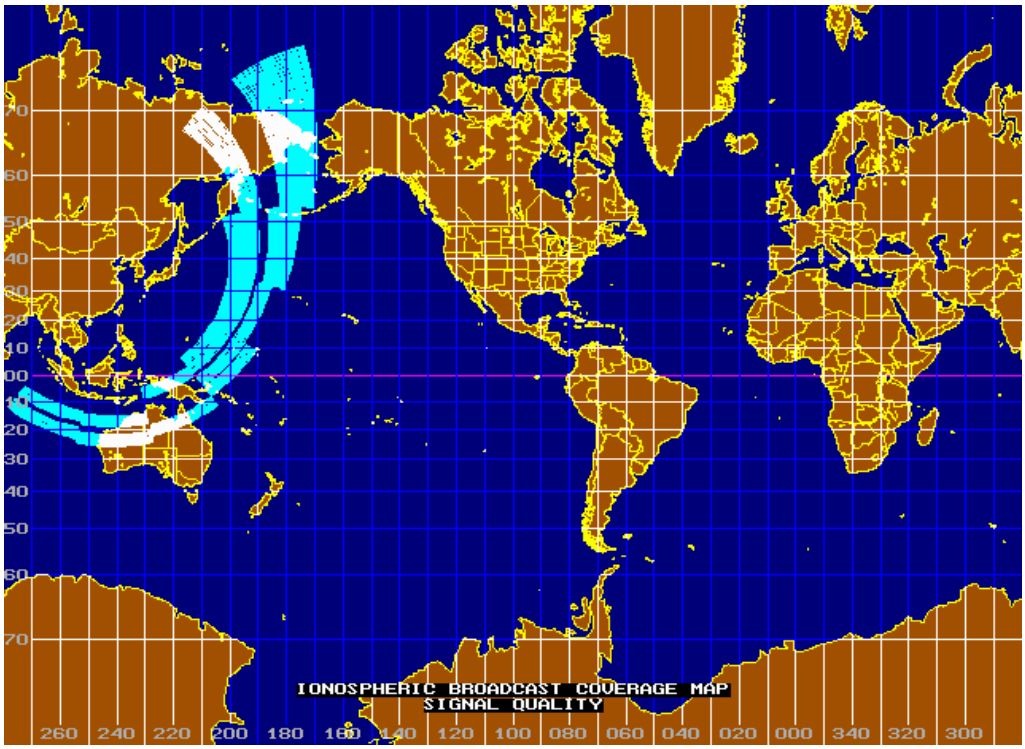

Figure 85. Signal Quality at 16 MHz Frequency for SSN = 30 and AI = 5 at 00:00 UTC 31 July 2007.

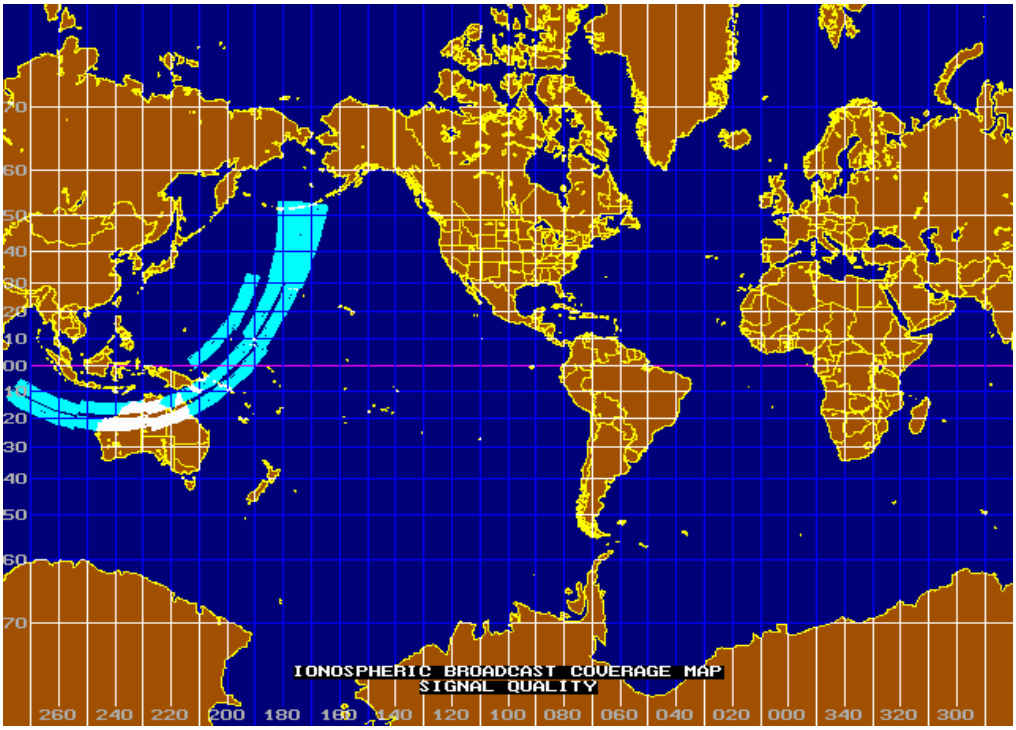

Figure 86. Signal Quality at 18 MHz Frequency for SSN = 30 and AI = 5 at 00:00 UTC 31 July 2007.

From the maximum and minimum FOTs shown in Figures 68 to 71, the signal quality broadcast coverage maps with the transmitter and the target separated by 3,500 km (as described in Chapter V section C) are generated in Figures 87 through 93 for the maximum/minimum FOTs at specific times (as described earlier), high/low SSN, and winter/summer parameters. The symbol "T" represents the Chinese OTH-B radar transmitter and symbol "X" represents the assumed target location which is 3,500 km away from the "T" symbol in the signal strength coverage maps in Figures 87 through 93.

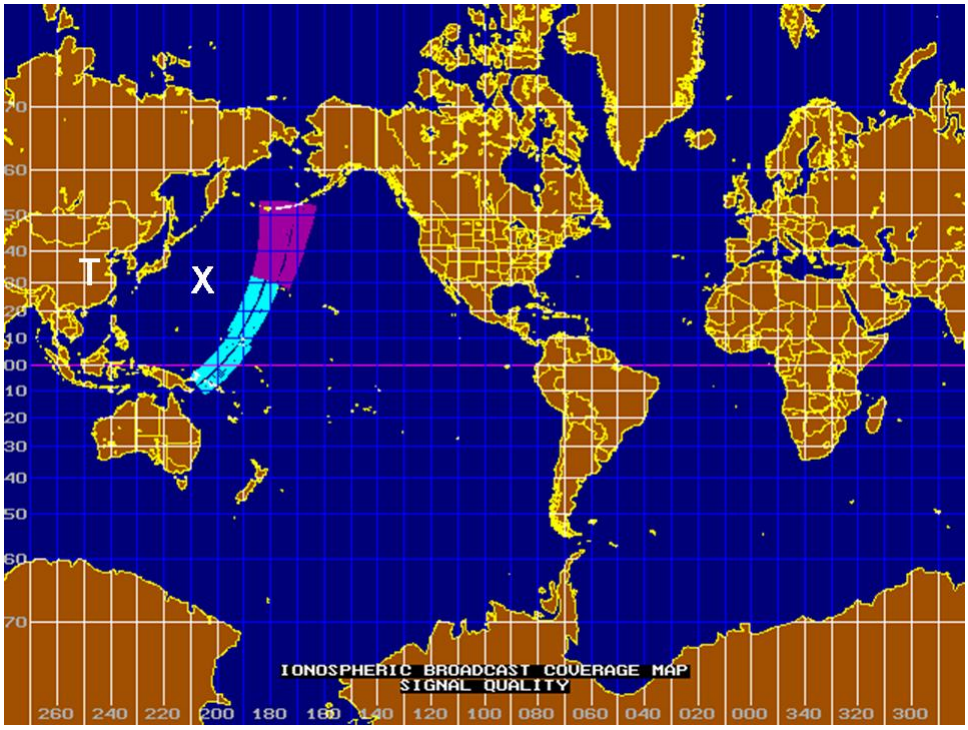

Figure 87. Signal Quality at High FOT = 25 MHz for SSN = 30 and AI = 5 at 01:00 UTC 2006/12/21.

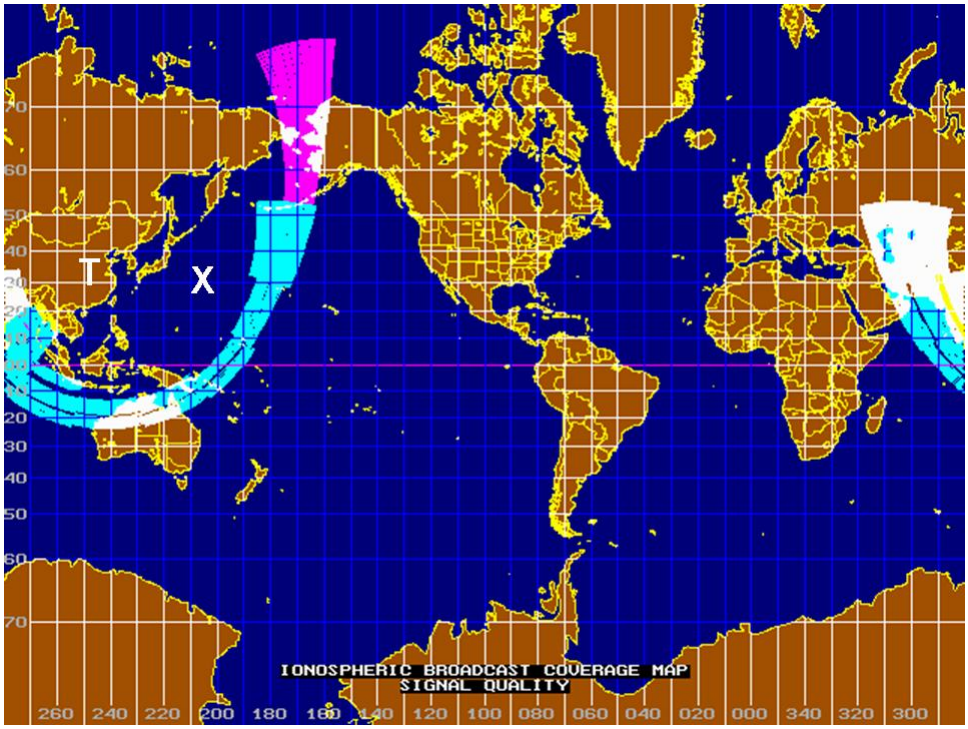

Figure 88. Signal Quality at Low FOT = 6.8 MHz for SSN = 30 and AI = 5 at 14:00 UTC 2006/12/21.

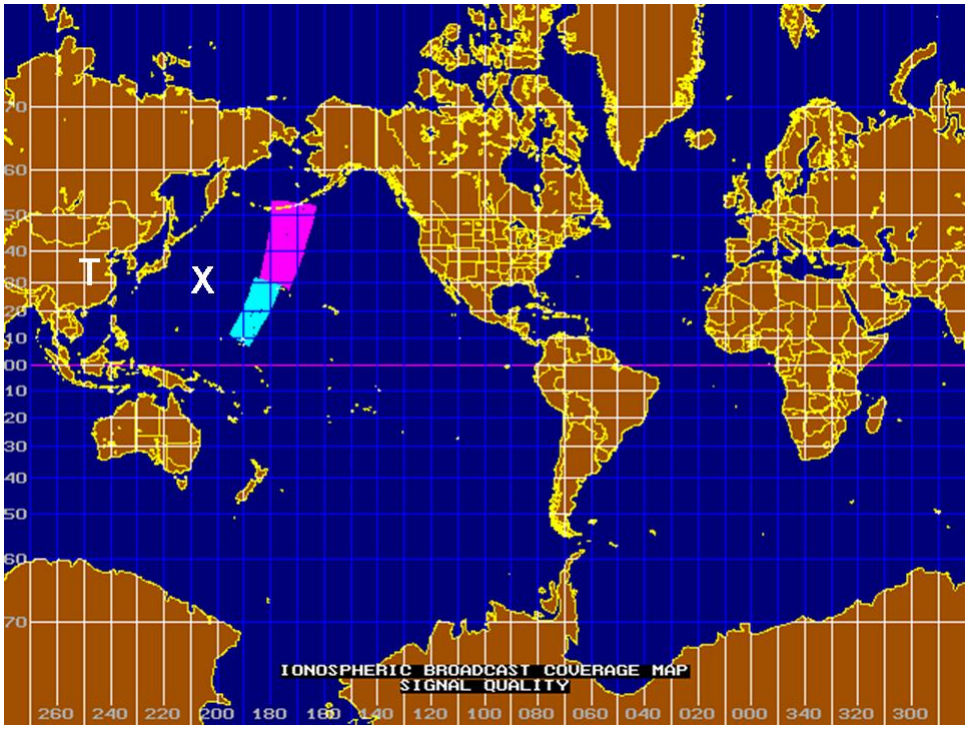

Figure 89. Signal Quality at High FOT = 38 MHz for SSN = 200 and AI = 5 at 01:00 UTC 2006/12/21.

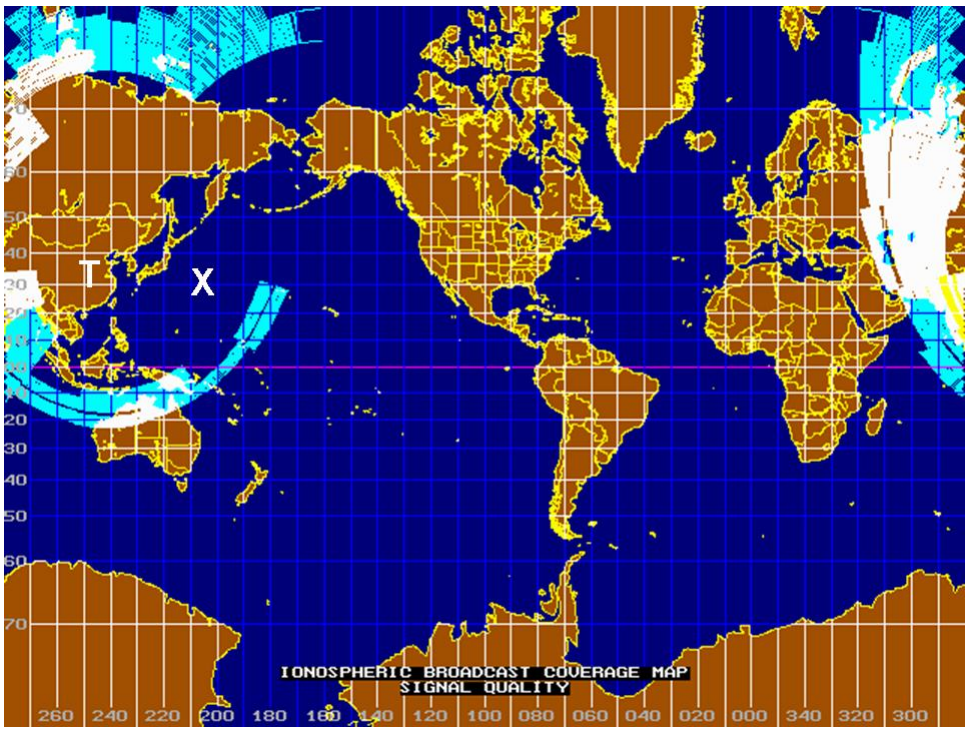

Figure 90. Signal Quality at Low FOT = 9.5 MHz for SSN = 200 and AI = 5 at 19:00 UTC 2006/12/21.

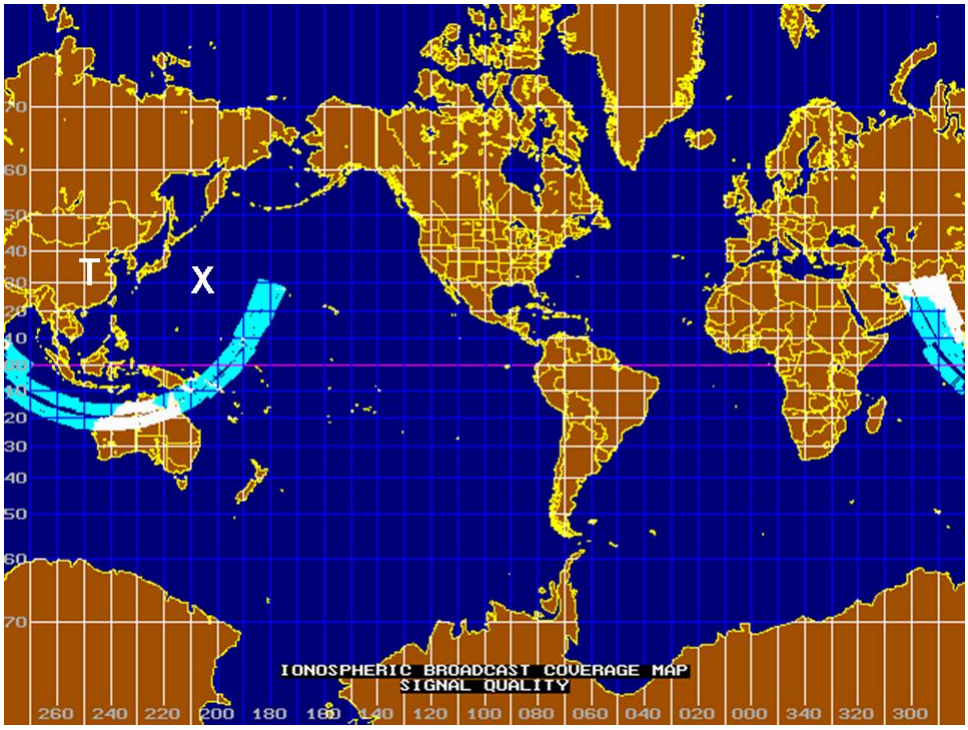

Figure 91. Signal Quality at High FOT = 22.5 MHz for SSN = 30 and AI = 5 at 08:00 UTC 2007/6/21.

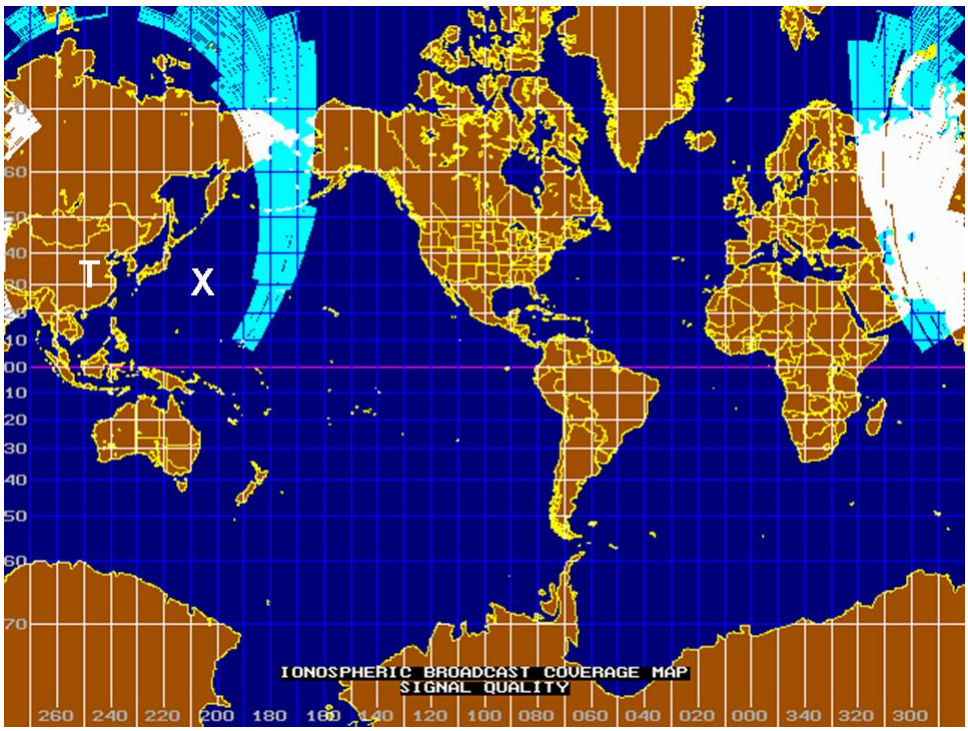

Figure 92. Signal Quality at Low FOT = 12.8 MHz for SSN = 30 and AI = 5 at 18:00 UTC 2007/6/21.

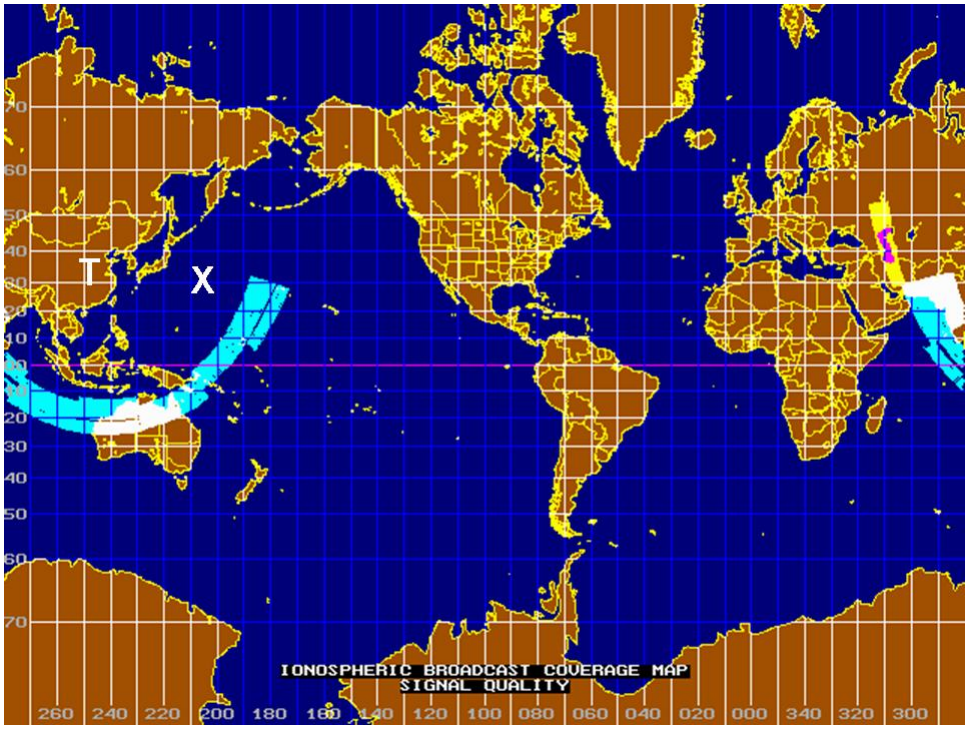

Figure 93. Signal Quality at High FOT = 28 MHz for SSN = 200 and AI = 5 at 08:00 UTC 2007/6/21.

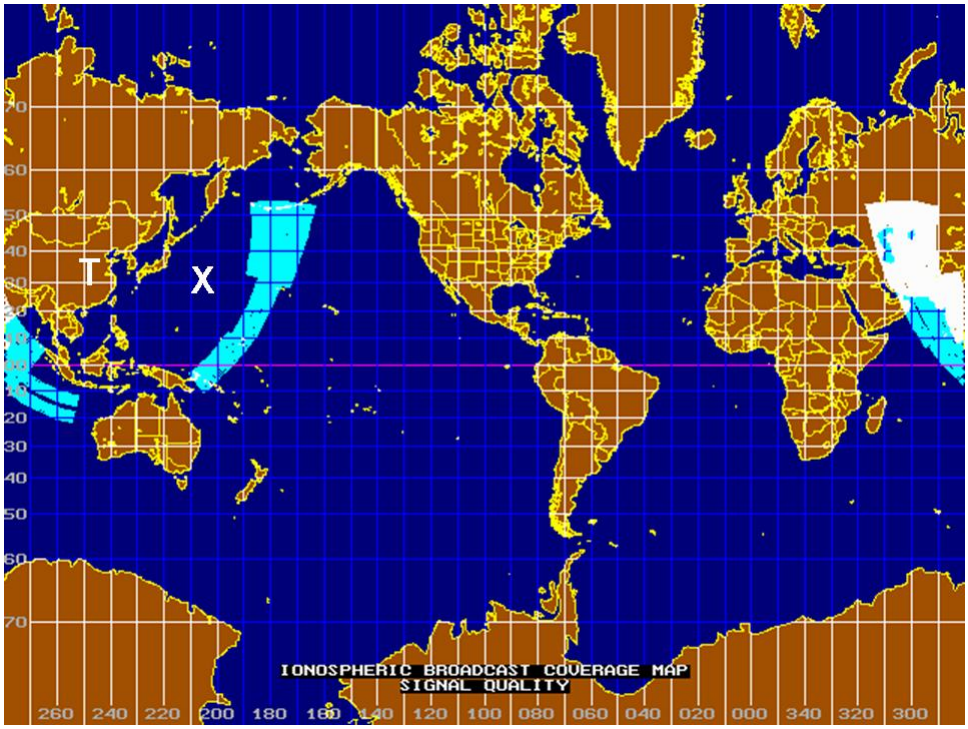

Figure 94. Signal Quality at Low FOT = 20 MHz for SSN = 200 and AI = 5 at 19:00 UTC 2007/6/21.

Based on the information analysis above, the signal propagation and area coverage is greatly dependent on the radar operating frequency, time of day, time of year, SSN and the elevation angles. The greater operating frequency does not actually result in better signal coverage area. The frequency needs to be within the boundary of the FOT and the average MUF of the E and the F-layer to have a better coverage area and good signal quality. The SSN is an important parameter when propagating a wave since the solar activities greatly affect the ionosphere and the skywave propagation.

Some questions regarding PROPLAB performance are observed here. The signal quality coverage maps do not match the ray trace results. The results shown in the signal quality broadcast coverage maps indicate that the signal coverage region is further than what we expected from the ray tracing screen. The other question is about the application of the antenna pattern. The default antenna pattern is shown in Figure 45 and has a maximum gain towards 085° in azimuth. It seems that PROPLAB doesn't apply the antenna pattern into the signal quality maps simulation since good to very good signal quality appears at many angles outside the azimuth beamwidth of the antenna.

LIST OF REFERENCES

1. Kong Min, Wang Guo-hong and Wang Xiao-Bo, "Coordinates Registration and Error Analysis based on Spherical Model for OTH Radar", IEEE International Conference on Radar, pp. 1-4, October 2006.

2. Simon Kingsley and Shaun Quegan, *Understanding Radar Systems*, Chapter 10, Scitech, Mendham, NJ, 1999.

3. A. A. Kolosov, et al., *Over-the-Horizon Radar*, Artech House, MA, 1987.

4. Mike D. E. Turley, "FMCW Radar Waveforms in the HF Band", Defense Science and Technology Organization, Australia, November 2006.

5. Department of Navy, *Naval Shore Electronics Criteria*, HF Radio Propagation and Facility Site Selection, Naval Electronic Systems Command, Washington DC, June 1970.

6. Y. Zhang, M.G. Amin and G. J. Frazer, "High-resolution time-frequency distributions for maneuvering target detection in over-the-horizon radars", Proc. of IEE Radar Sonar Navigation, Vol. 150, No. 4, pp. 299-304, August 2003.

7. PROPLAB-PRO version 2.0 User's Manual, High Frequency Radio Program Laboratory, 1994-1997.

8. The Earth's Ionosphere. http://www.utdallas.edu/research/spacesciences/ionosphere.htm (June 2007)

9. Ionospheric Model (IRI-2001). http://nssdc.gsfc.nasa.gov/nssdc_news/june01/iri.html (June 2007)

10. IRI Model, Space Physics Data Facility (SPDF). http://modelweb.gsfc.nasa.gov/models/iri.html (June 2007)

11. Kenneth Davies, *Ionospheric Radio Propagation*, chapter 3, U.S. Department of Commerce, National Bureau of Standards Monograph 80, April 1965.

12. P.L. Dyson and J.A. Bennett, BE, "Exact ray path calculations using realistic ionospheres", Proc. of IEEE Microwaves, Antennas and Propagation, Vol. 139, No. 5, pp. 407-413, October 1992.

13. C. J. Coleman, "A ray tracing formulation and its application to some problems in over-the-horizon radar", *Radio Science*, Vol. 33, No. 4, pp. 1187-1197, July-August 1998.

14. Thomas A. Croft and Harry Hoogasian, “Exact Ray Calculation in a Quasi-Parabolic Ionosphere With No Magnetic Field”, *Radio Science*, Vol. 3, No. 1, pp. 69-74, January 1968.

15. John C. Wise, J.C. Wise Associates, “Summary of Recent Australian Radar Developments”, *IEEE Aerospace and Electronic systems magazine*, December 2004.

16. “Jindalee Operational Radar Network (JORN)”, *Jane's Radar and Electronic Warfare Systems*, Land-Based Air Defence Radars**,** January 10, 2007.

17. Over the Horizon Radar.
http://www.canadaconnects.ca/space/main/1210/ (June 2007)

18. “SWR series High-Frequency Surface Wave Radars (HFSWR)”, *Jane's Radar and Electronic Warfare Systems, Naval/Coastal Surveillance and Navigation Radars***,** April 10, 2007.

19. Zhang Zhizhong, “Survey Paper – Radar Research and Development, People’s Republic of China”, Record of the IEEE International Radar Conference, pp. 136-138, April 28-30, 1980.

20. Weapons of Mass Destruction, WMD.
http://www.globalsecurity.org/wmd/world/china/oth-b.htm (April 2007)

21. “Chinese OTH radar”, *Jane’s C4I Systems* 2000-2001, *Intelligence Systems in Direction Finding*, January 8, 2002.

22. Chinese OTHR.
http://bbs.tiexue.net/post_1169441_1.html (June 2007)

23. Li Neng-Jing, “A Review of Chinese Designed Surveillance Radars -- past, present and future”, Record of the IEEE International Radar Conference, pp. 288-293, May 8-11, 1995.

24. Tang Xiaodong, Han Yunjie, and Zhou Wenyu, “Skywave Over-the-Horizon Backscatter Radar”, Proc. of the IEEE International Radar Conference, pp. 90-94, October 15-18, 2001.

25. Zhou Wenyu and Mao Xu, “Bistatic FMCW OTH-B experimental radar”, Nanjing Research Institute of Electronic Technology, Record of CIE International Conference on Radar (CICR-91), October 1991.

26. M. Six, J. Parent, A. Bourdillon and J. Delloue, “A New Multibeam Receiving Equipment for the Valensole Skywave HF Radar: Description and Applications”, *IEEE Transactions on Geoscience and Remote Sensing*, Vol. 34, No. 3, pp. 708-719, May 1996.

27. David Bourgeois, Christéle Morisseau and Marc Flécheux, “Over-The-Horizon Radar Target Tracking Using MQP Ionospheric Modeling”, *IEEE* 8th International Conference on Information Fusion (FUSION), Vol. 1, pp. 283-289, July 2005.

28. “French Radar Tracks Low-flying Light Aircraft”, *Jane’s International Defense Review, Weapons and Equipment*, June 1, 2002.

29. “CONDO-R Naval Radar”, *Jane's Radar and Electronic Warfare Systems, Naval/Coastal Surveillance and Navigation Radars*, January 16, 2006.

30. TPS-828, Italian Naval Coastal Radars. http://www.galileoavionica.it/A3_co1_inf.htm (June 2007)

31. “Japanese Over-the-Horizon (OTH) radar”, *Jane’s C4I Systems* 2000-2001, *Intelligence Systems in Direction Finding*, June 8, 2000.

32. “IRIDA Over-the-Horizon Surface Wave (OTH-SW) Radar”, *Jane’s C4I Systems* 2001-2002, *Intelligence Systems in Surveillance and Reconnaissance*, April 6, 2001.

33. “Over-The-Horizon Backscatter (OTH-B) Radar”, *Jane's Radar and Electronic Warfare Systems, Land-Based Air Defence Radars*, July 2, 2001.

34. New Radar in Short Wave. http://www.mediasuk.org/iw0hk/articolo_radar_hf.htm (July 2007)

35. “Transportable Over-The-Horizon Surface Wave (OTH-SW) radar”, *Jane's Radar and Electronic Warfare Systems, Land-Based Air Defence Radars*, November 9, 2001.

36. “Shipboard Over-The-Horizon Surface Wave (OTH-SW) radar”, *Jane's Radar and Electronic Warfare Systems, Naval/Coastal Surveillance and Navigation Radars*, November 9, 2001.

37. “Transportable Skywave Over-the-Horizon (SkW-OTH) radar”, *Jane’sRadar and Electronic Warfare Systems, Land-based Air Defence Radars*, November 9, 2001.

38. “Alenia Marconi Over-the-Horizon (OTH) radar”, *Jane’s C4I systems* 2001-2002, *Intelligence systems in Surveillance and Reconnaissance*, April 6, 2001.

39. Joseph F. Thomason, U.S. Naval Research Laboratory, “Development of Over-the-Horizon Radar in the United States”, Proc. of IEEE International Conference on Radar, pp. 599-601, September 3-5, 2003.

40. “AN/FPS-118 Over-The-Horizon radar”, *Jane's Radar and Electronic Warfare Systems, Land-based Air Defence Radars*, November 9, 2001.

41. Over-the-Horizon Radar, Wide Aperture Research Facility, 2007. http://www.sri.com/esd/rsed/oth.html (June 2007)

42. "AN/TPS-71 relocatable Over-The-Horizon Backscatter (OTH-B) radar", *Jane's Radar and Electronic Warfare Systems, Land-based Air Defence Radars*, March 14, 2007.

43. James R. Barnum and Erik E. Simpson, "Over-the-horizon radar target registration improvement by terrain feature localization", *Radio Science*, Vol. 33, No. 4, pp. 1077-1093, July-August 1998.

44. "NOSTRADAMUS Over The Horizon Radar - First sub-array experimentation", S. Saillant, IEEE International Conference on Radar, pp. 78-81, October 12-13, 1992.

45. James R. Barnum, "Ship Detection with High-Resolution HF Skywave Radar", *IEEE Journal of Ocean Engineering*, Vol. OE-11, No. 2, pp. 196-209, April 1986.

46. R. H. Khan and D. K. Mitchell, "Waveform Analysis for High-Frequency FMICW Radar", IEE Proceedings on Radar and Signal Processing, Vol. 138, No. 5, pp. 411-419, October 1991.

47. Pulse-Doppler Radar. http://en.wikipedia.org/wiki/Pulse_doppler (April 2007)

48. Byron Edde, *Radar Principles, Technology, applications*, Prentice Hall, New Jersey, 1995.

49. A.G. Stove, "Linear FMCW radar technique", IEE Proceedings on Radar and Signal Processing, Vol. 139, No. 5, pp. 343-350, October 1992.

50. Gary S. Sales, "OTH-B Radar System: System Summary", Phillips Laboratory, Air Force Systems Command, Hanscom Air Force Base, MA, May 1992.

51. Qiang Yong, Jiao LiCheng and Bao Zheng, "An Approach to Detecting the Targets of Aircraft and Ship together by Over-the-Horizon Radar", Proc. of CIE International Conference on Radar, pp. 95-99, October 2001.

52. Phillip E. Pace, *Detecting and Classifying Low Probability of Intercept Radar*, Artech House, Boston, 2004.

INITIAL DISTRIBUTION LIST

1. Defense Technical Information Center
   Ft. Belvoir, VA

2. Dudley Knox Library
   Naval Postgraduate School
   Monterey, CA

3. Phillip E. Pace
   Naval Postgraduate School
   Monterey, CA

4. Jeffrey B. Knorr
   Naval Postgraduate School
   Monterey, CA

5. James Michael (Bret)
   Naval Postgraduate School
   Monterey, CA

6. Dan C. Boger
   Naval Postgraduate School
   Monterey, CA

7. Mr. Richard Ritter
   Missile Defense Agency
   Washington, DC

8. Mr. Michael Young
   Missile Defense Agency
   Washington, DC

9. Ms. Denise Spencer
   Missile Defense Agency
   Washington, DC

10. Mr. Steve Hill
    Missile Defense Agency
    Washington, DC

11. Mr. Jan Young
Missile Defense Agency
Washington, DC

12. Ms. Genell Hausauer
Missile Defense Agency
Washington, DC

13. LTC. Scott LeMay, USAF
Missile Defense Agency
Washington, DC

14. Ms. Deborah Stiltner
Missile Defense National Team
Crystal City, VA

15. Mr. Tim Trapp
Missile Defense National Team
Crystal City, VA